Optimized control strategy for Venetian blinds in an event space with fully glazed facades

The case study of the Co-Creation Center

Master Thesis

Panagiota Theodoropoulou

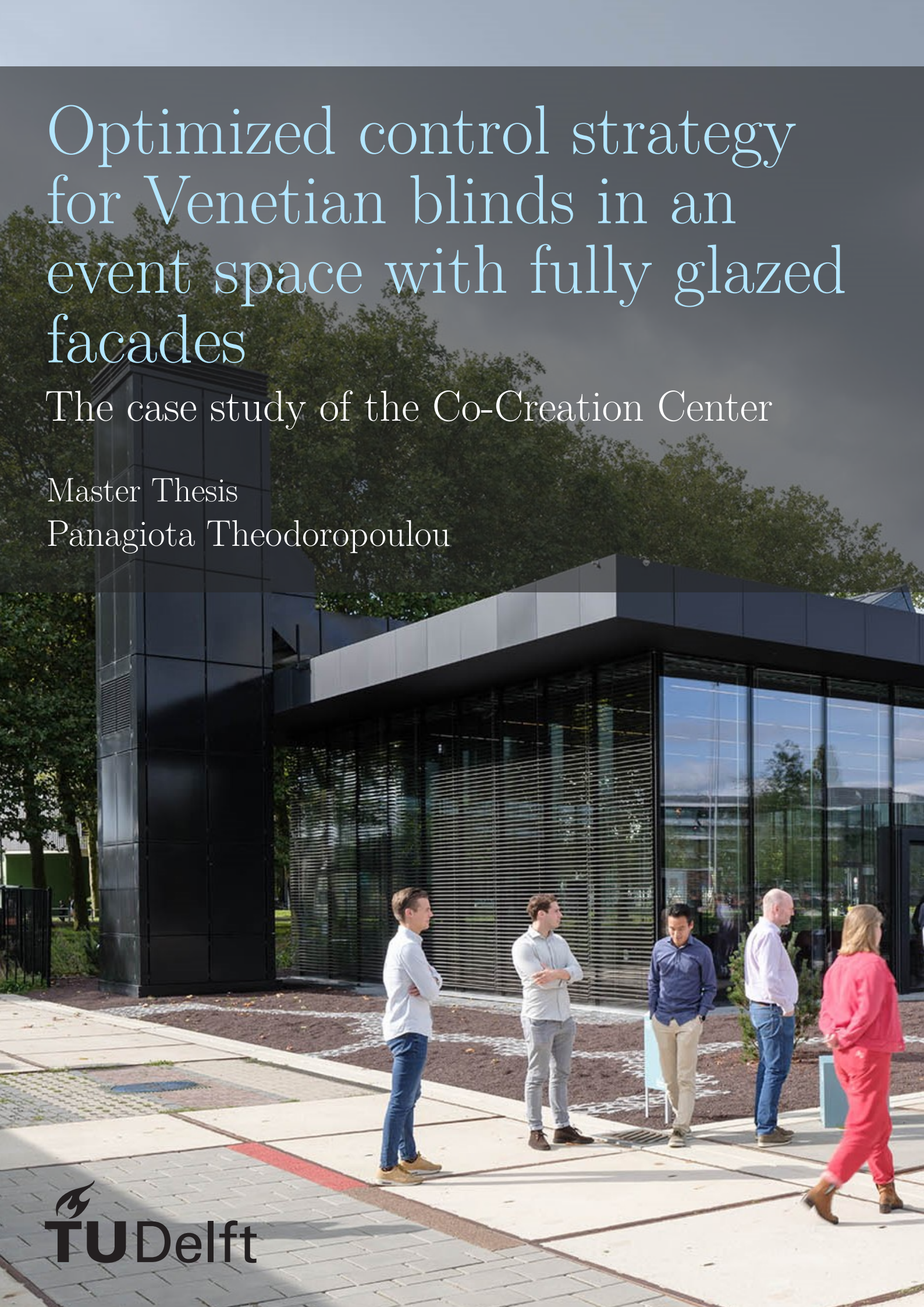

TU Delft

Delft University of Technology

Faculty of Civil Engineering and Geosciences

MSc Building Engineering

Master Thesis Report

Optimized control strategy for Venetian blinds in an event space with fully glazed facades

The case study of the Co-Creation Center

By

Panagiota Theodoropoulou
Student number: 5505127

to obtain the degree of Master of Science
at the Delft University of Technology,
to be defended publicly on July 6, 2023.

Thesis Committee:	Prof. dr. ir. P.C. Louter,	TU Delft - Chairman
	Dr. E. Brembilla,	TU Delft - Supervisor
	Dr. ir. H.R. Schipper,	TU Delft

Cover: The Co-Creation Center, The Green Village, TU Delft (Mecanoo, n.d.).

An electronic version of this thesis is available at `http://repository.tudelft.nl/`.

TU Delft

SUPPORTED BY
ONASSIS FOUNDATION

Acknowledgements

With the present Master thesis, my postgraduate studies at the faculty of Civil Engineering, at TU Delft are completed. On this occasion, I would like to thank everyone that contributed, directly or indirectly, to this accomplishment.

First and foremost, I want to thank my committee, Eleonora Brembilla, Christian Louter and Roel Schipper for their guidance and scientific assistance. Eleonora, thank you for our regular meetings, continuous support and advice. It has been a pleasure working with you, exchanging ideas and obtaining new knowledge. Christian and Roel, thank you for your insightful ideas during the committee meetings. The collaboration with all of you was a great experience that undeniably broaden my horizons. Moreover, I would like to thank Wouter Beck for his constant assistance during the thesis, providing useful information about the case study, as well as recorded data derived from the currently implemented control of the Co-Creation Center's shading system.

Furthermore, I would like to thank Onassis Foundation for the financial support during my Master's studies. Thanks to my scholarship, I was able to attend the Master's program, enlarge my knowledge in a wide range of scientific disciplines and innovative techniques, as well as to gain wonderful experiences living in Delft.

Last but not least, I want to express my gratitude to my friends and family for being supportive every single day, and for helping me overcome any difficulties. Especially, I want to thank my friends, Angelina and Anna, who went through this journey with me and made it so beautiful despite the hard times.

Penny Theodoropoulou
Delft, July 2023

"...Keep Ithaka always in your mind.
Arriving there is what you're destined for.
But don't hurry the journey at all.
Better if it lasts for years,
so you're old by the time you reach the island,
wealthy with all you've gained on the way,
not expecting Ithaka to make you rich.

Ithaka gave you the marvelous journey.
Without her you wouldn't have set out..."

C.P. Cavafy: *Collected Poems* (Princeton University Press, 1975)

Abstract

Nowadays, the integration of smart system technologies in buildings is a necessity to achieve pressing sustainability goals, but still, a challenge to design. Automatic operation of shading devices for the regulation of daylight entry is a commonplace passive technology that aims at occupants' visual comfort while limiting energy consumption for electric lighting. So far, automatic blinds controllers applied in practice are based on rule-based methods, which respond instantly to weather changes. However, their practical effectiveness is questioned, as they do not always respond to the actual visual needs of the occupants. On the other hand, Architectural Design Optimization (ADO) is getting popular among engineers that try to find optimal solutions, balancing conflicting aspects in their designs. Optimized control strategies are promising tools for optimal blinds operation, but their efficiency is still under research, as their high computational cost does not always allow for their real-life implementation.

The existing literature about control techniques for shading devices is mostly limited to simplified cases of side-lit rooms with certain view directions. Nevertheless, the constantly rising application of fully glazed facades in new designs complicates the assessment of indoor visual conditions, and hence the blinds' operation. Daylight Glare Probability (DGP), a widely-used metric for reliable glare assessment, and other image-dependent metrics, seem inappropriate in such cases, and thus the need for view-independent glare evaluation is raised. On the contrary, cylindrical illuminance (E_{cyl}) is the average of vertical illuminance in all directions around a viewpoint and hence it has the potential to assess glare risks regardless of the occupant's exact view direction.

The present Master thesis explores the implementation of a glare-based control strategy for Venetian blinds in buildings with totally transparent facades. The case study concerns the Co-Creation Center, a building located in the Green Village, TU Delft, that utilizes a combination of passive and active building system technologies to limit its environmental footprint. The building hosts three different types of events: presentations, meetings and workshops. The diverse occupancy patterns, coupled with the four fully glazed facades, make the effective blinds control a challenging task to achieve using a traditional rule-based approach. Therefore, in this project, an optimized control system is proposed, aiming at the minimization of visual discomfort due to glare, as well as the minimization of energy demands for electric lighting by increasing daylight entry. The control strategy is developed within *Grasshopper*, a promising tool for parametric and optimization problems. *Grasshopper* allows for the creation of a parametric model that can be adjusted to other similar buildings with fully glazed facades by modifying the input parameters. Radial Basis Function Optimization (RBFOpt), a model-based optimization method performed by *Grasshopper*'s component *Opossum*, is utilized for the computation of the optimal blinds' states.

The thesis yields results that help draw conclusions about the effectiveness of an optimized control algorithm, as well as the appropriateness of *Grasshopper* as a tool for the real-time operation of a shading device. Moreover, within the developed control strategy, E_{cyl} is used as a glare index, giving the opportunity to evaluate its performance. Results show that the developed algorithm can improve the existing visual conditions in the Co-Creation Center by an average of 80% for all activity types, although it led to an average increase of 7% in the time steps where electric lighting is needed, in comparison to the current control. The fact that the developed control logic worked overall effectively in such a complex case as the Co-Creation Center, suggests that it can meet requirements for a broader range of buildings and scenarios. Nevertheless, the time-consuming ray-tracing process performed by *Grasshopper* for each time step and the non-automated use of the RBFOpt component *Opossum*, slowed down the optimizations and made their use rather unsuitable for real-life implementation of the control strategy. Despite the impractical use of *Opossum*, RBFOpt was proved a promising optimization method. Finally, E_{cyl} displayed an overall agreement of 92.5% with DGP, proving that in spaces with multiple

windows and uncertain occupants' view direction, a view-independent index can predict glare risks adequately well, after being carefully correlated with another reliable view-dependent metric.

Contents

List of Figures

List of Tables

Nomenclature

Abbreviations

Abbreviation	Definition
ADO	Architectural Design Optimization
BSDF	Bi-directional Scattering Distribution Function
CAMS	Copernicus Atmospheric Monitoring Service
CBDM	Climate-Based Daylight Modelling
CCC	Co-Creation Center
CFS	Complex Fenestration Systems
CIE	Commission Internationale de l' Eclairage (International Commission on Illumination)
DA	Daylight Autonomy
DF	Daylight Factor
DGCC	Daylight Glare Comfort Class
DGI	Daylight Glare Index
DGP	Daylight Glare Probability
DGPs	simplified Daylight Glare Probability
DHI	Diffuse Horizontal Irradiance
DNI	Direct Normal Irradiance
eDGPs	enhanced simplified Daylight Glare Probability
EPW	*EnergyPlus* Weather
FN	False Negative
FP	False Positive
GA	Genetic Algorithm
GHI	Global Horizontal Irradiance
GLANCE	CLare ANnual Classes Evaluation
HDR	High Dynamic Range
HVAC	Heating, Ventilation and Air Conditioning
IES	Illuminating Engineering Society
MTI	Minimum Target Illuminance
Opossum	OPtimizatiOn Solver with Surrogate Models
RBFOpt	Radial Basis Function Optimization
rMBE	relative Mean Bias Error
TI	Target Illuminance
TMY	Typical Meteorological Year
TN	True Negative
TP	True Positive
UDI	Useful Daylight Illuminance
UGP	Unified Glare Probability
UGR	Unified Glare Rating

Symbols

Symbol	Definition	Unit
$\mathbf{C}_{dc}$	Daylight Coefficient matrix	[−]
E	Illuminance	[lx]
$\mathbf{E}$	Illuminance matrix	[lx]
$\mathrm{E}_{ceiling}$	Horizontal illuminance at the ceiling	[lx]
E_{cyl}	Cylindrical illuminance	[lx]
E_{hor}	Horizontal illuminance	[lx]
$\mathrm{E}_{middle,wp}$	Horizontal illuminance at the middle point of the workplane (desk level)	[lx]
E_{v}	Vertical illuminance	[lx]
$\mathrm{E}_{v,eye}$	Vertical illuminance at the eye level	[lx]
$\mathrm{E}_{v,in}$	Vertical indoor illuminance of glazing	[lx]
$\mathrm{E}_{v,out}$	Vertical outdoor illuminance of glazing	[lx]
E_{wp}	Horizontal illuminance at the workplane (desk level)	[lx]
L	Luminance	[cd/m^2]
R^2	Coefficient of determination	[−]
$\mathbf{S}$	Sky matrix	[cd/m^2]
ρ	Reflectance	[%]
τ	Transmittance	[%]

1

Introduction

1.1. Motivation for the design of shading control systems

Daylight plays a significant role in the comfort of indoor environments, affecting human circadian rhythm, and hence occupants' health and well-being in the long term. Visual comfort depends on the amount and distribution of light in the indoor space. Allowing penetration of large amounts of daylight into the building can ensure sufficient indoor illuminance, limiting the need for electric lighting. Furthermore, sunlight is beneficial for indoor thermal comfort during winter, since it allows solar heat gains into the building while reducing heating energy demands.

In order to take advantage of the benefits of the incoming daylight, more and more buildings have been constructed with fully glazed facades over the last decades. However, concerns regarding visual and thermal discomfort that may occur due to excessive daylight, were quickly raised. On the one hand, stray light reaching users' eyes can provoke disability glare, resulting in a reduction of their visibility (Vos, 1984). On the other hand, long exposure to excessive direct sunlight results in discomfort glare that may cause eye fatigue, headaches and dizziness (Osterhaus, 2005). In addition, during summer, large amounts of incoming solar energy lead to overheating of indoor spaces, and hence to higher cooling energy needs.

To overcome those obstacles, but simultaneously maintain the benefits of daylight for building occupants, multiple shading devices and complex fenestration systems have been developed, in order to improve buildings' performance and keep a balance between visual comfort and thermal efficiency (Konstantoglou & Tsangrassoulis, 2016). Manual operation of blinds was initially sufficient to ensure visual comfort based on the exact needs of the occupants, but usually at the cost of energy consumption. Nevertheless, the gradual application of automatically controlled shading systems proved that they are a promising mechanism for the manipulation of the amount of admitted solar radiation, balancing visual comfort and energy demands at the same time (Nielsen, Svendsen, & Jensen, 2011). Besides, automatic shading systems replaced the blinds' distractive manual operation in open space buildings that host a large number of occupants (e.g. presentation rooms, meeting rooms, galleries etc). The automatic control of shading devices, based on sensor measurements or model simulations, is usually combined with automatic lighting, heating and cooling systems. Then, all systems work complementarily to achieve visually and thermally comfortable indoor environments in a sustainable way.

Even though automatic shading systems have been applied to an increasing number of buildings over the last few years, their efficiency is still under investigation. Multiple control parameters have been tested to identify their suitability for different spaces and their capability to represent the actual expected performance. Depending on the complexity of the space configuration and the occupants' behavior, control strategies vary to perform effectively under certain conditions. Despite the scientific and technological advancements, developing a valid and fast control model for shading devices and lighting

systems in real time is still a challenge. This is because, state-of-the-art model-based algorithms achieve well-performing controls, sacrificing their computational speed, while traditional rule-based algorithms have low computational effort, but at the cost of their accuracy and effectiveness.

The present Master thesis investigates an innovative glare-based control strategy of the shading system of a building with totally transparent facades and diverse occupancy patterns. More specifically, the project focuses on the development of an efficient model-based optimized algorithm that will automatically determine the blinds' positions and luminaires' dimming level, aiming at the maximization of visual comfort and the minimization of energy consumption. Visual comfort comprises illuminance sufficiency in the indoor space, as well as glare prevention. Energy consumption refers to the energy required to meet visual needs via the use of electric lighting. Within the limits of the specific study, the heating and cooling performance of the building is not taken into account.

1.2. Background information about the Co-Creation Center

The case study of the Co-Creation Center (CCC) serves as the basis of this research, therefore the developed control strategy directly concerns this particular building. *Grasshopper* is used for the development of a parametric control model, as it is a promising tool for daylight simulations and optimization analyses. This parametric algorithm allows for adjustments by modifying its input parameters, enabling its general use in various similar existing buildings and future projects.

The Co-Creation Center (CCC) is an example of a conference and meeting space, located at the Green Village, TU Delft (Figure 1.1). It was conceived within the CONVERGE research project, aiming at the limitation of energy demands to almost zero, through a combination of passive and active building system technologies, including the smart control of blinds and electric lighting.

Figure 1.1: The Co-Creation Center in the Green Village, TU Delft (Si-X, 2021).

As seen in Figures 1.1 and 1.2, the Co-Creation Center is a single-story building with four fully glazed facades 5.20 m high. The surface area of the building is around 315 m^2 and its length and width are equal to 22.8 m and 13.8 m respectively. The short facades consist of 9 window panes, while the long ones consist of 15 panes. With a flexible open floor plan and varying furniture arrangements, the CCC serves as an event center and offers space to up to 240 guests (Mecanoo, n.d.). The longitudinal axis of the building is tilted at -22° from due North (Figure 1.3).

This building is an example of innovative techniques utilized towards a sustainable future. The structure of the building consists of state-of-the-art recyclable triple-glazing panels and glass fins, while its foundations are made out of recycled concrete. The Nonohouse, connected by a small corridor to the

CCC and serving as an annex, is made of CLT and has a water-retaining roof with sedum that absorbs nitrogen (Mecanoo, n.d.).

Figure 1.2: Co-Creation Center and the Nonohouse, TU Delft (Mecanoo, n.d.).

Figure 1.3: Satellite photo of the Co-Creation Center and its surroundings. North is towards the top of the figure (Google Maps).

The material choices are not the only ones that serve the sustainability goals of the building. A special ventilation system with a climate tower has been installed next to the CCC to drive the fresh air into the building and ensure a comfortable internal climate (Wassink, 2018). In the cooling season, four North-oriented skylights and five doors at the western and eastern façades can also be used for natural ventilation during the day and for cooling at night.

To ensure a visually and thermally comfortable indoor environment, external Venetian blinds are mounted on the facades and controlled automatically. The blinds of each facade move simultaneously and they are operated separately from the rest of the facades. The slats can rotate with a tilt angle from -30° to 72°, in steps of 2°, whereas there are only two possible states of blinds' increments, either fully raised or fully lowered. The currently implemented control strategy of the blinds has two modes of operation. On the one hand, when the building is occupied, the priority is the maximization of indoor illuminance, preventing glare and high lighting energy demands. On the other hand, when the building is empty, the blinds' control is determined by future energy needs for heating and cooling, aiming at their minimization.

In case of an occupied building, the algorithm predicts earlier glare risks that may occur during a session and then moves the blinds to the appropriate state that will prevent glare in the near future. This "predictive" logic, which tries to avoid blinds' movements during a session, uses direct irradiance forecast data to determine whether the luminous exitance threshold for a facade (6000 lx) is exceeded during a planned event. If so, the blinds are scheduled to go down before the event commences. To prevent solar beam penetration when a façade is lit by direct radiation higher than 100 W/m^2, a sun-tracking control strategy is used, meaning that the tilt of the blinds' lamellas is controlled in a way that always blocks direct sunlight (cut-off angle). In fact, the slat angle for all blinds on a facade is set to 2° more than the cut-off angle. When a façade receives mostly diffuse radiation (beam radiation less than 70 W/m^2) and the blinds are already lowered, the slat angle is set to 0° to allow maximum outdoor view. If the blinds are down for at least 30 minutes and the direct radiation falls below 50 W/m^2, the blinds are raised. In order to make the rotation of the slat angles unnoticeable to the occupants, the control algorithm ensures that the tilt angle varies smoothly over time.

In case of zero occupancy, the algorithm predicts the probability of the indoor temperature falling out of the comfort band during a planned session. Hence, it tries to constantly maintain a comfortable temperature. The energy model of the control algorithm is based on the thermal performance of the building during the previous five days and calculates the running mean temperature. Depending on the available solar energy and the heating required at any specific moment, it decides how to operate the blinds, in order to block or allow solar radiation.

The current control system also operates electric lighting. The lighting system in the CCC consists of 32 LED luminaires, each with a power of 66 W and a luminous flux of 8800 lm. The luminaires are placed at the ceiling in four parallel rows along the longitudinal direction (N-S). The light intensity can be dimmed by setting a percentage of the maximum lighting output. Moreover, the light intensity can be adjusted in steps between 0 and 15, with 0 corresponding to warm white light (2700 K) and 15 to cool white light (5000 K). The lighting control currently implemented in the CCC adjusts the lighting intensity to supplement daylight entry and reach the desired horizontal illuminance at desk level. If no occupancy is detected for more than 15 minutes, the lighting system is switched off (Brembilla, 2022b).

There are three activity modes defined for the determination of the desired horizontal illuminance. The current blinds' operation is the same for all occupancy modes. The latter can be visualized in the sketches of Figure 1.4, which demonstrates an example of the space configuration for each case. The three activity types are described below:

- Presentation: The orientation of the audience's view is predetermined, albeit not always the same. The audience stares at one or two projection screens. The desired illuminance at desk level is set to 300 lx, to ensure sufficient light for taking notes.
- Meeting: There is no specific orientation of the occupants. All of them sit around a desk. There may be a projection screen. The desired illuminance at desk level is set to 500 lx.
- Workshop: There is no specific orientation of the occupants. Many desks are placed in the building and the users are distributed around them, working in groups. The people may be seated or standing. There may be one or two projection screens. The desired illuminance at desk level is set to 750 lx.

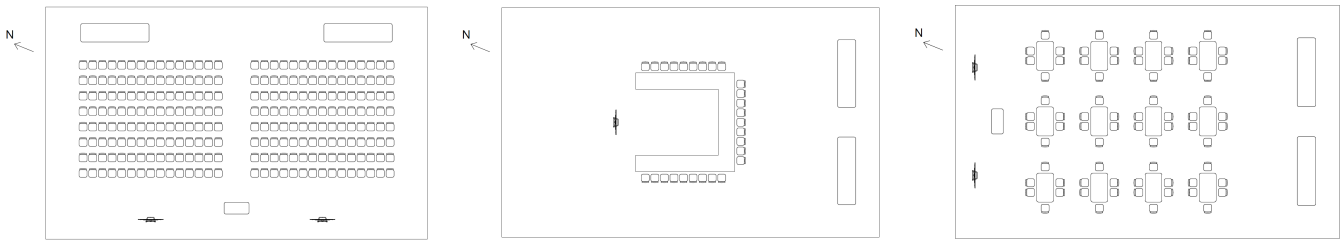

(a) **(b)** **(c)**

Figure 1.4: Example of the space configuration for each of the occupancy modes: (a) presentation, (b) meeting, (c) workshop.

Regarding the HVAC systems and indoor comfort of the CCC, research has been implemented within the CONVERGE project (Van den Engel et al., 2022). In the following paragraphs, the research on the daylight performance of the building will be highlighted.

The building is equipped with a commercial pyranometer (Priva weather station) placed on the roof, which records Global Horizontal Irradiance (GHI) every 5 minutes. Based on the measurements of the roof sensor, the control system can "read" the weather conditions, so as to operate the blinds accordingly. The validation of data collected by the pyranometer was done, by comparing its measurements with the irradiance data (diffuse, direct, global) gathered by a research-grade pyranometer installed on the roof of the nearby building of the EWI faculty. The latter is a 90-meter-tall building, unaffected most of the time by the shadows of surrounding trees and buildings and therefore its measurements are used as a benchmark. The pyranometer of the EWI building logs measurements every 1 minute. Results showed that, although the shadowing obstructions during sunny days affect the measurements of CCC's pyranometer underestimating the GHI, there is a good agreement between the two instruments overall (Figure 1.5). This enables us to use the recordings of the roof's weather station, in order to simulate the sky model in the developed control algorithm.

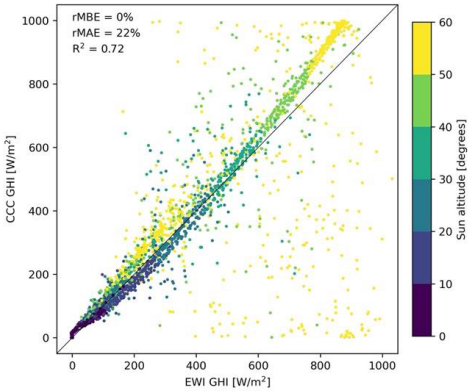

Figure 1.5: Scatterplot showing the correlation between Global Horizontal Irradiance (GHI) values (in W/m^2) recorded by a research grade pyranometer on the EWI building on campus and by the commercial pyranometer installed on the CCC's roof (Van den Engel et al., 2022).

Additionally, Brembilla (2021) tested the accuracy of GHI derived from satellite observations of the Copernicus Atmospheric Monitoring Service (CAMS) with a 15-minute resolution. The GHI of the three sources (CCC pyranometer, EWI pyranometer and CAMS) was compared for a sunny and a cloudy day. Results demonstrated an overall underestimation of GHI on clear sky days by CAMS, and an overestimation on overcast days. Furthermore, it should be noticed that the lower temporal resolution of CAMS leads to lower accuracy for days with variable weather conditions (Figure 1.6). Consequently, it is concluded that CAMS recordings are rather unreliable for the accurate simulation of weather conditions at the CCC's region.

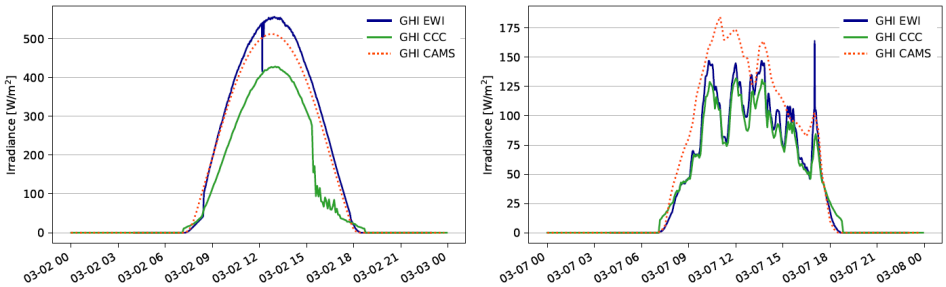

Figure 1.6: GHI time series for a sunny day (left) and a cloudy day (right) from the three sources (Brembilla, 2021).

Moreover, Brembilla (2021) indicated that the Skartveit (Skartveit & Olseth, 1987) and Reindl (Reindl, Beckman, & Duffie, 1990) splitting models can perform quite well for the estimation of Diffuse

Horizontal Irradiance (DHI) and Direct Normal Irradiance (DNI), derived from the GHI given by the CCC's weather station. Even though an overestimation of DNI and an underestimation of DHI were addressed, the two models seemed to be reliable. However, a validation of the sky model will need to be implemented to ensure its accuracy before using it in the control algorithm.

A glare assessment study was also implemented in the CCC, in order to evaluate the effectiveness of various glare indices for three different control modes of the blinds (Brembilla, 2022a). The results proved that Daylight Glare Probability (DGP) and Unified Glare Probability (UGP) represent better reality in the three cases. Nevertheless, these two metrics have limitations that hinder their applicability in the CCC. On the one hand, DGP was derived from a small office room with the occupants not looking straight towards the window (Wienold & Christoffersen, 2006). On the other hand, UGP considers quite low vertical illuminance values (< 2500 lx), thus it cannot identify saturation effects (Hirning, Isoardi, & Cowling, 2014). In addition, both of them are view-dependent, whereas the four fully transparent facades and occupancy variety make glare assessment much more complex than a simple evaluation of HDR images with a certain view direction.

Finally, Brembilla (2022b) conducted an analysis on the electric lighting of the CCC and proposed a control strategy for it. The research showed that energy savings can be achieved during night-mode, by setting lower intensities in the three scenarios; the desk illuminance of 300 lx, 500 lx and 750 lx can be reached by setting a relative intensity of 30%, 50% and 80% respectively. This means, that during the day, lower intensities than the aforementioned percentages are needed for the three activity modes, although the recorded data show that usually a 100% lighting intensity is actually applied. Furthermore, it was noted that in the presentation mode, desk illuminance is not a solid indicator of visual comfort, since occupants' view is mainly towards the screen. Vertical illuminance at the eye level should be used as a supplementary index for checking overall visual conditions in the presentation case.

1.3. Problem Statement

Based on the background information described above, the currently implemented control for the lighting and blinds system of the CCC seems to have room for improvement. First of all, the fact that the blinds of each façade move simultaneously to only two increment states (fully up/fully down), results in an inflexible operation of the shading device. On the contrary, an independent movement of the blinds with more increment steps could offer higher flexibility in balancing daylight sufficiency, glare risks and movements' smoothness. In addition, the early prediction of zero glare risks may not be always successful, resulting in glare issues during a session, which are not resolved, as the blinds usually remain stable over that time period.

Moreover, artificial lighting is not well integrated with admitted daylight, leading to pointless additional energy consumption. This was indeed confirmed during a visit to the CCC, where the lights were already switched on while there was no activity taking place and there was sufficient daylight in the space. The high glass percentage and the dark ceiling and floor produce high contrast and create the feeling of insufficient light, making the occupants turn on electric lighting. This effect can be compensated by opening the louvers in a strategic way, allowing adequate diffuse daylight to enter the building. Furthermore, the early glare prediction may lead to less useful daylight entry throughout an event's duration, resulting in higher energy demands for electric lighting. Finally, solar beam radiation, used as blinds' trigger metric, is not always representative of the actual visual conditions in the building, as glare risks may occur when high contrast between the dim indoor space and the bright admitted daylight is created. Therefore, a more effective metric-based control strategy should be tested and evaluated.

Apart from overcoming the practical problems of the case study, this thesis is challenged to fill the missing research gaps in the scientific field concerning visual conditions assessment and blinds control techniques. The vast majority of the existing research projects tend to simplify the conditions under which the control strategy is implemented, by tackling cases of side-lit rooms with certain spatial and temporal occupancy patterns and low window-to-wall percentages, such as office rooms and classrooms.

These features simplify the assessment of visual conditions and hence the shading control. Nevertheless, nowadays, there is a wide range of buildings that embed a high percentage of transparency in their architectural design, like the CCC. Most of them have usually irregular occupancy patterns, such as conference spaces, galleries, meeting places, shops etc. These complex building conditions require more complicated control approaches and the use of different daylight and glare indices than usual.

In addition, most scientific papers study image-dependent indices, such as Daylight Glare Index (DGI) and Daylight Glare Probability (DGP), which evaluate the glare conditions of a certain scene. Nevertheless, when dealing with buildings with multiple daylight sources (i.e. windows) and diverse occupancy scenarios, a view-independent glare indicator would be more suitable to assess glare risks in multiple directions around a point.

The fact that the existing literature mostly focuses on rule-based control strategies, sets another challenge to this thesis. Real-life applications have shown that rule-based techniques are not always reliable to provide indoor visual comfort. Consequently, the present research gives the opportunity to test the effectiveness of a more advanced, optimized control design under complex daylight conditions.

Finally, although *Grasshopper* is gaining more and more ground as a user-friendly visual-programming tool and it is constantly improved in daylight simulations, developers of control algorithms tend to avoid it. This is reasonable, as *Grasshopper*'s visualization tools are expected to slow down the iterative simulations of a controller. However, its capabilities in parametric model-based algorithms should be further tested, especially for such complex cases of buildings with variable occupancy and fully glazed facades. Also, the optimization tools embedded in *Grasshopper* should be checked and evaluated as appropriate –or not– means, for the development of a control system for optimal visual conditions.

In summary, the final target of this thesis is to discover a more effective control system for the specific case study, as well as to contribute to gradual research advancements in this scientific discipline. Based on the problem statement, the objective and research questions of the project can be identified.

1.4. Thesis objective and Research questions

The objective of the present study can be defined as the development of a parametric model that will control Venetian blinds using an optimization method, aiming at the maximization of visual comfort (prevention of glare and illuminance sufficiency), as well as the minimization of energy demands for electric lighting, in a multi-occupancy building with fully glazed facades. In this manner, this Master thesis will solve the problems of the existing control system in the CCC and will recommend a more efficient way to manipulate artificial and natural light for the provision of a visually comfortable indoor space, with as high as possible energy savings. Within the scope of this research, the occupied mode of the building is investigated, thus the focus is on visual comfort, whereas the heating and cooling energy demands are not included in the control strategy.

It should be noted that the CCC is the starting point for the development of a new advanced algorithm for the automatic operation of Venetian blinds in buildings with fully transparent facades and variant occupancy. However, the algorithm can also be utilized in cases of similar buildings in the future. The parametric character of the model will serve this aim. Of course, the logic behind the proposed control system could be generally applied to any kind of space, e.g. side-lit offices and classrooms.

Based on the objective of the thesis, the main research questions and sub-questions can be stated as follows:

- *How does an optimized control of Venetian blinds in a multi-occupancy building with fully glazed facades affect visual comfort and lighting energy demands?* Automatic operation of blinds for optimal indoor visual conditions in buildings like the CCC is a demanding task, as daylight should be carefully used in the occupants' interest for each time step of the year. With the developed control model, using optimization tools, conflicting aspects need to be balanced. On the one hand, the algorithm should take advantage of solar radiation to minimize electric lighting use, while, on

the other hand, it should block direct or diffuse daylight when glare risks occur. The following sub-questions can steer the process to find the answer to the above main question:

  - *Which daylight simulation method is more appropriate for real-time control of Venetian blinds with a short operational time-step?*
  - *Can optimization tools be used for the development of a real-life control algorithm, responding almost instantly and effectively to weather changes?*

- *Which glare index can act as a trigger metric for efficient glare-based control of an automatic shading system in a building with fully transparent facades and diverse occupancy patterns?* There are multiple ways to assess glare risks, based on various indices. The existing studies have indicated that DGP and UGP have generally a good potential for glare prediction. Nevertheless, their limitations raise concerns about their efficiency in the special case of CCC and other similar buildings. Thus, the next sub-questions are generated and need to be answered within the present research project:

  - *Which glare metrics are suitable for view-independent assessment of discomfort glare?*
  - *How can a view-independent glare index be successfully correlated with image-dependent metrics?*
  - *Is a view-independent glare index solely sufficient for glare assessment in rooms with multiple glare sources, based on simulation results?*

The above research questions serve as guidelines for the gradual progress of the present Master thesis. They are gradually answered based on the literature study and the conclusions derived from the simulations performed during the thesis.

1.5. Outline

The outline of the thesis is structured as summarized below:

Chapter 2 (*Literature Review*) presents the theoretical background of daylight simulations and gives information about indices for glare and light sufficiency evaluation. It also describes various shading control systems that have been tested within other research studies and are useful for a clear understanding of a control's logic and limitations depending on the case.

Chapter 3 (*Methodology*) describes the construction of the parametric 3D model, as well as its calibrations to ensure getting reliable results from the daylight and glare analyses. Moreover, it explains the developed control strategy and how its effectiveness is validated.

Chapter 4 (*Results*) demonstrates the results of the various analyses done throughout this research, for the construction of a valid model and the development of an effective control strategy. The results are then commented on, helping us to draw useful conclusions.

Chapter 5 (*Discussion*) presents a reflection on the results of the thesis and its limitations, as well as some general considerations about control strategies for shading systems.

Chapter 6 (*Conclusion*) sums up the conclusions derived from the whole study, answering the research questions.

Chapter 7 (*Recommendations*) gives recommendations for improvements and further research to overcome problems faced in this thesis and proposes ways to use the developed *Grasshopper* model and control strategy in practice.

2

Literature Review

The starting point of the project is a literature study based on a wide variety of scientific papers, that sets the foundations of this research. Based on it, the background theory can be explicitly enlightened and studies encountering similar problems can guide, inspire or challenge the present research. The literature study provides general information that steers the decisions taken during the thesis and its research approach. In particular, in this chapter, general information regarding various metrics for the assessment of indoor visual conditions is given. Then, some typical control strategies of shading systems are described. In the end, some basic points of background theory about daylight simulations are highlighted.

2.1. Indices for Visual Comfort Assessment

There is a wide variety of indices that can be used to evaluate the (day)lighting performance of an indoor space for a specific moment or on an annual basis. Over the years, more metrics are added to this list and they are gradually embedded into contemporary guidelines. In an attempt to create a list of some visual comfort metrics and describe their characteristics, Carlucci et al. (2015) divided them into two categories; indices for the assessment of light quantity and metrics for evaluation of glare risk. In the following subsections, some useful indices are concisely presented, whereas metrics considered out of the research limits of the thesis are omitted.

2.1.1. Quantity of light

Illuminance (E) constitutes the basis of most light indices as, by definition, it is a metric that represents the amount of light emitted by a source at a given rate that falls on a surface per square meter.

Daylight Factor (DF) is adopted by traditional guidelines and used to be the main index to draw conclusions about the sufficiency of daylight in a building. By its definition, DF is computed under CIE standard overcast sky conditions, which do not represent reality on a yearly basis. For that reason, with the development of CBDM and within the scope of the current thesis, DF is considered rather obsolete as a metric for daylight performance assessment.

Daylight Autonomy (DA) is an index that expresses the percentage of occupied hours when a minimum illuminance threshold (usually 300 lx or 500 lx) is met by sole daylight at a certain point of the sensor grid. To make DA a single-value metric for a room, $sDA_{300/50\%}$ was introduced to represent the percentage of points of the analyzed area which meets or exceeds the horizontal illuminance threshold (300 lx) for at least 50% of the occupied hours over a Typical Meteorological Year (TMY). According to the committee of Illuminating Engineering Society (IES), a preferred minimum percentage of 75% of floor area for $sDA_{300/50\%}$ is recommended (Wagdy & Fathy, 2015).

Useful Daylight Illuminance (UDI) is another climate-based daylight metric that demonstrates the percentage of occupied hours where the illuminance level falls into certain ranges. It is calculated at each sensor point and then it can be averaged over the plane. According to Mardaljevic et al. (2012), achieved UDI is defined as the annual occurrence of daylight illuminances that are between 100 lx and 3000 lx. The UDI range is further subdivided into two ranges called UDI-supplementary and UDI-autonomous. The former corresponds to illuminance levels between 100 lx and 300 lx and indicates that additional electric lighting may be needed to supplement daylight. The UDI-autonomous gives the occurrence of daylight illuminances in the range of 300 lx to 3000 lx, where additional electric lighting will most likely not be needed. For illuminance values above 3000 lx (UDI-exceeded), visual discomfort occurs due to excessive daylight. In older research studies, instead of 3000 lx, the upper limit for UDI was usually set equal to 2000 lx (Nabil & Mardaljevic, 2006). The decision on the upper UDI limit is left to the engineer's discretion.

NEN-EN 17037 (2018) gives recommendations for daylight sufficiency in an indoor space. For openings in the façade and for 50% of daylight hours, daylight design should achieve a target illuminance (TI) across 50% of the floor area and a minimum target illuminance (MTI) should be achieved across 95% of the area. Table 2.1 details the recommended illuminance limits. The three levels of recommendation for the TI values are employed by the current control strategy in the CCC for the three activity modes respectively.

Table 2.1: Recommendations of daylight provision by daylight openings in vertical and inclined surface (EN 17037).

Level of recommendation	TI (lx)	Fraction space for TI (lx)	MTI (lx)	Fraction of space for MTI (lx)	Fraction of daylight hours (%)
Minimum	300	50%	100	95%	50%
Medium	500	50%	300	95%	50%
High	750	50%	500	95%	50%

2.1.2. Disability and Discomfort Glare

Glare assessments are based on the calculation of Luminance (L) of a given light source seen from a given observation point. Luminance (L) is defined as the amount of light emitted or reflected by a surface at a given rate within a solid angle per square meter. To take into account the luminance contrast of objects in the visual field of an observer, most glare indices consider the luminance, the position and the solid angle of the glare source, as well as the background luminance as seen from the observer's position.

All those values can be calculated based on High Dynamic Range (HDR) images, which record the luminance field over an entire hemisphere by using a fish-eye lens. To assess glare, *Honeybee* in *Grasshopper* utilizes the software *Evalglare* as a *Radiance* tool. *Evalglare* analyses a 180° fish-eye HDR image, it calculates the location and luminance of each pixel and it subsequently computes crucial values such as the luminance, position and solid angle of a glare source (Suk & Schiler, 2013). Based on them, *Evalglare* returns various glare indices, some of which will be discussed in the following paragraphs. It can be concluded from the above information that, as a general rule, glare metrics are view-dependent.

Daylight Glare Index (DGI) can predict glare provoked by large sources, such as windows. The fact that it refers only to uniform light sources, makes it an inappropriate glare index when direct sunlight is in the field of the observer's view. In addition, DGI is not reliable when source illuminance has values close to the background illuminance.

Unified Glare Rating (UGR) is a metric used to evaluate glare risks from small sources, thus electric luminaires. Usually, glare indices for electric lighting are not useful for spaces with high transparency percentages, where daylight is the main glare source. By applying a regression coefficient of 3.2×10^{-2} to the original UGR equation, Hirning, Isoardi, and Cowling (2014) recommended Unified Glare Probability (UGP) as a metric to predict glare probability in a more robust way for both natural and electric lighting systems. The index identifies a glare source when its luminance is 5 times larger than the average luminance in the field of view.

Daylight Glare Probability (DGP) was proposed and evaluated by Wienold and Christoffersen (2006) as a glare metric highly correlated with users' response. DGP expresses the percentage of occupants that would be disturbed by discomfort glare for a given scene and it is valid for values between 0.2-0.8 and for vertical eye illuminance ($E_{v,eye}$) above 380 lx. Contrary to the above-described indices that focus only on the contrast effect, DGP equation consists of two terms; the first one evaluates the level of illuminance perceived by the observer ($E_{v,eye}$), while the second term represents the contrast ratio between the background average luminance and the glare source luminance. This fact makes DGP a robust index for glare assessment, as multiple studies have proven (Jakubiec & Reinhart, 2012b; Suk & Schiler, 2013).

To improve the costly computational behavior of DGP as an image-dependent index, the simplified DGP (DGPs) was proposed by Wienold (2009). The calculation of DGPs does not require HDR image assessment and is based only on the saturation effect, i.e. the amount of light perceived by the observer's eye ($E_{v,eye}$). Although fast calculations are a relieving feature of DGPs, its accuracy is low when glare sources are in the field of view, i.e. when direct sunlight or specular reflections fall onto the observer's eyes (Konstantzos, Tzempelikos, & Chan, 2015). In order to maintain a short computational time, but also take into account glare sources in the field of the observer's view, Wienold (2009) introduced enhanced simplified DGP (eDGPs). This glare metric is based on vertical eye illuminance ($E_{v,eye}$) and simplified images, and it allows for a comprehensive analysis of yearly data, requiring much smaller computational effort than using DGP.

According to Wienold et al. (2019) and Mardaljevic et al. (2012), the cut-off values for the above metrics that represent the limits between the four Daylight Glare Comfort Classes (DGCC), are the ones given in Table 2.2.

Table 2.2: Cut-off values for the glare metrics presented in the literature review.

	Imperceptible –	Noticeable –	Disturbing –	Intolerable
DGI	19.0	19.9	22.4	
UGP	0.79	0.83	0.95	
DGP	0.35	0.40	0.45	

The glare categories are explained as follows:

- Imperceptible: glare is mostly not perceived.
- Noticeable: glare is perceived but mostly not disturbing.
- Disturbing: glare is perceived and often disturbing.
- Intolerable: glare is perceived and mostly intolerable.

All the above glare indices are view-dependent, meaning that a specific view is evaluated to determine glare risks. Nevertheless, when assessing glare probability for spaces with multiple windows or with uncertain users' view directions, a metric that can assess glare sources for all orientations around an observer's position would be a useful tool. Furthermore, a real-time glare-based control strategy requires the fast computation of glare metrics, which is not met when employing image-dependent indices.

These problems are resolved by cylindrical illuminance (E_{cyl}) that was initially proposed by Hewitt, Bridgers, and Simons (1965). Cylindrical illuminance (E_{cyl}) is defined as the total luminous flux falling on the curved surface of a very small cylinder located at a specified point, divided by the curved surface area of the cylinder (Duff, 2012). It represents the average of all vertical illuminances in all directions around a considered point. Adequate level of mean E_{cyl} at eye level in the activity space (at least 50 lx in general, or 150 lx for spaces where visual communication is important) means sufficient illumination to highlight objects, reveal texture and good integration of daylight with electric lighting. Of course, these minimum limits are easily exceeded in spaces with high transparency ratios. Apart from visual recognition of the surrounding space, E_{cyl} can be used for view-independent glare assessments. Torres and Lo Verso (2015) proved that E_{cyl} can predict glare accurately and agree with DGP evaluations, after correlating the two indices. The fact that E_{cyl} does not entail the evaluation of an HDR image, saves computational effort and time. In addition to the aforementioned benefits, by using E_{cyl} for

glare evaluation, daylight is integrated effectively with electric lighting (Nassar et al., 2003). Those advantages encourage the use of E_{cyl} in the proposed control strategy of the thesis.

2.1.3. Comparison of Indices

By checking the correlation between the various indices, conclusions can be drawn about their accuracy and applicability. As regards glare, DGI and UGR are overall in agreement, although they are not reliable when direct sunlight enters the space (Hirning, Isoardi, & Cowling, 2014; Jakubiec & Reinhart, 2012b). Wienold et al. (2019) noted that those indices, which are based only on the contrast effect, have the lowest performance and robustness in comparison to other indices, especially when dealing with large-sized glare sources (i.e. windows), where contrast is essentially low.

On the contrary, vertical eye illuminance ($E_{v,eye}$), which is based only on the saturation effect, performs better than contrast-based metrics, although it cannot be totally reliable in dim environments (Wienold et al., 2019). This raises concerns about the performance of E_{cyl} in the CCC, where the dark ceiling and floor, create noticeable contrast to windows (i.e. bright light sources) and the feeling of a dim environment. Thus, its effectiveness should be carefully investigated in the present thesis.

Multiple studies that tackled small office rooms or classrooms with occupant's position adjacent to the window, proved the high reliability and robustness of DGP (Wienold et al., 2019). However, Hirning, Isoardi, and Cowling (2014) who studied open plan spaces, showed a bad correlation of DGP to discomfort, probably due to the large number of windows. This makes the appropriateness of DGP in buildings with fully glazed facades generally doubtful.

Furthermore, the relation between DGP and indices that evaluate the amount of daylight in space was tested by Konstantzos and Tzempelikos (2014), who showed that there is a fair correlation between DGP and workplane illuminance (E_{wp}). This statement was verified also by Mardaljevic et al. (2012), who compared the discomfort assessments of DGP and UDI and concluded that there is a good relation between them. It should be clear that this information does not encourage the researchers to rely solely on E_{wp} for glare evaluation, but it shows the correlation between a discomfort index and a design factor, that can be used complementary to achieve a visually comfortable environment.

Finally, Konstantzos and Tzempelikos (2014) revealed that DGP is mostly dominated by the vertical illuminance term, especially when there is no significant contrast effect. Besides, this can be justified by the definition of DGP. This constitutes an encouraging hint to use E_{cyl} as a reliable view-independent index based on the average vertical illuminance at the eye level, although more tests should be done.

2.2. Control Strategies for Shading Systems

Keeping a balance between occupants' comfort and energy savings is a challenging task. For this reason, multiple studies have been conducted, proposing various automatic control strategies for shading systems and electric lighting, and testing their effectiveness regarding indoor visual comfort and energy demands.

The most commonplace control strategy of a shading device is based on the calculation of outdoor illuminance or irradiance, either vertically on the façade or horizontally on the roof. When the value of outdoor illuminance is above a certain threshold, the blinds close completely. This is a rule-based technique, implemented in most of the buildings that use smart control systems. Of course, this control system is not always effective in relation to occupants' current needs for shading, daylight and outdoor view. In addition, it isn't environmentally sustainable, as totally closing the shades for long intervals during the day results in high energy demands for electric lighting and heating.

The above-described technique is usually combined with the cut-off angle method, the most typical manner to prevent glare when using Venetian blinds. This is a geometrical control strategy, according to which, the lamellas of the blinds are rotated to a certain angle, so as to block direct solar beams passing through the envelope (Bueno et al., 2015; Chan & Tzempelikos, 2013; Eltaweel & Su, 2017; Zhang

& Birru, 2012). Nevertheless, Chan and Tzempelikos (2013) argued that the cut-off angle is not always effective either for specular or diffuse Venetian blinds, as it may create a second reflection between the slats, that leads reflected solar beams into the room and may cause glare. To resolve this issue, they proposed the rotation of lamellas perpendicularly to direct solar rays, which block a significant amount of daylight, resulting in zero glare risks, but also low indoor illuminance levels.

Furthermore, Chan and Tzempelikos (2013) suggested that the slats' reflecting ability may be used by redirecting solar radiation deeper into the space and away from the occupants' positions. A similar approach was adopted by Eltaweel and Su (2017) who presented the Heliotropic response of slats. According to this, the reflecting side of the lamellas follows parametrically the sun position and redirects the solar radiation toward the ceiling of the room. In this way, as much as possible daylight is used to ensure a good illuminance distribution in the room. However, although this control strategy is efficient in side-lit rooms, where reflective surfaces, such as white walls and ceiling, can re-diffuse the light to the back of the room, it could not work in buildings with totally glazed facades and dark ceilings.

In lieu of a geometrical control of Venetian blinds, a rule-based strategy steered by metrics describing indoor conditions, can be generally implemented. In this case, the desired visual conditions can be achieved by operating blinds in a way that ensures certain values of daylight and glare indices in the indoor space. The thresholds of daylight metrics used in a control system, may be defined as fixed set-points by the designer of the algorithm. To determine the trigger metrics' limits for a certain building, either literature research is done, or experiments are executed to discover the set-points that achieve better visual comfort for the occupants (Le et al., 2022; Lee, Cho, & Jo, 2021; Naderi et al., 2020; Nagy et al., 2015; Xiong et al., 2019; Yao, 2014). However, thanks to machine learning, the metrics' thresholds may be gradually adjusted to users' wishes, making the control strategy more efficient and satisfying towards the occupants' preferences. This requires standard occupancy temporal and spatial patterns, which usually concern offices or classrooms (Guillemin & Morel, 2001; Gunay et al., 2014; Gunay et al., 2017). On the contrary, in event spaces, where the occupancy pattern of a room is uncertain and the users are not able to freely override automatic changes of blinds and electric lighting, artificially intelligent adjustments of those set-points cannot be applied.

Many different control strategies based on daylight metrics and sun position have been studied over the years trying to identify their strengths and weaknesses. Some of them are of interest to the present research and will be broadly discussed below. However, it is worth mentioning that the conclusions drawn from these studies correspond to specific rooms with certain location, orientation, geometry and occupancy. Thus, their scientific approach cannot be followed blindfolded in the case of the CCC and similarly complex buildings.

A way to control indoor conditions is by implementing the DELTA blind controller, proposed by Guillemin and Morel (2001), which follows a similar approach as the one currently implemented in the CCC. More specifically, this system consists of two control modes depending on user presence or absence. When the building is occupied, the priority of the controller is to define the maximum blinds aperture that prevents glare and maximizes the indoor illuminance levels above a user-defined set-point. In the zero occupancy case, the algorithm takes action to minimize energy consumption for heating or cooling. Generally, such glare-based control strategies are coupled with an electric lighting control system that is switched on to contribute to desired indoor illuminance in case of daylight insufficiency when the users are present (Guillemin & Morel, 2001; Le et al., 2022; Nagy et al., 2015; Xiong & Tzempelikos, 2016). Guillemin and Morel (2001) concluded that this kind of blinds' controller provides a high comfort level for both lighting and thermal aspects and gives at the same time very good results concerning energy consumption.

An effective shading control system was proposed by Konstantzos, Tzempelikos, and Chan (2015), who argued that the blinds should move to a position that hinders direct solar beams from falling on the workplane and simultaneously prevents excessive illuminances ($E_{wp} > 2000$ lx) at the desk level. This shading control seemed to protect users from glare most of the time, while maintaining satisfactory illuminance levels. However, such control strategies, that depend on the location of the workplane, cannot be easily applied in workshop and conference rooms, like the CCC, where the desks are not

placed at certain locations.

Another advanced rule-based control method for Venetian blinds was demonstrated by Chan and Tzempelikos (2013). Based on the configuration of the space and the fenestration system, DGP thresholds can be correlated with the corresponding values of transmitted illuminance. The control system consists of a bimodal (on/off) blind operation. When the transmitted illuminance exceeds the illuminance set-point, DGP values would be unacceptable (>0.35) for the vast majority of working hours, resulting in glare risks, so the blinds would rotate to the "off" position. Otherwise, the slats remain horizontal to allow daylight transmission and outdoor view ("on" position). The tilt angle of the "off" position is the one that ensures that the percentage of occupied time with DGP>0.35, is less than 5%. The study concluded that this method is efficient in providing high DA values without the risk of glare.

Later, Xiong and Tzempelikos (2016) tested three control criteria to ensure visual comfort in office spaces. In the first control strategy, DGP should be below 0.35, in the second one vertical illuminance at the eye level ($E_{v,eye}$) should not exceed 2500 lx, while in the third strategy the average workplane illuminance (E_{wp}) should be less than 2000 lx. In all cases, E_{wp} had to be more than 500 lx; in case sole daylight cannot achieve this limit, the lights are switched on at their appropriate intensity. The results of the study showed that the DGP-based and $E_{v,eye}$-based control systems had similar efficiency regarding glare, but they were stricter for E_{wp}. On the other hand, the E_{wp}-based controller led to high values of DGP and $E_{v,eye}$, generating high glare risks.

An interesting approach to identify time-varying glare conditions in large spaces with many possible user positions was proposed by Giovannini et al. (2020), who presented GLANCE (GLare ANnual Classes Evaluation). This method is based on the calculation of $E_{v,eye}$ values for many viewpoints and their comparison to $E_{v,eye}$ thresholds defined after correlating $E_{v,eye}$ with DGP. In this manner, each viewpoint is characterized by a certain Daylight Glare Comfort Class (DGCC). Although this technique is promising, it is not applicable to CFS yet, and it concerns only cases where all occupants have the same view orientation.

Recently, Lee, Cho, and Jo (2021) followed a stepwise method of shading control: first, the control algorithm determines the blind states that prevent glare; from them, the algorithm chooses the states that lead to low primary energy usage; finally, from the states defined in the second step, the controller determines the blind position that results in the highest indoor illuminance. The glare control of the first step is based on two simultaneous criteria; glare occurs when the external vertical irradiance is higher than 50 W/m^2 and the solar altitude is less than a certain profile angle that depends on the room's geometry. This study proved that energy savings and visual comfort achieved by an automatic control system depend on the priority given to its objectives.

Finally, Wang, Weibin, and Wang (2022) used multiple daylight and glare metrics, as well as energy ones to ensure visual and thermal comfort in a space. These metrics acted as objectives of a multi-objective optimization tool that aimed to find the optimal fenestration configuration for maximum visual comfort and minimum energy demand. A similar approach was followed by Čongradac et al. (2012) and Mahdavi (2008). The latter proposed a trained algorithm, which tests a set of candidate blind and lighting states in each time-step and decides the blinds position and luminaires' dimming levels for the subsequent time-step. The final decision is taken by a single-objective optimization algorithm that aims to minimize energy usage and the deviation of indoor illuminance from the desired value.

The determination of optimal shading states and electric lighting levels entails the use of optimization algorithms that check a wide range of possible solutions by performing iterative daylight analyses, so as to identify the optimal solution for a specific moment. In such complex problems, the relation between the variables and the objective is not defined as a formula, but as a parametric model with numerical simulations, and therefore the shape of the objective function is initially unknown. These cases can be tackled using black-box (or derivative-free) optimization methods. Global black-box optimization techniques do not require mathematical formulations of optimization problems and, contrary to local optimization methods, they do not get stuck to local optima, but instead consider the whole design space. There are three types of global black-box optimization algorithms: metaheuristics, direct

search and model-based (Wortmann, 2017). Figure 2.1 summarizes their main characteristics.

Metaheuristic algorithms, such as genetic algorithms, are stochastic, inspired by genetic evolution. They are time-consuming since they have to iterate multiple simulations in order to formulate the fitness landscape. With this kind of algorithm, there is little guarantee that the optimum will be discovered. Despite their drawbacks, metaheuristics algorithms are the most popular optimization method in the engineering society as they can be easily implemented, being applicable to a wide variety of optimization problems (Talbi, 2009; Wortmann et al., 2017).

Direct algorithms follow a deterministic process when they search for a new solution. They do not try to approximate the design space, but they investigate the original simulation-based model to determine the fitness landscape. Direct algorithms offer a high guarantee for finding the optimal objective. This implies that the algorithm always ends up at the same optimal solution, if it runs for a long time. However, direct optimizations' effectiveness is limited to low-dimensional problems, with no more than 20 variables (Wortmann, 2017; Jones, 2001).

Model-based optimizations approximate the design space, by constructing surrogate models of the implicit mathematical relations of the simulation-based models. Surrogate models demand shorter computational time than simulations and hence they can accelerate the optimization process. Practically, the algorithm checks various possible designs and based on them it tries to approximate the shape of the fitness landscape. Every time the algorithm executes a new calculation, it improves the fitness landscape, by gradually building and refining the surrogate model. Consequently, the model-based algorithm improves its model's accuracy during the optimization process. This technique saves significant computational time, as the algorithm creates the fitness landscape with only a few iterations, without exhaustively repeating the time-intensive simulations. In other words, model-based optimization methods find robust results within a small number of evaluations. The high speed of convergence is important for sustainable design problems regarding daylighting and building energy, where a single simulation takes several minutes to complete. To construct the surrogate model, global model-based algorithms follow either a statistical (e.g. Polynomial regression) or a machine-learning approach (e.g. Radial Basis Functions). Due to their ability to model complex design spaces, Radial Basis Functions are particularly suitable for architectural simulation-based problems. Although the algorithm requires additional calculations to gradually build the surrogate model, the needed time is eventually negligible in comparison to the simulations' computational cost. The model-based algorithms are stochastic or deterministic and have a good potential to find the optimal result (Wortmann, 2017; Forrester, Sobester, & Keane, 2008).

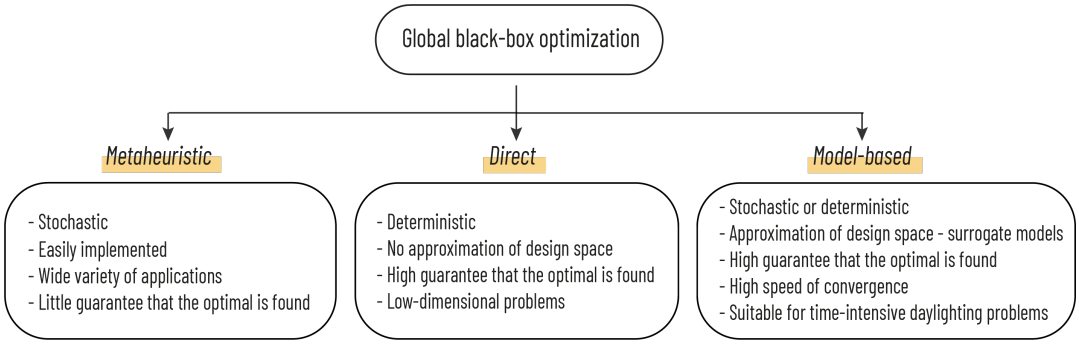

Figure 2.1: Global black-box optimization methods and their main characteristics.

2.3. Daylight Simulations

The need for accurate simulation of annual weather conditions to determine the amount of daylight penetrating the envelope of a building led to the development of Climate-Based Daylight Modelling (CBDM), which was first proposed by Mardaljevic (2000). CBDM concerns year-round daylight simulations based on real sun and sky conditions derived from standard meteorological datasets (Mardaljevic,

2006).

The most widespread lighting simulation engine is *Radiance*, which provided the basis for CBDM development since the 1990s (Mardaljevic, 1995). *Radiance* is an open-source suite of commands that can be used in custom scripts or can be embedded in several other building simulation software (e.g. *Honeybee*), which often provide a graphic interface to it. Based on the sky luminance distribution, the scene (geometry, landscape, materials) and the area of interest (viewpoints, sensor grids), *Radiance* simulates the redistribution of light in space by sending random rays from a point towards a light source (sun, sky), while keeping track of which of these rays reach it and how many reflections (ambient bounces) are needed. This process is called backward ray-tracing (Jakubiec & Reinhart, 2012a).

There are multiple methods of *Radiance*-based CBDM simulations, namely the 4-component method, DAYSIM, the 2-phase method, the 3-phase method, the 4-phase method, the 5-phase method and the 6-phase method. The adequacy of each simulation technique is dependent on the scope of the simulation, the used daylight metrics and the computational settings.

Figure 2.2 demonstrates how the programs used in the thesis interconnect and work. *Rhino 3D* contains all geometrical information of a model and acts as a visualization tool for analyses results produced by *Grasshopper*. The latter is a parametric software that allows the creation of adjustable models dependent on the imported variables. *Grasshopper* can execute daylight and energy simulations, thanks to the plug-in *Ladybug* - *Honeybee*. *Ladybug* imports standard *EnergyPlus* Weather (EPW) files into *Grasshopper* and provides a variety of 3D interactive graphics for better visualization of the calculations. The EPW file contains weather data of a Typical Meteorological Year (TMY) for different geographical locations. The weather data include hourly values of Direct Normal Irradiation (DNI) and Diffuse Horizontal Irradiation (DHI), which are used to characterize the sky conditions in terms of luminance distribution (i.e. the amount of light emitted by the sky) over the sky hemisphere, hour by hour, for a full year. The Perez All-Weather sky model generates continuous luminance distributions that represent the most likely sky conditions given direct and diffuse irradiation values (Subramaniam, 2017).

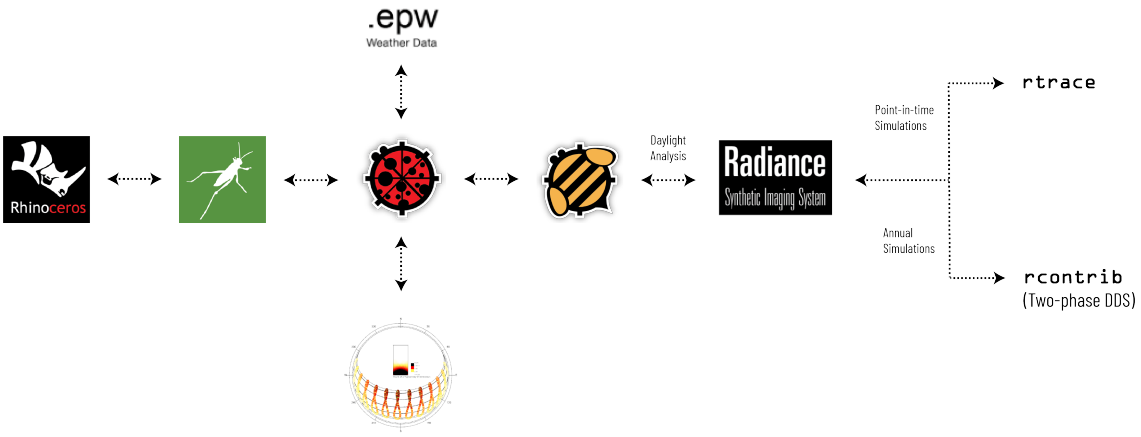

Figure 2.2: Interconnections between the software used in the present thesis.

Honeybee allows for daylight simulations in the parametric environment of *Grasshopper* via *Radiance*. In its latest version, *Honeybee* employs the *Radiance rtrace* command for instantaneous (point-in-time) daylight simulations. With this command, the illuminance distribution over the surfaces is continuous, because the illuminance values of neighboring ambient points are interpolated. The results of these point-in-time simulations are smooth renderings with a realistic impression of illuminance distribution.

On the contrary, when executing annual analyses or analyses for a period with dynamic sky conditions, *Honeybee* implements a modified version of the 2-phase method, which is called 2-phase DDS (Subramaniam, 2017). The 2-phase method does not use *rtrace*, but instead, it employs the *rcontrib* command. Then, the sky hemisphere is divided into luminous patches. A luminance value is assigned

to each sky patch for every time-step of the analysis period. With the regular 2-phase method, the sun luminance is assigned to the three sky patches closest to the actual sun position and the sky subdivision can have a variable resolution, by subdividing each segment into smaller parts. It should be noted that the higher degree of sky discretization, the longer the simulation runtime, but the higher the accuracy of the calculations. When using *rcontrib*, the illuminance between adjacent sampling points is not interpolated (i.e. -aa 0, -as 0, -ar 0), leading to noisy render images. The zero ambient interpolation aims at the prevention of sampling errors, while the ray-tracing relies on the number of ambient divisions (-ad), which should be high enough to secure accurate results (Brembilla et al., 2017; Brembilla, Hopfe, & Mardaljevic, 2018).

When using the 2-phase method, the program generates two matrices, one for the Daylight Coefficient and one for the sky. In this case, the calculation of illuminance over a sensor grid for a certain time-step of the analyzed period, is expressed as the multiplication of two matrices, as shown in equation 2.1:

$$\mathbf{E} = \mathbf{C_{dc}} \times \mathbf{S} \tag{2.1}$$

In equation 2.1, $\mathbf{C_{dc}}$ represents the Daylight Coefficient matrix and $\mathbf{S}$ corresponds to the sky vector. For each time-step, the ray-tracing simulation computes how much of each sky patch a specific sensor point sees, and stores this information in the Daylight Coefficient matrix. The core principle behind Daylight Coefficients is that the daylight, directly or indirectly incident on a surface inside a room, can be accounted for by considering two independent factors: the sky luminance and the geometry and optical properties of the surrounding surfaces. The $\mathbf{C_{dc}}$ matrix has a number of rows equal to the amount of the sensor points and as many columns as the sky patches (i.e. $[N_{sensors} \times N_{skypatches}]$). The sky vector consists of luminance values equal to the number of sky segments (i.e $[N_{skypatches} \times 1]$). The resulting illuminance vector $\mathbf{E}$ contains the illuminance values of the grid points (i.e. $[N_{sensors} \times 1]$). In the end, for an annual analysis, the dimensions of the sky matrix are $[N_{skypatches} \times 8760]$, and hence the dimensions of the resulting illuminance matrix are $[N_{sensors} \times 8760]$. From this matrix, annual CBDM metrics are derived (Chapter 2.1).

Brembilla et al. (2019) have shown that the regular 2-phase method cannot represent realistically daylight patterns in a room, because it tends to average sunlight peaks passing through shading devices. Consequently, the 2-phase method usually shows a higher frequency of low-intensity sunlight instants. These inaccuracies are due to the representation of sun position with three sky patches instead of a point, which results in a great overestimation of the sun's size. Nevertheless, the 2-phase DDS method employed by *Honeybee* accomplishes representing direct sunlight better. This is because the modified version of the method "erases" the inaccurate sun position and replaces it with a point after recalculating the exact sun position.

Although the 2-phase DDS method is the default technique that *Honeybee* uses for annual simulations, the 3-phase method and the 5-phase method can also be implemented manually in Grasshopper. The 3-phase method was the first CBDM technique able to simulate Complex Fenestration Systems (CFS), by using Bi-directional Scattering Distribution Function (BSDF) materials. CFS refer to all non-specularly transmitting fenestration technology including layers that provide shading and layers that improve interior lighting (McNeil et al., 2013). A non-specular transmission occurs when an incident ray is redirected by CFS. Venetian blinds constitute one of the most commonplace CFS. BSDF is a computational tool that has been developed to accurately describe the optical properties and daylight performance of CFS.

With the 3-phase method, the light transport is divided into three stages: exterior transport, fenestration transmission (BSDF material) and interior transport. Despite its augmented accuracy and its ability to perform annual daylight simulations in an operationally acceptable time span, the 3-phase method tends to average incident light over large solid angles, losing the details of the blinds and the shadows and thus being unsuitable for precise representation of direct sunlight and glare evaluations (Brembilla et al., 2019). However, the 5-phase method enables simulations of CFS at a higher accuracy. More specifically, the 5-phase method uses the results of the 3-phase method and it recalculates the direct sunlight component in a more accurate way. Hence, the 5-phase method is a good tool to perform

daylight and glare simulations accurately for a time period (Brembilla, Hopfe, & Mardaljevic, 2018).

The light calculations are influenced by the simulation parameters, which are determined by the simulation user, based on the desired level of detail/accuracy, the simulation method and the daylight metrics employed for the analysis. The definitions of the main simulation parameters that are usually the most result-affecting are listed in Table 2.3 (Kharvari, 2020).

Table 2.3: *Radiance* ambient parameters for *rtrace*.

Parameter	Abbreviation	Definition	Higher accuracy
Ambient bounces	-ab	Maximum number of diffuse bounces computed by the indirect illuminance calculation.	Higher values
Ambient accuracy	-aa	Maximum error permitted in the calculation of indirect illuminance interpolation. A value of zero implies no interpolation.	Lower values
Ambient resolution	-ar	Distance between ambient calculations by determining the maximum density of ambient values used in interpolation.	Higher values
Ambient divisions	-ad	Number of initial sampling rays sent from each ambient point into the hemisphere to determine the indirect incident light. The error in Monte Carlo calculation of indirect illuminance will be inversely proportional to the square root of this number.	Higher values
Ambient super-samples	-as	Number of extra rays that will be used to sample areas in the divided hemisphere. Super-samples are applied only to the ambient divisions which show a significant change.	Higher values (at most one half of -ad)

Many studies propose frameworks to appropriately determine ambient parameters that secure the solidity of the computational output. Mardaljevic (2000) argued that -ab should be 4 or more, to ensure 10% accuracy of illuminance prediction. More recent studies have proposed specific values of ambient parameters for various simulation methods (Kharvari, 2020). However, these recommendations cannot be followed blindfolded, since they refer to very specific models with certain geometry, materials and simulation methods. Thus, the determination of ambient parameters' values should be done from scratch when implementing a daylight simulation for a particular model.

Finally, in order to correctly calibrate the model and acquire sound values of daylight metrics, attention should be paid when setting the input optical properties of the model's materials. Kharvari (2020) showed that a difference of 0.1 in reflectance factors can noticeably affect the simulation results. Hence, acquiring information from manufacturers or executing in-situ measurements under overcast sky conditions is recommended.

3

Methodology

This chapter describes the step-by-step methodology followed for the creation of a parametric model, based on which the optimized control strategy for Venetian blinds is deployed. First, the parametric model is constructed, setting the basis for the daylight and glare analyses performed by the control system. The accuracy of the model is ensured by performing iterative tests and simulations that calibrate the multiple parameters imported into the model. Subsequently, the correlation between DGP and E_{cyl}, the metric used for glare assessment in the control strategy, is explicitly presented. In the end, the decision-making algorithm is constructed and its effectiveness is then validated.

3.1. Initial modelling setup

The main part of the present research is modeling a parametric algorithm that will determine the optimal states of Venetian blinds and electric lighting usage throughout the year, based on glare assessment and daylight quantity. For this purpose, a valid and accurate model of the Co-Creation Center and its surroundings should be created in *Grasshopper*. The latter is chosen as the basic software, because it combines three beneficial characteristics. First, it is a parametric program, meaning that the script can adapt to different conditions when the input parameters change. Second, *Grasshopper* can be connected to *Radiance* through the plug-in *Honeybee*, having the ability to execute daylight simulations in its environment. In addition, it includes a wide variety of single and multi-objective optimization tools that can be easily employed for discovering optimal blinds' states. Finally, *Grasshopper* is equipped with a *Python* component, that allows for more complex programming conditions.

The first step in the development of the model is the determination of initial input elements, which can be modified to adjust it accordingly. The whole *Honeybee* model is dependent on these inputs, which can be divided into three categories; fixed parameters, sensor data and variables. The fixed parameters are standard inputs that do not change for a particular model. They are only modified to adjust the model to different cases. The fixed parameters are sub-divided into three sub-categories:

- Scene: It contains all information regarding the building's geometry, location and orientation, the electric lighting characteristics, the landscape and the materials' optical properties. As for the shading geometry, the designer should define:
  - the height of the facades,
  - the distance between the slats of the louvers,
  - the depth of the louvers,
  - the offset distance between the blinds and the facades,
  - the geometry of the louvers (curved or straight),
  - the radius of curvature of the louvers (in case of curved ones) and
  - the location of the blinds (internal or external).

  As regards the electric lighting, the user should import into the model:

  - the number of luminaires,
  - the luminous flux per luminaire and
  - the power per luminaire.

- Area of interest: This parameter is basically the viewpoints and the grids of virtual sensors used for various daylight and glare analyses. It is considered a fixed input, as it remains constant during the analyses.
- Space usage: It consists of three occupancy/activity scenarios, i.e. meeting, workshop and presentation. The designer can choose the one that suits better to their case study. The space usage is considered a fixed input, as it remains constant during the analyses.

The sensor data refer to the measurements of the weather station installed on the CCC's roof. The recorded irradiance measurements are inserted into the model to represent the sky conditions for the specific location and time instance.

Finally, the variables concern the increments of the blinds and the angles of the slats. These inputs are basically the variables that the control strategy determines for each time step. Hence, they are allowed to change and are represented by sliders in *Grasshopper*.

In the next sections, the procedure followed for the development of the control algorithm is described, divided into six main stages:

1. Geometrical model
2. *Honeybee* model
3. Calibration of the model
4. Correlation of E_{cyl} with DGP
5. Control strategy
6. Validation of the control strategy

3.2. Geometrical model

The geometrical model of the case-study building and its surroundings must be accurate. However, the level of detail should be carefully determined, so as to avoid exhaustively complicated simulations. The fact that the building's facades are fully glazed already increases the computational effort. The 3D *Rhino* model of the CCC and the surrounding landscape is provided with a high level of detail, containing the ground, surrounding buildings, trees and the canal. The geometry has to be simplified wherever the details would add computational time without significantly augmenting the accuracy of the calculations. In Figures 3.1 and 3.2, the original *Rhino* model and the simplified one are shown.

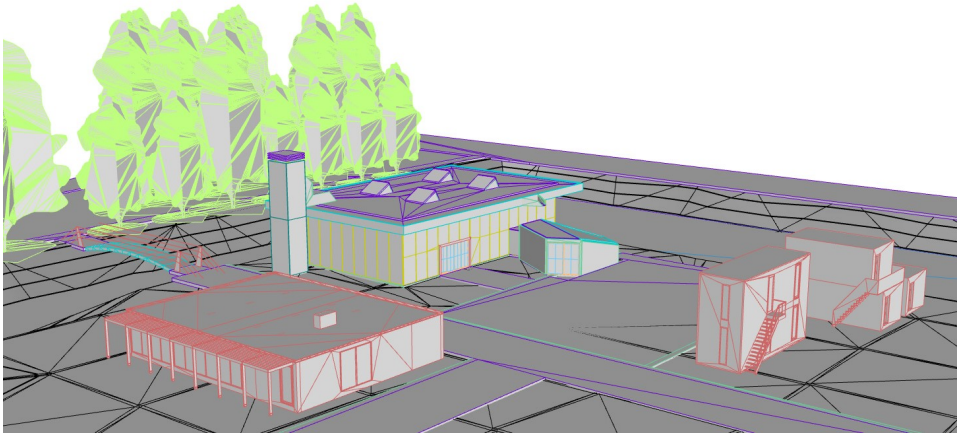

Figure 3.1: Original Rhino model of the CCC and its context, with a high level of detail.

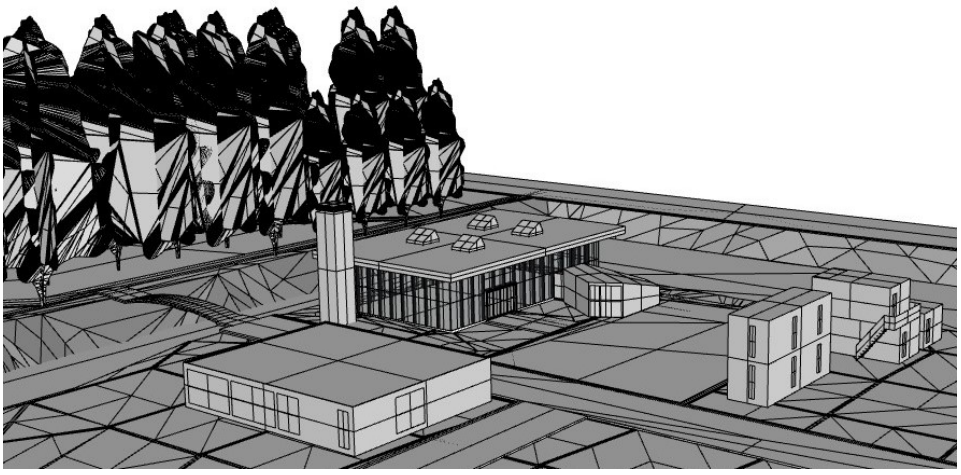

Figure 3.2: Simplified Rhino model of the CCC and its context, with a medium level of detail.

The various surfaces of the simplified *Rhino* model are inserted into *Grasshopper* as *Geometries*. It is worth mentioning that all meshes would better be converted from the beginning into surfaces, otherwise *Honeybee* would demand extra computational time in every run. The geometries inserted into the model are divided into two categories: the building in consideration (now the CCC) and its context/surroundings. The geometrical parameters of the CCC used as fixed inputs in its digital model are listed in Table 3.1.

Table 3.1: Geometrical input parameters for the case study.

Height of facades	5.20 m
Distance between blinds' louvers	0.07 m
Depth of louvers	0.08 m
Distance between blinds and facades	0.07 m
Geometry of louvers	Curved
Radius of curvature of louvers	0.12 m
Location of blinds	External

The most challenging part is the creation of the Venetian blinds' geometry that shade the facades of the building. The fact that the Venetian blinds may generally be curved or straight, makes the use of the default component *HB Louver Shades* inappropriate since the latter creates only straight louvers. Hence, the Venetian blinds for each orientation are manually modeled.

Generally, the windows of the facades may not have the same height. In the case study, the eastern and western facades include doors, which act as emergency exits and open towards the outside. Therefore, for security reasons, the doors are not covered by blinds, while only the windows above them are shaded by the blinds. The small windows (above the doors) have around half of the height of the facades.

The proposed control system aims to approach an as-independent-as-possible movement of the blinds for each facade, with the totally independent movement of the blinds of each window pane being the most advanced case (Figure 3.3). The blinds of each window are operated by two variables: one for the increment of the louvers and one for their angle. As regards the angle variable, the numbers range between -30° and 72° in steps of 2°. The movement of the blinds is simulated as a gradual reduction of the distance between them. The possible states of the blinds follow increments of 20%. To generate the 20% increment of blinds' movements, the distance between the slats is multiplied by a factor ranging from 0 to 1 in steps of 0.2. This constitutes the increment variable, with 0 representing blinds totally up and 1 representing blinds totally down. A special adjustment is applied to the increments of the short panels' blinds (above the doors), to make their movement "follow" the steps of the long blinds' movement.

In order to make the model easily adjustable to a building with a different number of glass panes, two *Gene Pools* (each consisting of 50 sliders) are used for the louvers' increments and angles of each façade. In this manner, depending on the number of windows of each façade, the algorithm is obliged to use only the sliders that correspond to the actual number of panels. For example, for the North façade of the CCC, which has 9 window panels, the algorithm uses only the 9 first sliders of each *Gene Pool*.

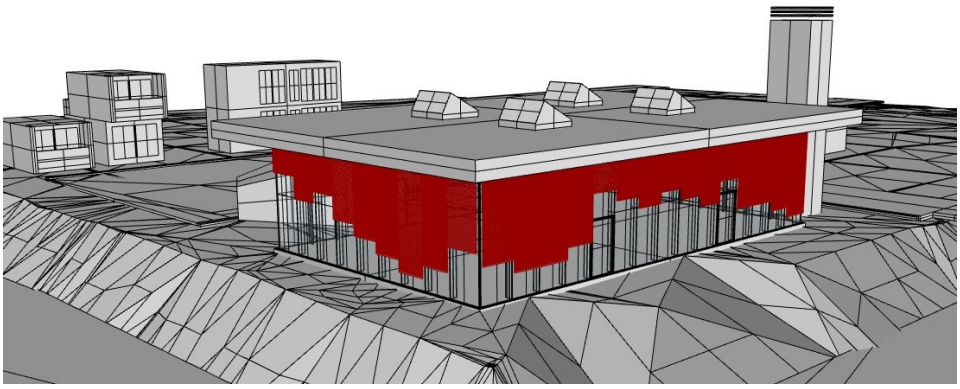

Figure 3.3: Geometry of Venetian blinds from the North-West view of the CCC, representing the highest degree of independence in the blinds' movement.

3.3. Honeybee model

The construction of the *Honeybee* model starts with converting the geometrical surfaces into *Honeybee* objects (*HB Aperture*, *HB Shade*, *HB Face*, *HB Door*). Then, the optical properties of those objects are determined. More specifically, the reflectance of opaque materials and the transmittance of transparent surfaces are set. Specularity and roughness are mainly used for visualization effects and setting them to values other than zero risks to slow down the simulation. In general, specularity and roughness values should be lower than 0.1 and 0.2 respectively. For the scope of this study, they are both set equal to zero.

In an attempt to import realistic transmittance and reflectance values into the model, the materials' properties were measured in the field, under overcast conditions. The in-situ measurements were performed using an illuminance meter and a luminance meter, assuming that all surfaces display Lambertian reflectance and hence are perfectly diffusing. The reflectance (ρ) of an opaque surface is calculated based on equation 3.1 after measuring its illuminance (E) and luminance (L). Table A.1 in the Appendix demonstrates the iterative measurements and calculations for various opaque materials in the CCC and its context. For each material, the average of the calculated reflectance values is used in the model.

$$\rho(\%) = \frac{L\pi}{E} \times 100 \tag{3.1}$$

The transmittance of the windows and the skylights in the CCC are given by the manufacturers (Saint-Gobain, 2019; Velux, 2022). However, the transmittance is lower most of the time due to dirt and dust on the glass. Table A.2 in the Appendix presents multiple measurements of the indoor and outdoor vertical illuminance values ($E_{v,in}$, $E_{v,out}$) for the window panes and the doors, which are used to calculate their transmittance (τ) as shown in equation 3.2. For each glazing, the average of the calculated transmittance values is used in the model. Since access to the skylights was difficult, the manufacturers' properties reduced by 15% are used.

$$\tau(\%) = \frac{E_{v,in}}{E_{v,out}} \times 100 \tag{3.2}$$

Eventually, Table 3.2 lists the surfaces of the building and its context, with the corresponding *Honeybee* objects and their optical properties as inserted into the model. In the end, all simulated objects of the building and the landscape are then incorporated into the total *Honeybee* model (Figure 3.4). This

procedure should be manually done by the designer, depending on the exact 3D model.

Regarding the materials listed in the table, it should be clear that the walls of the CCC are basically surfaces that extend to the four façades and are almost 100% covered by their transparent sub-surfaces (i.e. windows and doors). As a result, the remaining surfaces of the walls, which are not glass, are considered silicone around the panels. This silicone is a black matte material, which composes also the doors' frames and hence the walls and the frames have the same reflectance.

The roof of the CCC and the surrounding buildings have a finish of satin black steel that also covers the climate tower, with a measured reflectance value of 0.01. On the contrary, the roof of the Nonohouse consists of two opaque parts, one covered by glass and one by greenery. The glazed roof does not allow light entry and thus it is considered a surface with a typical glass reflectance of 0.10, whereas the green roof has a general reflectance value of 0.20 for grass. Furthermore, between the CCC and the Nonohouse, there is a corridor enclosed by two glazed walls and a glazed roof. Their transmittance is assumed the same as the doors of the CCC's facades.

Since the indoor conditions of the surrounding buildings are not under investigation, the transmittance of their windows is not useful for the present study on the CCC. Thus, the windows are simulated as apertures with a common outdoor reflectance of 0.10. According to the literature, a typical reflectance value for the ground, including concrete pavement and grass-covered areas, is around 0.20 (Brembilla, Hopfe, & Mardaljevic, 2018; Jakubiec, 2022). The average light reflectance for clear canal water is assumed equal to 0.5. Finally, the trees are simulated as transparent surfaces with an arbitrarily specified transmittance value of 0.10, indicating that only a small percentage of light passes through the leaves when the trees flourish.

Table 3.2: *Honeybee* objects and initial optical properties.

Geometrical surface	HB objects	Material	Reflectance	Transmittance
Building (Co-Creation Center)				
Walls	Face	Matte black material	0.03	-
Windows	Aperture	Glass	-	0.60
Doors	Door	Glass	-	0.80
Venetian blinds	Shade	Matte black material	0.04	-
Floor	Face	Carpet	0.03	-
Ceiling	Face	Acoustic ceiling	0.03	-
Skylights	Aperture	Glass	-	0.65
Roof/Overhang	Shade	Satin black steel	0.01	-
Columns/Fins	Face	Glass	-	0.60
Frames	Shade	Matte black material	0.03	-
Sill	Face	Light-colored metal	0.30	-
Context				
Dark-colored walls of surrounding buildings	Face	Wood	0.04	-
Light-colored walls of surrounding buildings	Face	Wood	0.08	-
Walls between CCC and Nonohouse	Face	Glass	-	0.80
Black roofs of surrounding buildings	Face	Satin black steel	0.01	-
Green roof of Nonohouse	Face	Greenery	0.20	-
Glass roof of Nonohouse	Face	Glass	0.10	-
Glass roof between CCC and Nonohouse	Face	Glass	-	0.80
Windows of surrounding buildings	Aperture	Glass	0.10	-
Ground	Face	Soil & Pavement	0.20	-
Canal	Face	Water	0.50	-
Plants	Face	Trees/Leaves	-	0.10
Climate tower	Shade	Satin black steel	0.01	-

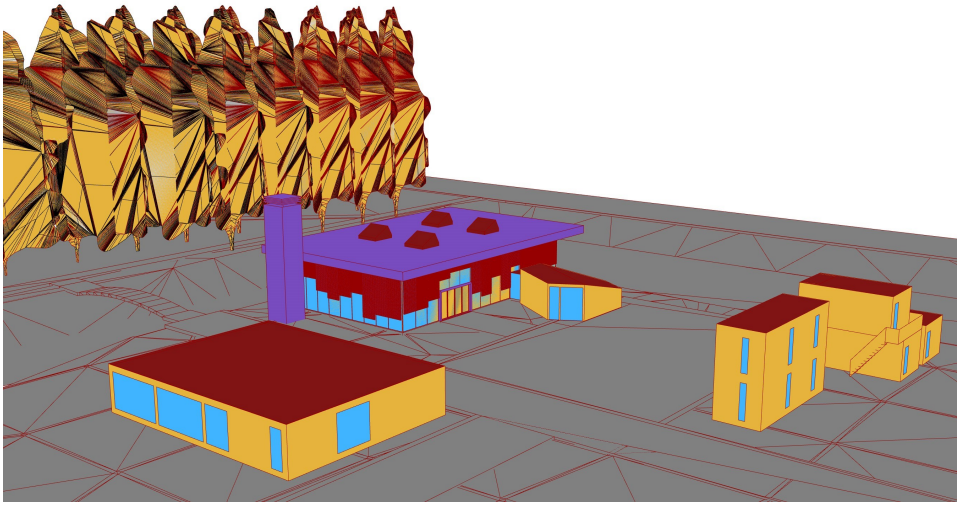

Figure 3.4: *Honeybee* model of the CCC and its context.

3.4. Calibration of the model

3.4.1. Calibration of ambient parameters

The accuracy of simulations' outputs is greatly dependent on the main *Radiance* ambient parameters, which are the ambient bounces (-ab), ambient accuracy (-aa), ambient resolution (-ar), ambient divisions (-ad) and ambient super-samples (-as). They are all described in detail in Chapter 2.3 (Table 2.3). In order to produce reliable results, high precision of calculations is desired. However, the higher the accuracy, the larger the computational effort and hence, the longer the runtime. To achieve a good balance between sufficient accuracy and reasonable computation runtime, the main simulation parameters of *Radiance* should be investigated and calibrated. The calibration of the rendering parameters entails an iterative simulation process for the identification of the most suitable set of ambient parameters. The iterations that need to be done consist of repeated instantaneous (point-in-time) simulations for a different set of *Radiance* parameters.

For Climate-Based Daylight Modelling (CBDM), the real weather conditions are imported into the algorithm. This is done by utilizing the Global Horizontal Irradiance (GHI) measured by the CCC's roof sensor and splitting it into Direct Normal Irradiance (DNI) and Diffuse Horizontal Irradiance (DHI) with the Skartveit model, which was proved to work adequately well. It should be noted that the sensor's measurements that are currently available for the case study refer to 2022, because this is the first complete year that the weather station has recorded. Although the roof sensor logs measurements every 5 minutes, the time series of GHI are inserted into the model in hourly time steps. In reality, if the control system was actually implemented at the CCC, real-time sensor measurements would be used.

The iterative point-in-time simulations for the calibration of *Radiance* parameters calculate the horizontal illuminance at the middle point of the workplane, at a height of 0.85 m above the floor ($E_{middle,wp}$). These simulations are executed for an overcast day, which is the worst-case scenario. Based on the measurements of the weather station on the CCC's roof, the instant that is chosen for the calibration is on 22.09.2022 at 9.00 am. The aim of the calibration is to find the rendering parameters that lead to a converged value of $E_{middle,wp}$. The convergence test consists of running multiple simulations and gradually increasing the "resolution" of the ray-tracing process by changing one parameter at a time. First, -ad and -as are determined, then -ar follows, subsequently -aa is chosen and finally -ab is defined. This process is followed twice, once with blinds up and once with blinds down and horizontal slats. The step-by-step procedure is shown in detail in Tables A.3 and A.4 of the Appendix.

3.4.2. Validation of sky model

In order to achieve a reliable and realistic control algorithm, the simulated sky and sun conditions should be validated, confirming their agreement with the actual weather conditions. The sky model is created after importing the GHI data recorded by the roof weather station and dividing it into DNI and DHI. These irradiance values, along with the corresponding month-day-hour data and geographic coordinates, are employed to create a custom luminance sky definition through the Perez Sky Model.

The validation of the simulated annual climatic conditions is performed by comparing the measurements of the four illuminance sensors mounted on the CCC's roof with the corresponding results of the calculations. A successful validation would arise if all relative Mean Bias Errors (rMBEs) were below 20%. It should be noted that one sensor is placed horizontally and looks upward, while the rest are positioned vertically and look towards East, South and West respectively (Figure 3.5).

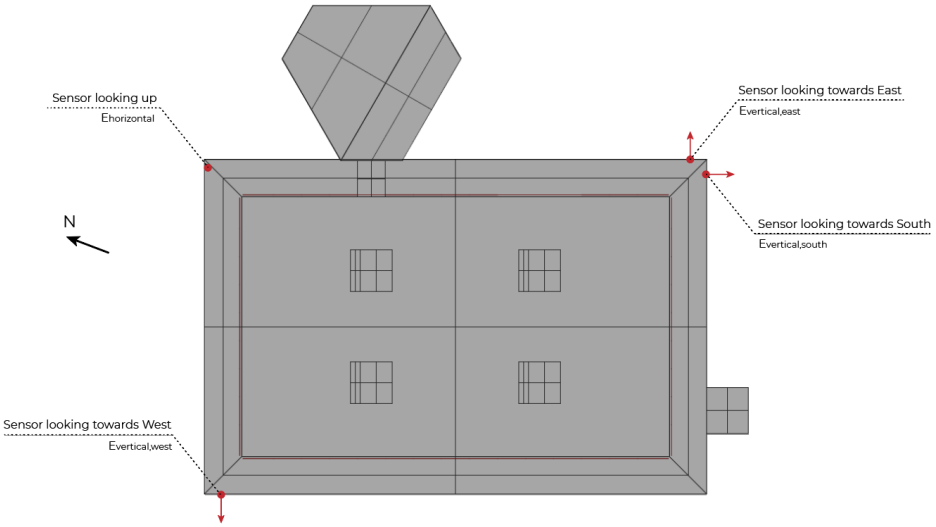

Figure 3.5: Scheme demonstrating the locations of the four roof sensors.

For the validation process, multiple point-in-time simulations are executed for the calculation of vertical and horizontal illuminance (E_v, E_{hor}) at the four virtual sensor points respectively. The simulations are performed for a week in winter under an overcast sky (19.12.2022 – 25.12.2022) and in summer under a clear sky (04.07.2022 – 10.07.2022) in hourly time steps.

3.4.3. Calibration of optical properties

Finally, the reliability of the model depends on the input material properties. The field measurements are a good starting point, but they depend on the exact environmental conditions during the time of the measurements. Moreover, many materials' characteristics were assumed, particularly for the landscape. Thus, the optical properties of the surfaces should be calibrated, aiming at increasing the model's accuracy, so as to properly represent reality. Of course, a 100% representation of reality cannot be accomplished, due to geometrical inaccuracies, unstable measurement conditions and multiple simulation parameters. However, calibrating the optical properties of the materials to make calculations correspond to measurements, is an important step to succeed in creating a precise model.

Calibration of context materials' properties

Firstly, the calibration of properties of the context materials is implemented. This concerns mainly the ground and the canal, as their reflectance could not be easily and accurately measured in the field. Additionally, the calibration process includes the specification of the deciduous trees' transmittance, with the gradual falling of leaves being simulated as a transmittance shift over the year.

For this purpose, multiple simulations for the calculation of vertical illuminance (E_v) at the three roof sensors (West, South and East) are executed, in order to compare the results with the measured val-

ues. This is done for an overcast day (24.12.2022) and a sunny day with high solar altitude (09.07.2022), in hourly time steps. To simulate the trees around the CCC more accurately, a sunny day with low solar altitude (02.10.2022) is also checked. The aim is to identify the optical properties of the ground, canal and trees that lead to an approximate maximum rMBE of 20% for all sensors for both overcast and clear-sky conditions. The properties of the remaining outdoor materials, which were obtained through field measurements, are considered reliable, and hence they remain stable. Besides, the calibration process shows that they do not influence significantly the results.

The calibration is executed manually by modifying initially the properties of one material at a time, so as to observe the influence the specific material has on the results. The extent to which the properties of each material are increased or reduced depends on the distance between the calculations and the measurements. Apart from identifying the impact of the changes on the results, we can notice any local effects, e.g. shadows from the trees on the western and eastern sensors. Then, various sets of the three materials' optical properties are tested to obtain sufficiently good results. Section A.2.2 in the Appendix explains explicitly the procedure followed for the calibration of the optical properties of the ground, the canal and the trees.

Calibration of building materials' properties

As demonstrated in Figure 3.6, the ceiling of the CCC is equipped with 9 sensors that calculate the horizontal illuminance at the ceiling ($E_{ceiling}$). After simulating the ceiling sensors at their exact locations, the optical characteristics of the CCC's surfaces can be adjusted, in order to approach the measured illuminance values at the ceiling. Each sensor is simulated as a small 3×3 grid of virtual sensors around it. The average $E_{ceiling}$ of each grid represents the calculated illuminance of the sensor.

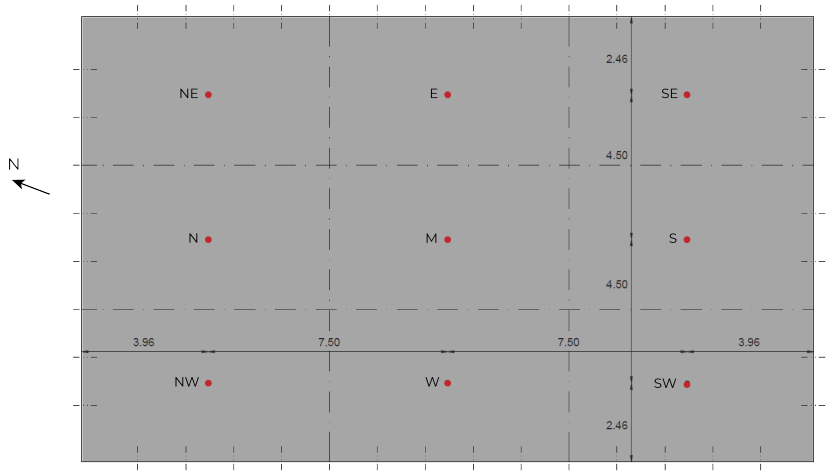

Figure 3.6: Scheme demonstrating the locations of the nine ceiling sensors.

The calibration process consists of iterative simulations performed for an overcast day (24.12.2022) and a sunny day with low solar altitude (02.10.2022) in hourly time steps. For those two days, the blinds' states decided by the current control system are inserted into the model. Since the two chosen days are weekend days, the building is not occupied, thus the blinds' movements are limited and the electric lighting is off. The aim is to identify the optical properties of the CCC's materials that lead to an approximate maximum rMBE of 30% for all sensors for both overcast and clear-sky conditions. To achieve this goal, small or large adjustments of the reflectance and transmittance values of various elements should be applied to the model.

As previously, the calibration process starts by manually modifying the properties of one material at a time, but mainly focusing on the most affecting surfaces, i.e. the facades, the floor and the ceiling. Subsequently, many combinations of various materials' optical properties are tested to obtain as close results as possible to the sensors' measurements. However, tweaking multiple optical parameters to simultaneously achieve the desired results of nine sensors for two test days is a challenging task. Section

A.2.2 in the Appendix explains how the iterative simulations were performed for the calibration of the optical properties.

3.5. Correlation of E_{cyl} with DGP

In the proposed control strategy, the metric employed for glare assessment is cylindrical illuminance (E_{cyl}), because it is capable of imageless and view-independent glare evaluation with low computational cost. However, the fact that E_{cyl} does not introduce cut-off values for the distinction of the four glare classes (imperceptible, noticeable, disturbing, intolerable) entails the need for determination of those thresholds after correlating E_{cyl} with DGP. The latter is chosen as a benchmark, since previous studies have shown that it can assess glare effects more reliably than other glare metrics in the CCC (Brembilla, 2022a). Besides, according to Torres and Lo Verso (2015), E_{cyl} can be a reliable glare index only after correlating it with another glare metric that works well in a certain space, meaning that this process should be done from scratch when the analyzed building changes. This ensures the trustfulness of E_{cyl} as a glare metric in the specific space. As only imperceptible glare is allowed in the proposed control strategy, the DGP threshold of 0.35 is used in order to find the respective value for E_{cyl}.

For the correlation of the two indices, the approach of Torres and Lo Verso (2015) is followed. The correlation process between the two indices commences with the selection of three test days with clear-sky conditions, various solar altitudes and different trees' sunlight transmittance. Thus, the chosen test days are 08.03.2022, 09.07.2022 and 02.10.2022. For those days and with an hourly time resolution, the glare inside the CCC is assessed under two facades' conditions; blinds fully raised and blinds fully lowered with horizontal slats. Consequently, the glare evaluation is performed for six cases in total. Then, a grid of nine viewpoints, evenly distributed in the space, is defined (Figure 3.7). For each of those points, vertical illuminance (E_v) is calculated in eight directions at the height of 1.20 m (eye level of a seated person) and the average value is used to compute E_{cyl}. Finally, hemispherical fish-eye images are produced in each of the eight directions and DGP is calculated from them. For each of the six cases explained above, the highest DGP value of each point for each daylit hour is compared with the corresponding E_{cyl} value. In this manner, a large sample of couples of values (E_{cyl}, DGP) is collected.

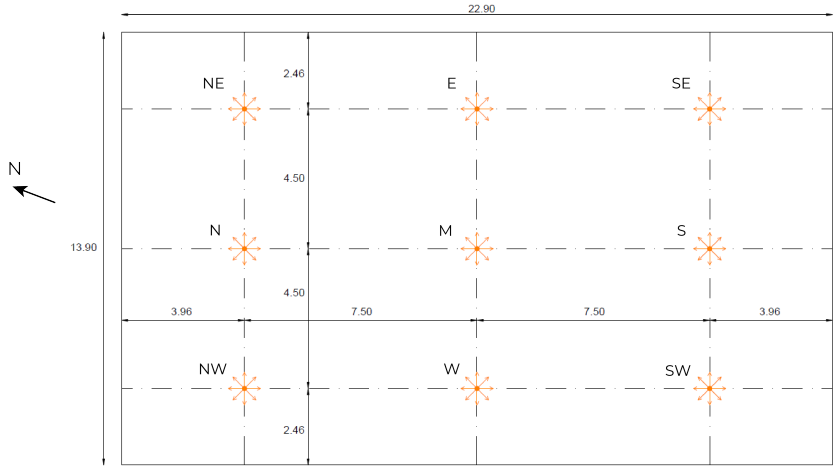

Figure 3.7: Grid of viewpoints where DGP and E_{cyl} are calculated for the correlation of the two indices.

The next step is the arbitrary determination of a certain threshold for E_{cyl}. For this value, the following check is implemented for each couple of E_{cyl} and DGP values:

- "True positive" (TP): DGP $>$ 0.35 and E_{cyl} over the chosen threshold. This proves a correspondence between DGP and E_{cyl} in identifying a glare condition.
- "True negative" (TN): DGP $<$ 0.35 and E_{cyl} below the chosen threshold. This proves a correspondence between DGP and E_{cyl} in identifying a non-glare condition.

- "False positive" (FP): DGP < 0.35 and E_{cyl} over the chosen threshold. This does not show a correspondence between DGP and E_{cyl}.
- "False negative" (FN): DGP > 0.35 and E_{cyl} below the chosen threshold. This does not show a correspondence between DGP and E_{cyl}.

This check is repeated for multiple optional thresholds of E_{cyl}. The value providing the highest percentage of TP and TN results, and hence the highest agreement with DGP, is chosen as the final threshold, below which only imperceptible glare occurs.

3.6. Control strategy

The proposed control strategy of the blinds for indoor visual comfort is steered by an optimization process, that leads to a theoretically ideal operation of the shading system. Within this thesis, instead of a rule-based control approach, an optimized one is developed, in order to identify its capabilities and limitations, as well as to give feedback for future research and improvements. Besides, rule-based operating systems are already thoroughly examined in an extensive list of research papers (Chapter 2.2). Contrary to rule-based techniques, nowadays, architectural design optimization (ADO) for solving design problems is gaining more and more ground and demands explicit research.

The optimization employed here is based on the Radial Basis Function Optimization (RBFOpt) algorithm, which can be performed by *Grasshopper*'s component *Opossum* (OPtimizatiOn Solver with SUrrogate Models). RBFOpt is a black-box model-based optimization method, which has the ability to find robust results within a small number of evaluations, rather than requiring an exhaustive search to find them, as already explained in Chapter 2.2. The Radial Basis Function model is continuously updated, identifying quickly promising areas of the design space (Wortmann, 2017). This constitutes a significant advantage in comparison to other optimization algorithms, especially in the complex case study of the CCC, and it justifies why it is chosen in the present study.

The aim of the optimized control system is the regulation of the amount of daylight entry, balanced by glare risks. The former is quantified by the average horizontal illuminance on the workplane (E_{wp}) calculated at a sensor grid 0.85 m above the floor and 1 m offset from the facade, whereas the latter are evaluated by the maximum value of cylindrical illuminance (E_{cyl}) between nine viewpoints (Figure 3.7). It should be clear that the priority of the control system is occupants' visual comfort avoiding glare, while the limitation of lighting energy consumption allowing large amounts of daylight entry is a subjacent goal.

As illustrated in Figure 3.8, the model characteristics are inserted into the control system as inputs. These inputs consist of the variables (blinds' increments and angles) and the fixed parameters, which include the sky conditions (sensor data) for a specific time step, the scene, the area of interest (sensor grid) and the space usage (workshop, meeting, presentation). The fixed inputs do not change during the optimization process. For a certain set of variables, the model calculates the average E_{wp} and the maximum E_{cyl} through point-in-time *Radiance* simulations. Based on these calculations, the optimization algorithm decides the optimal blinds' states that result in satisfactory values of E_{wp} and E_{cyl}. The optimization process is constrained by the limits of E_{wp} and E_{cyl}. In particular, to ensure an adequate quantity of light in the space, E_{wp} should be more than 300 lx, 500 lx and 750 lx for presentation, meeting and workshop respectively. At the same time, only imperceptible glare is allowed by employing the upper threshold of 1400 lx for E_{cyl}. This threshold was obtained by the results of the correlation between E_{cyl} with DGP, as can be seen in Chapter 4.2.

Setting E_{wp} and E_{cyl} as two objectives in the control algorithm requires the implementation of multi-objective optimization (MOO). However, having more than one objective tends to complicate exponentially the algorithm, while it produces a set of equally good solutions (Pareto front) and not the optimal one. This means that the designer is the one that manually decides the final solution, choosing among the best Pareto front ones. On the contrary, a control strategy should act automatically, defining the best solution by itself. After performing a MOO optimization, having E_{wp} and E_{cyl} as two objectives, it is proven that, in the vast majority of the cases, as daylight entry increases, the values of

E_{wp} and E_{cyl} increase as well (Tables A.13, A.14, A.15 in the Appendix). The fact that E_{wp} and E_{cyl} have overall similar trends as functions of the daylight quantity in the space, allows us to use only one of them as the objective of an SOO control algorithm.

In the case of meetings and workshops, the aim is to prevent glare, while maximizing the amount of daylight so as to achieve low energy demands for electric lighting. Those two targets are competing. Since visual comfort is prioritized and only imperceptible glare is allowed, the largest amount of daylight entry can be achieved only when E_{cyl} has a value close to 1400 lx, but still lower than this threshold. In this manner, noticeable glare is prevented, while the maximum possible E_{wp} is accomplished.

On the contrary, for the presentation scenario, apart from preventing glare, the aim is to allow for small amounts of daylight entry, enough to meet the 300 lx requirement. This is because, during a presentation, the light levels should be low, but sufficient to write down notes. In this case, the two targets are non-competing. The aim now is to minimize daylight entry until E_{wp} has a value close to 300 lx, but still higher than this limit. At the same time, a very low E_{cyl} value is accomplished ($<$ 1400 lx), ensuring zero glare risks.

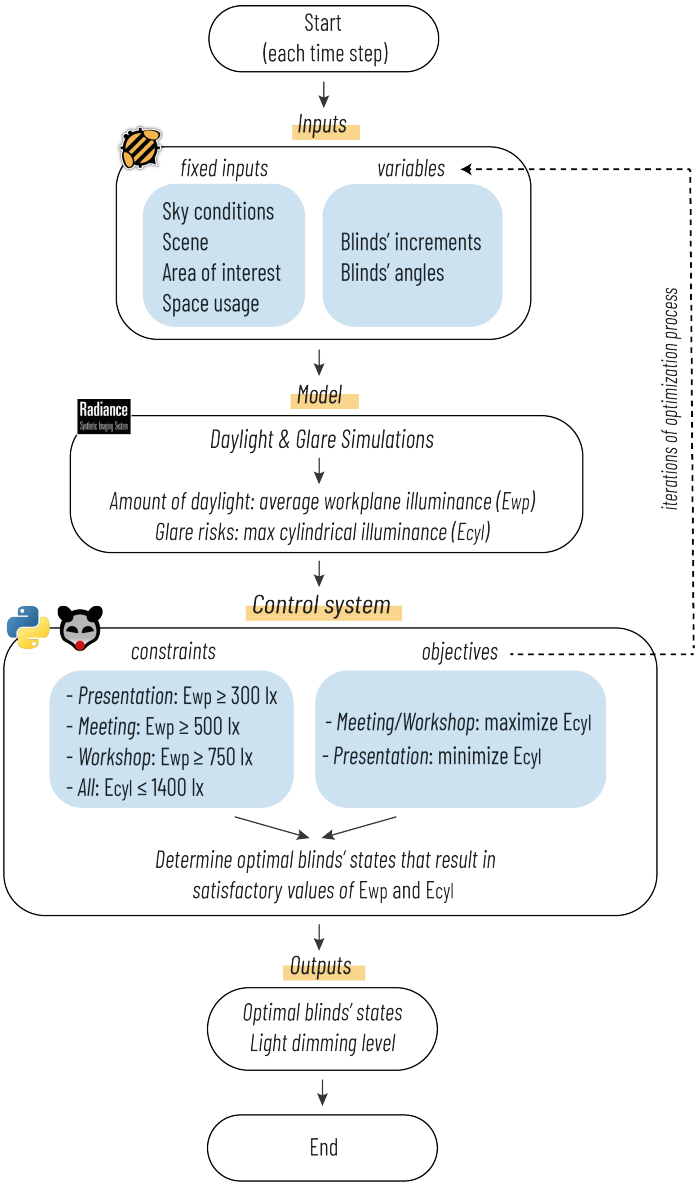

Figure 3.8: Flowchart of the developed control strategy.

After testing a large list of possible optimization algorithms, the one that outperforms is described by the objective function of Equation 3.3, where E_{cyl} is multiplied by a penalty factor. The calculation of the objective function is performed within a Python script in *Grasshopper* [1]. It should be mentioned that the multiple optimizations done to identify the most appropriate control algorithm, are tested for a sunny day with low solar altitude (02.10.22 at 10.00), which represents the worst-case scenario, as the low solar position is more likely to cause glare. Those initial optimizations were performed with the simplest operation of the shading system, where all blinds of each facade move simultaneously.

$$ObjectiveFunction = penalty \times E_{cyl} \tag{3.3}$$

During workshops and meetings, the control system tries to maximize the objective function, whereas during presentations its minimization is targeted. The penalty is derived from the optimization constraints and is applied to enforce the algorithm to find values for E_{wp} and E_{cyl} within their limits. The objective function is harder penalized when E_{cyl} is above 1400 lx, as glare prevention is prioritized.

For each time step, the optimization consists of a certain number of iterations specified by the designer, creating a loop in the process. The more the iterations, the better the results. In this way, it is more likely to find the optimal solution (blinds' states and corresponding values of E_{wp} and E_{cyl}). However, RBFOpt has a high convergence speed, which allows for a relatively small number of iterations per time step, saving computational time. Eventually, when the optimal blinds' states are determined, the algorithm decides the light dimming levels needed to supplement daylight, in case the average E_{wp} provided solely by daylight is not sufficient (Figure 3.8). Based on the dimming levels, the energy demand for electric lighting can be also calculated.

3.7. Validation of the control strategy

In order to validate the effectiveness of the proposed control model, its performance for the three activity modes is compared with the currently applied control system. The key performance indicators refer to:

- the amount of daylight in the space, expressed by the average E_{wp};
- the glare risks, evaluated by the maximum values of both E_{cyl} and DGP among the nine viewpoints, allowing to draw conclusions about the performance of E_{cyl} as a glare index;
- the quality of view towards the outdoors, quantified as the average percentage of the occupants' view that is not blocked by the context geometry (i.e. blinds). A person's view is defined as the 360° horizontal view band bounded on top and bottom by a 30° offset from the horizontal plane (human cone of vision);
- the energy demands for electric lighting (in kWh);
- the solar heat gains (in kWh), giving insight into the energy performance of the proposed control strategy, although the limitation of energy demands for heating/cooling was not included in its scope.

The view percentage is calculated in *Grasshopper* using the component *LB View Percent*. This analysis is done for a point grid distributed over the floorplan at the eye level of a seated person (1.20 m above the floor). The view percentage is calculated in 145 view directions for each grid point. Those 145 view vectors are evenly distributed in the space around a point. An average view percentage of 100% for a point would result from the case where all facades are unshaded, allowing a free view towards the outdoor environment. In the end, the average value of the view percentages over the point grid is utilized to quantify the overall view quality of the space for a time step.

The validation is initially done for a time period under sunny conditions and with relatively low sun altitudes, during which an event took place. This period represents the worst-case scenario and refers to 18.03.2022 between 10.00-16.00. Additionally, to obtain a more general overview of the control's actions, another interval with lower, but more fluctuating, GHI values is also tested. This time period refers to 24.10.2022 between 9.30-12.30 and includes varying weather conditions (cloudy and sunny sky), being useful to investigate how the control strategies respond to them. In Figure 3.9, the GHI, DNI,

[1] `https://github.com/pentheod/Optimized-control-strategy-CCC-TU-Delft`

DHI data are given for the two test periods.

The above test periods are considered representative of the control's daylight performance under sunny conditions and variable sky models. However, both of them belong to the heating season, meaning that high solar heat gains are desired. A more complete validation of the control would also include testing time periods in summer, during which the building was occupied. This would give the opportunity to observe the controls' energy performance also in the cooling season, when high solar heat gains are unwanted. Unfortunately, data limitations didn't provide information about the summer period, and hence it is excluded from the present validation.

As the current blinds' operation does not make a distinction between the three activity modes, there is no information about the exact type of activity that took place during those certain periods. Therefore, the results obtained by the three optimized controls (for the three modes respectively) will be compared with the corresponding results of the existing control, which is the same for the three cases. Since the current algorithm and its documentation are not available, its daylight, glare and energy calculations can be obtained by importing into the model the blinds' states resulting from the currently implemented system. A time step of 15 minutes is chosen for the comparison of the two control models, using the louvers' increments and tilt angles on the exact instant. With a time step of 15 minutes, we can assure that the system responds to weather changes, without causing a distraction to occupants.

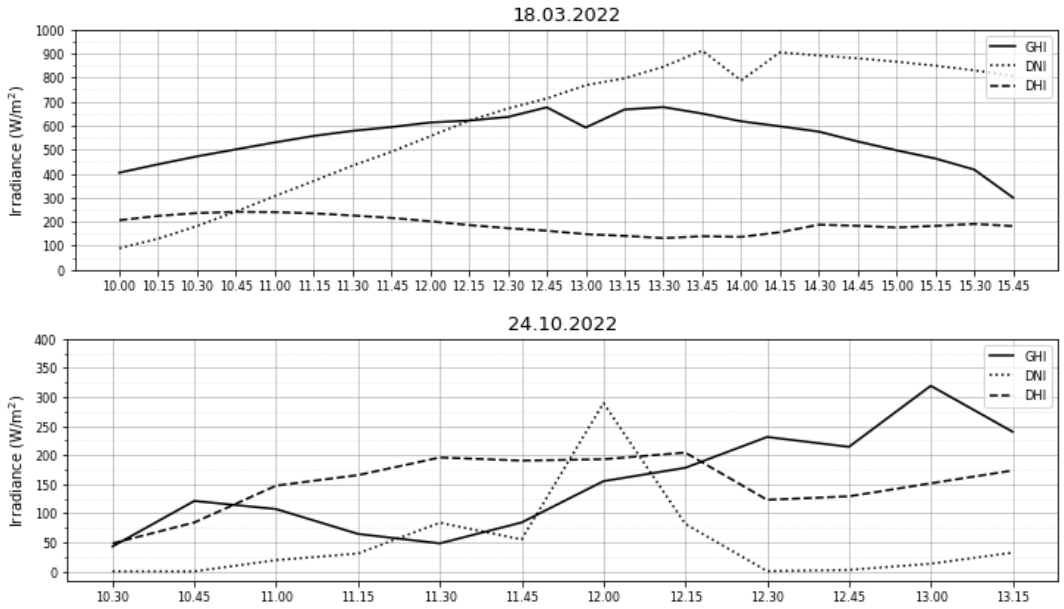

Figure 3.9: Global Horizontal Irradiance measured by the CCC's roof sensor, as well as the respective Direct and Diffuse Irradiance calculated through the Skartveit model for the two test periods.

4

Results

In this chapter, the results derived from the multiple analyses described in Chapter 3 are demonstrated and commented on. First, the results of the calibrations for the development of a valid model are given. Then, the upper threshold of E_{cyl} for imperceptible glare is decided, based on its correlation with DGP. In the end, some first outputs of the developed blinds' control are presented, followed by the validation results that prove the overall effectiveness of the control strategy.

4.1. Calibration of the model

4.1.1. Calibration of ambient parameters

Figure 4.1 illustrates the convergence graphs derived from *Radiance* parameters' convergence tests. The final ambient parameters that result in a converged value of $E_{middle,wp}$ for both raised and lowered blinds are: -ab 5, -aa 0.2, -ar 64, -ad 4096, -as 2048. It should be highlighted that the ambient parameters must be redefined when adjusting the model to different cases, because the complexity of the model affects the *Radiance* parameters needed to achieve the desired accuracy.

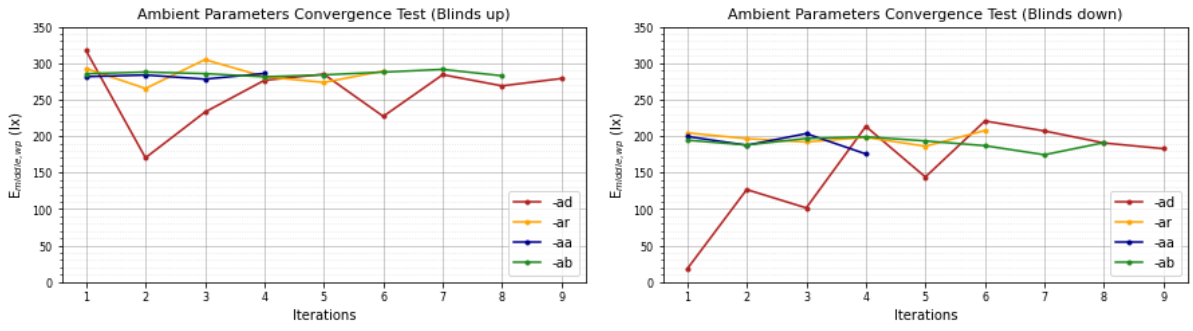

(a) **(b)**

Figure 4.1: Convergence test of ambient parameters for blinds (a) up and (b) down.

The convergence tests show that even with lower values of ambient bounces (-ab 2 or 3), the results are accurate enough. This can be explained by the fact that the CCC does not have opaque walls that would create many reflections. On the contrary, the four fully glazed facades do not reflect the light indoors, but they mostly transmit it outdoors again. Nevertheless, it is safer to use a higher value of -ab, i.e. 5.

4.1.2. Validation of sky model

The results derived from the sky validation process indicate that there is a sufficient correlation between roof sensors' illuminance calculations and measurements for both winter and summer. More specifically, the relative mean bias error (rMBE) is below 20% for all sensors, with the highest values observed at the southern sensor in winter and at the eastern one in summer (Figures 4.2, 4.3). In order to achieve a small error in the calculations of the western sensor, the geometry of the trees had to be slightly corrected at the beginning by adding more of them to the west of the building.

Overall, the coefficient of determination (R^2), which represents the percentage of the measured data variations that can be predicted by the simulations, ranges between 85% and 94%, with the lowest values corresponding to the illuminance recordings of the western and southern sensors during the winter and summer week respectively. This observation implies that there is a higher uncertainty of agreement between the simulation results and the measurements for those two sensors. This can be explained by the highly approximated plants' geometry and the uncertain optical properties of the trees and the canal, which clearly affect the sunlight reflections towards the western and southern roof sensors.

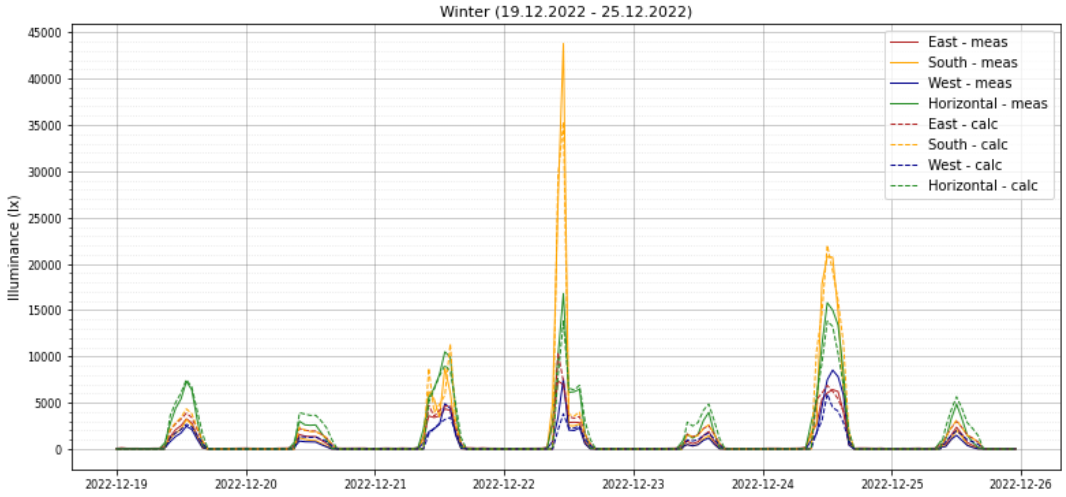

(a)

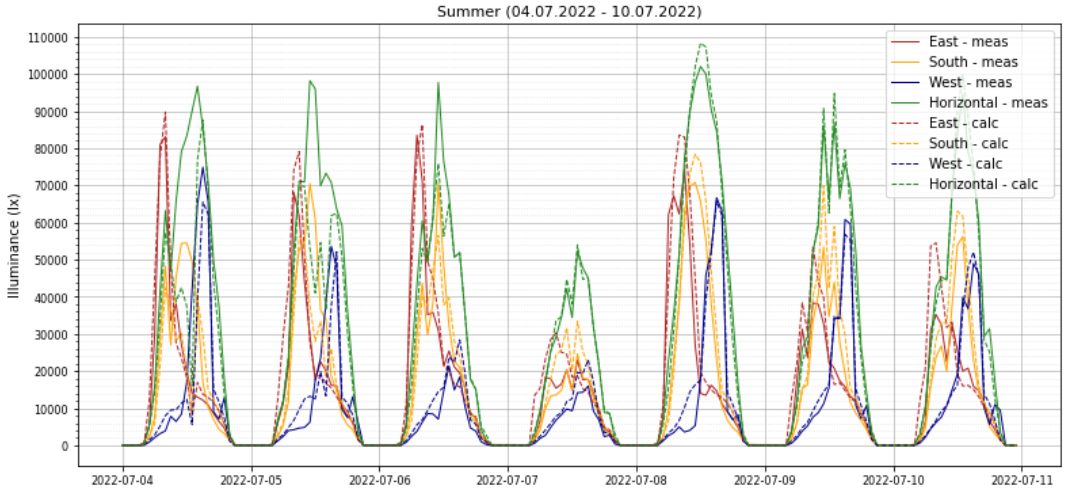

(b)

Figure 4.2: Illuminance measurements and calculations for the four roof sensors during the test period (a) in winter and (b) in summer.

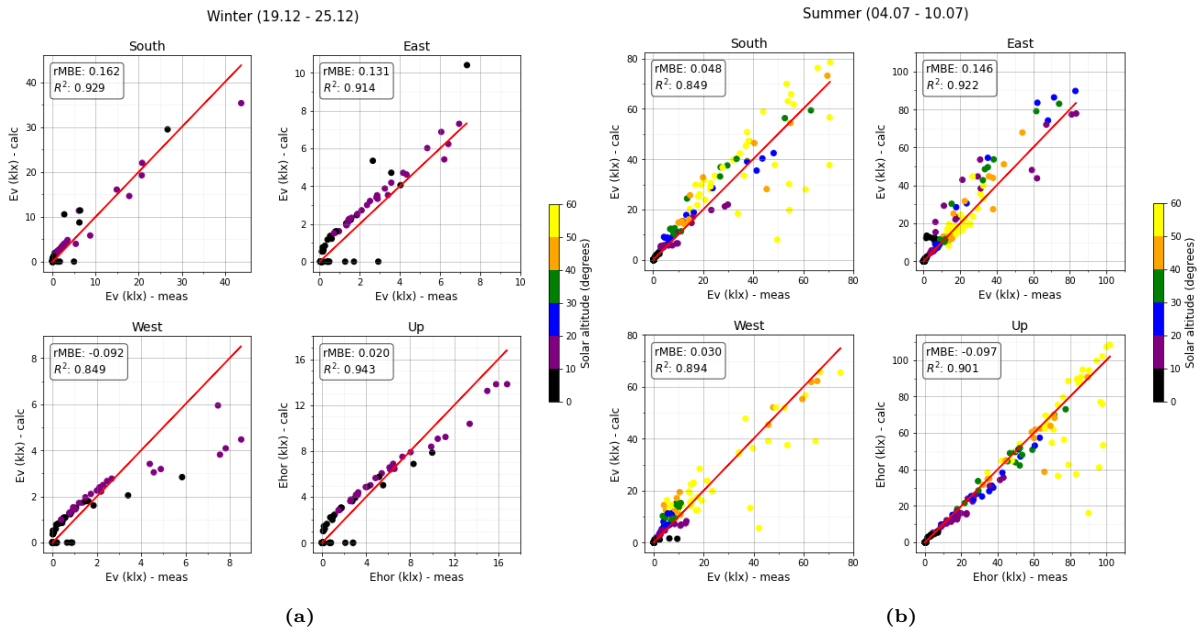

Figure 4.3: Scatterplots of illuminance measurements and calculations for the four roof sensors during the test period (a) in winter and (b) in summer.

Consequently, it is concluded that the sky model is adequately reliable and it can be used for the simulations as a good representative of actual weather conditions in the region of the Co-Creation Center.

4.1.3. Calibration of optical properties

Calibration of context materials' properties

The initial reflectance values assigned to the ground and water were 0.2 and 0.5 respectively, while the initial transmittance value of the plants was 0.1 for totally leafy trees. After testing various combinations of reflectance and transmittance values and running iterative simulations, the chosen reflectance values for the ground and the canal are 0.25 and 0.3 respectively, whereas the transmittance of the trees is set to 0.1 from April to October (leafy trees) and 0.8 from November to March (bare trees). In addition, extra trees were added to the east of the building, in order to achieve the desired results.

For the chosen optical properties and the trees' modifications, the rMBEs between the E_v calculations and measurements at the three roof sensors, range between 2% and 19%, with the highest values observed at the southern sensors for the two days with clear sky (Figures 4.4, 4.5). Those errors are considered acceptable, taking into account the fact that trees and other surrounding elements located at a long distance from the CCC, which could influence the incident sunlight on the southern sensor, are not simulated for reasons of simplicity and computational cost. The coefficient of determination (R^2) is above 85% for all sensors, indicating a satisfactory agreement between the simulations and measurements.

Eventually, the final optical properties resulting from the calibration process can be found in Table 4.1, where only the modified material properties are presented.

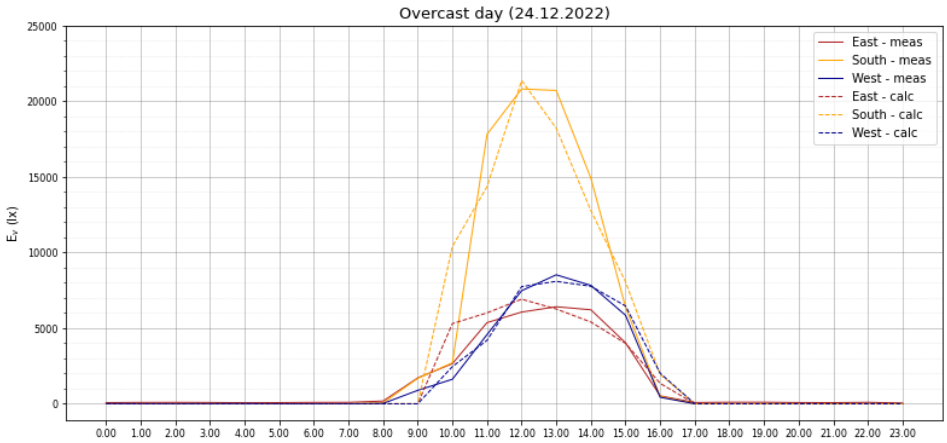

(a)

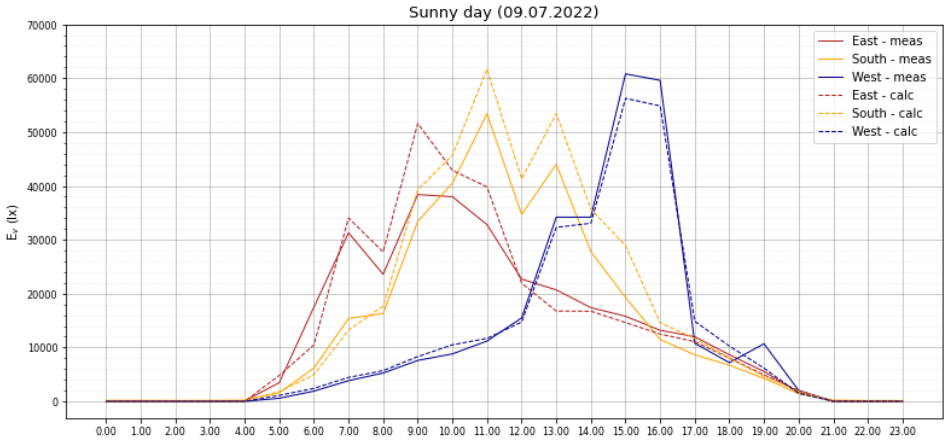

(b)

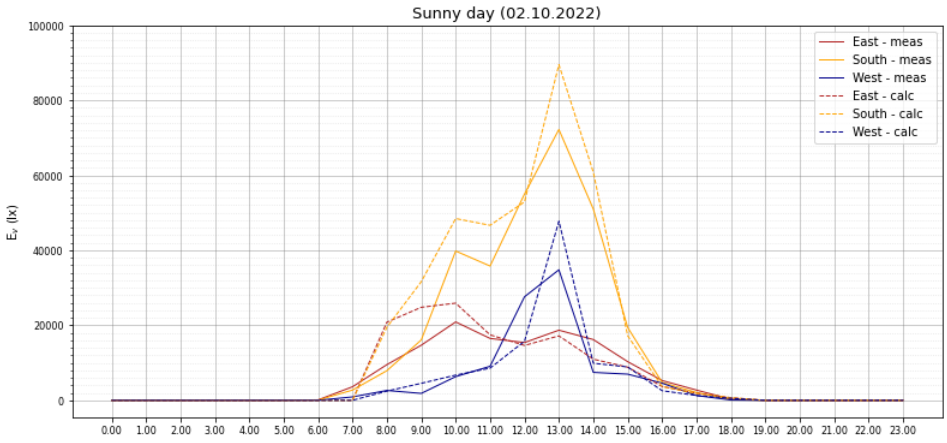

(c)

Figure 4.4: Illuminance measurements and calculations for the three roof sensors during (a) an overcast day, (b) a sunny day with high solar altitude and (c) a sunny day with low solar altitude .

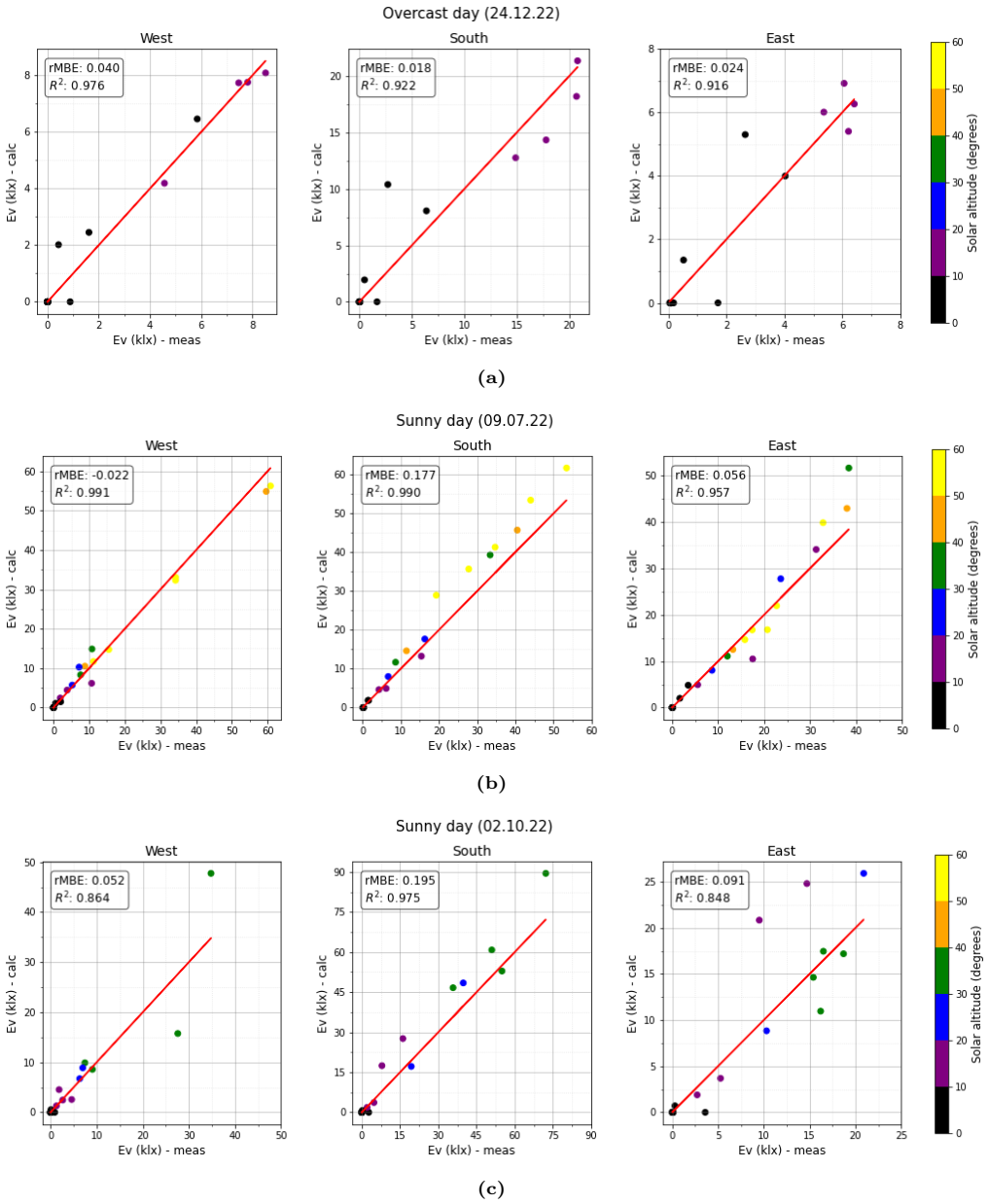

Figure 4.5: Scatterplots of illuminance measurements and calculations for the three roof sensors during (a) an overcast day, (b) a sunny day with high solar altitude and (c) a sunny day with low solar altitude.

Calibration of building materials' properties

After finishing the calibration of the materials in the CCC, the elements with new optical properties are the facades' windows and their glass fins, the skylights, the floor, the ceiling and the frames. The transmittance of the facades and the skylights inserted initially into the model were 0.60 and 0.65, while the final values are 0.68 and 0.80 respectively. The field measurements showed a reflectance of 0.03 for the floor carpet, assuming an equal value for the acoustic ceiling. However, after tweaking the properties to achieve the desired results, the final reflectance value for both elements equals 0.30. The large difference can be explained by the fact that the acoustic ceiling is equipped with reflective metal beams and the floor is usually covered by furniture with a high reflectance value, such as tables. Finally, the reflectance of the frames increased slightly from 0.05 to 0.08.

For the final optical properties, the rMBEs between the calculated and measured $E_{ceiling}$ values, managed to be below 30% for all simulations, except for the North sensor where an underestimation with an error of 46% is noticed for both days (Figures 4.6, 4.7). This observation indicates that there

is a local effect that significantly increases the illuminance values measured by the sensor. Probably the regular placement of the presentation screen at the northern side of the building, which has a high reflectance due to its polished finish, explains this local dramatic increase in the measured illuminance. Another possible reason that explains the locally high error could be the North sensor's malfunction and need for replacement. Overall, the coefficient of determination (R^2) varies between 85% and 97% proving the good agreement between the simulations' and the measurements' variations.

Table 4.1: *Honeybee* objects and final optical properties of the calibrated materials.

Geometrical surface	HB objects	Material	Reflectance	Transmittance
Building (Co-Creation Center)				
Windows	Aperture	Glass	-	0.68
Floor	Face	Carpet	0.30	-
Ceiling	Face	Acoustic ceiling	0.30	-
Skylights	Aperture	Glass	-	0.80
Columns/Fins	Face	Glass	-	0.68
Frames	Shade	Matte black material	0.08	-
Context				
Ground	Face	Soil & Pavement	0.25	-
Canal	Face	Water	0.30	-
Plants	Face	Trees/Leaves	-	0.10 or 0.80

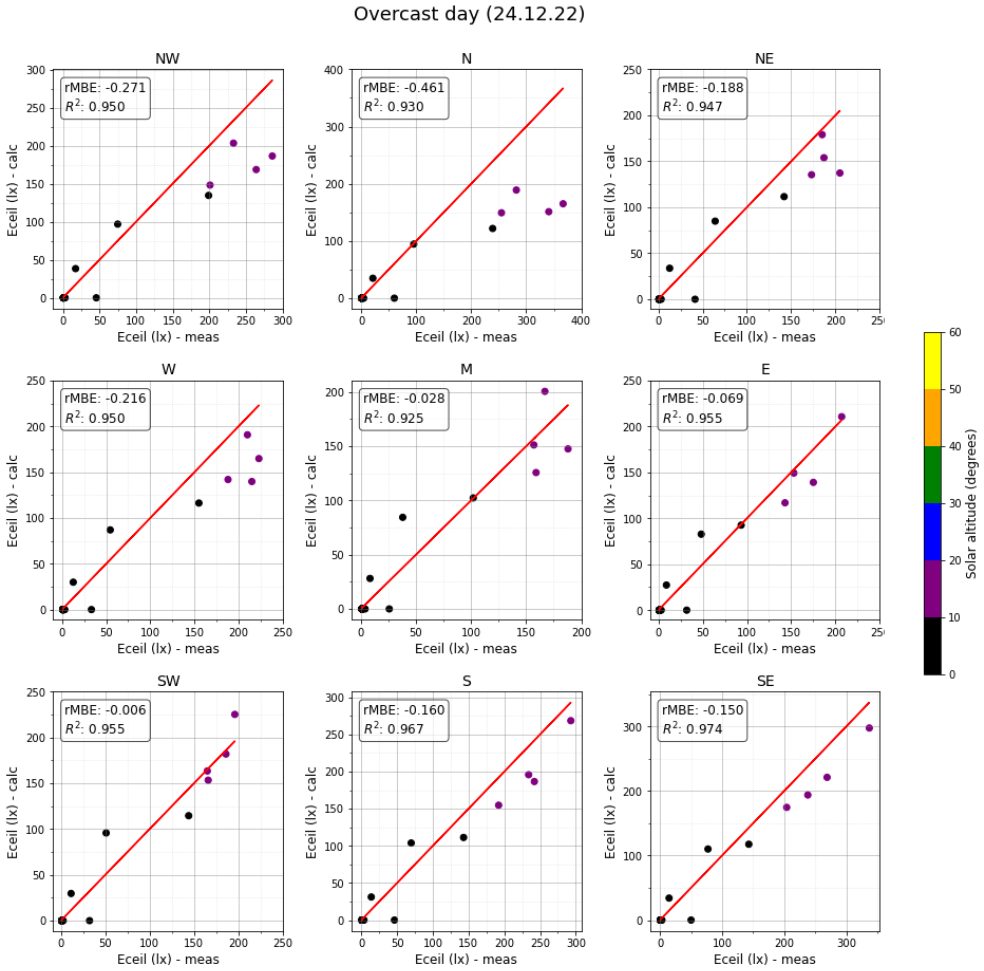

Figure 4.6: Scatterplots of illuminance measurements and calculations for the nine ceiling sensors during an overcast day.

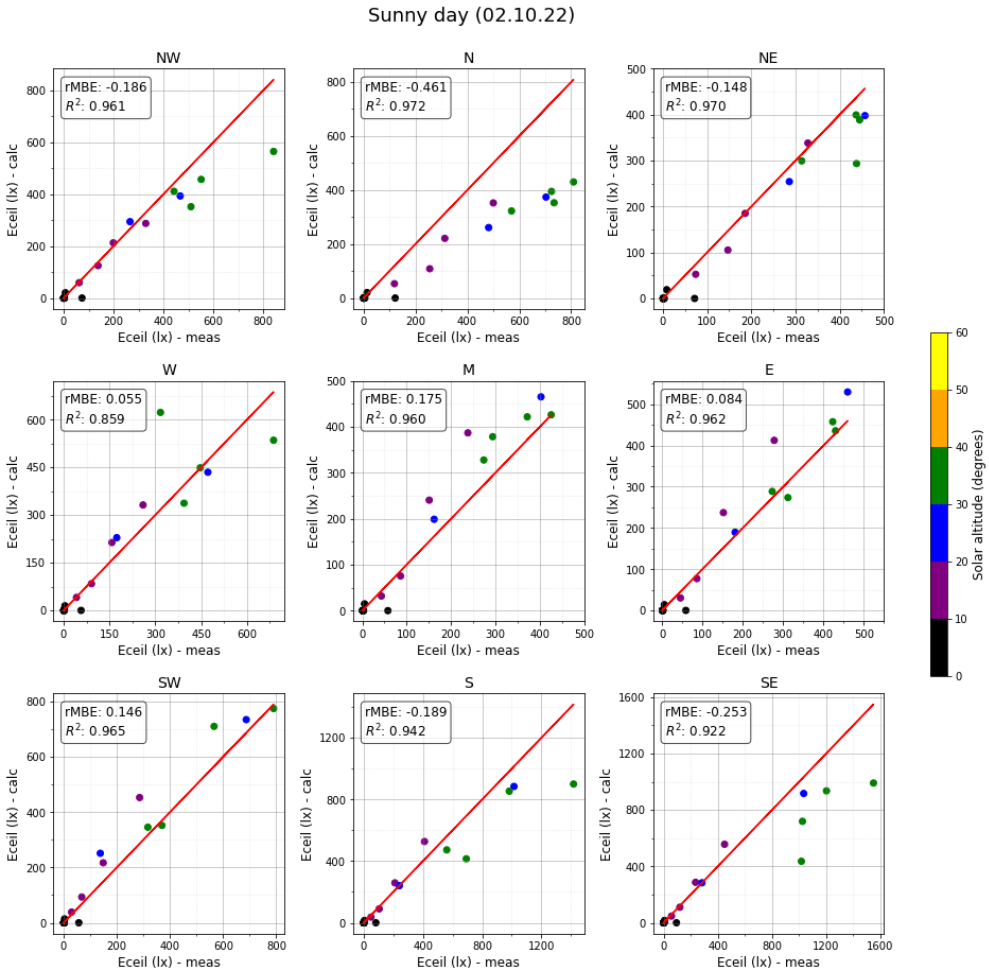

Figure 4.7: Scatterplots of illuminance measurements and calculations for the nine ceiling sensors during a sunny day.

4.2. Correlation of E_{cyl} with DGP

Figure 4.8 demonstrates the distribution of the percentage of TP and TN cases for various optional values of the E_{cyl} threshold. The value yielding the highest percentage of TP and TN results is adopted as the best-correlated E_{cyl} threshold. Thus, the value of E_{cyl} = 1400 lx is employed in the proposed control strategy as the highest limit of imperceptible glare, because it shows a 93% agreement with the corresponding cut-off value of DGP (red line in Figure 4.8).

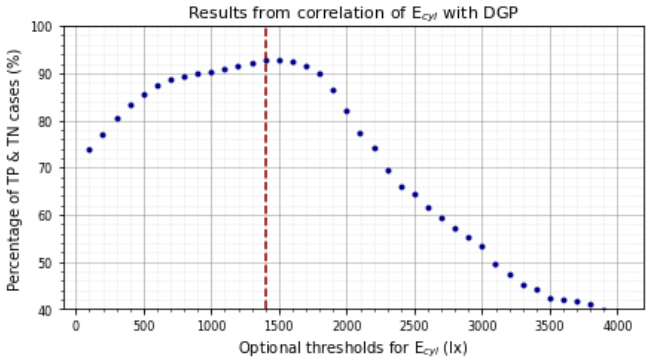

Figure 4.8: Percentage of TP and TN cases for optional thresholds of E_{cyl}.

4.3. Control Strategy

When starting developing the optimized control, the number of variables is set equal to 8, which corresponds to the blinds' increment and angle for each facade. This characterizes the simplest operation of the shading device, where all blinds of each facade move simultaneously, as currently implemented. Nevertheless, the aim is to approach an independent movement of the blinds per window pane, providing a more flexible operation of the shading system and daylight entry. Then, the number of variables increases and the complexity of the problem raises exponentially, as shown in Table 4.2. This means that the number of iterations needed to find a satisfactory and converged solution is very large, resulting in a prohibitive computational cost.

Table 4.2: Optimization's complexity depending on the number of variables.

Case	Number of variables	Complexity
All blinds of each facade move simultaneously	8	x
The blinds move independently in sets of three	32 = 8×4	x^4
All blinds move independently	96 = 8×12	x^{12}

After performing the developed control strategy for 02.10.2022 at 10.00 under sunny conditions for the three activity modes using 8 variables, results show that after 20 iterations, the algorithm finds the blinds' states that provide satisfactory E_{wp} and E_{cyl} values (Figure 4.9a). For the meeting and workshop modes, as satisfactory results, we consider an E_{cyl} value close to its maximum threshold with the respective E_{wp} value. On the other hand, for the presentation mode, as satisfactory results, we consider an E_{wp} value close to its minimum limit with the respective E_{cyl} value. Consequently, 20 iterations are considered sufficient to discover a good solution balancing optimization effectiveness and computational time. More than 20 iterations could not improve dramatically the results. On an Nvidia RTX 3080 graphics card, using *Accelerad*, the optimization with 8 variables takes around 1 hour per each instant.

In Tables A.16, A.17, A.18 of the Appendix, the results for each iteration of the optimization for the three scenarios, are presented. From the detailed presentation of the results, it can be noticed that although higher E_{cyl} values generally lead to higher E_{wp} values, sometimes the opposite occurs, leading to lower E_{wp} values. This can be explained by the fact that the daylight calculation by *Honeybee* is not deterministic, meaning that running the same problem under the same conditions will not produce the exact same results. Hence, these discontinuities in the parallel increasing or decreasing trends of the two metrics are reasonable and, since they do not influence the convergence and efficiency of the algorithm, they are considered acceptable. It is also worth mentioning that, based on the results for the meeting and workshop cases, E_{wp} never exceeds 3000 lx, hence discomfort due to excessive daylight never occurs. This is because the maximum threshold of E_{cyl} significantly limits daylight entry and constricts E_{wp} well below 3000 lx.

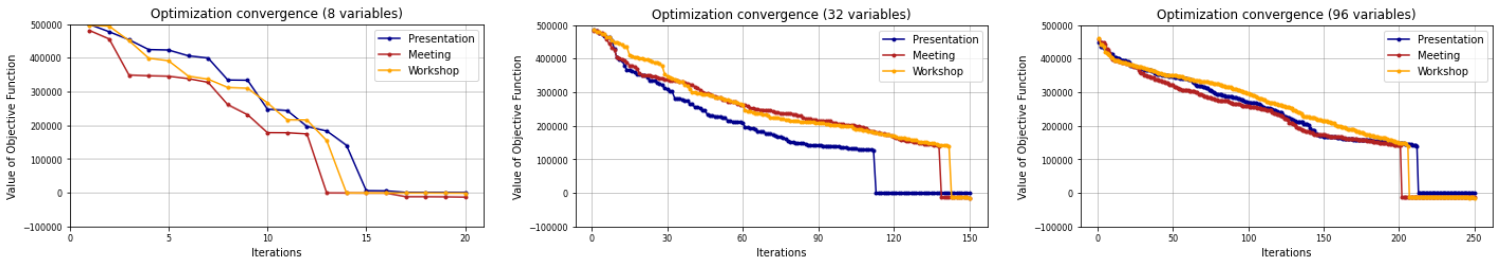

(a) **(b)** **(c)**

Figure 4.9: Convergence of optimization process for the three activities (a) after 20 iterations, using 8 variables, (b) after 150 iterations, with 32 variables and (c) after 250 iterations, using 96 variables.

When having 32 variables, the time needed to reach a good solution is approximately 8 hours, corresponding to 150 iterations (Figure 4.9b). In the extreme case of 92 variables, operating each blind independently, satisfactory results occur at least after 250 iterations, lasting around 16 hours (Figure 4.9c). In Tables A.19, A.20, A.21, A.22, A.23, A.24 of the Appendix, the results of the 32- and 96-variable optimizations for the three activity modes can be seen.

In Figure 4.10, the final values (E_{wp}, E_{cyl}) of the three optimization cases for the three activity modes are demonstrated as a bar chart. Comparing the results of the three blinds' operation modes (simultaneous movement of blinds, independent movement of blinds in sets of three, totally independent movement of blinds), it can be noticed that all techniques present the desired performance in most of the cases. In the case of meetings and workshops, the two operation techniques with a higher degree of blinds' movement independence seem to slightly outperform, providing higher values of E_{wp} and thus ensuring zero energy demands for electric lighting, especially for the workshop mode. Regarding the presentation scenario, the 96-variable optimization displays some difficulty to converge to low E_{wp} values, providing acceptable results, but worse than the other two optimizations. This means that more iterations are probably needed to further improve the solution. On the contrary, the 8- and 32-variable optimizations converge faster and give very similar results. Table 4.3 summarizes the relative errors between the results of the three blinds' operations, having the 8-variable optimization as a reference.

In general, the simplest blinds' operation performs very well in comparison to the other two techniques, producing similar solutions that meet the goals of the optimized control strategy. This leads to the conclusion that moving the blinds of each facade simultaneously, in increment steps of 20% and angle steps of 2°, is flexible enough to handle effectively daylight entry, avoiding the high computational cost of using many optimization variables.

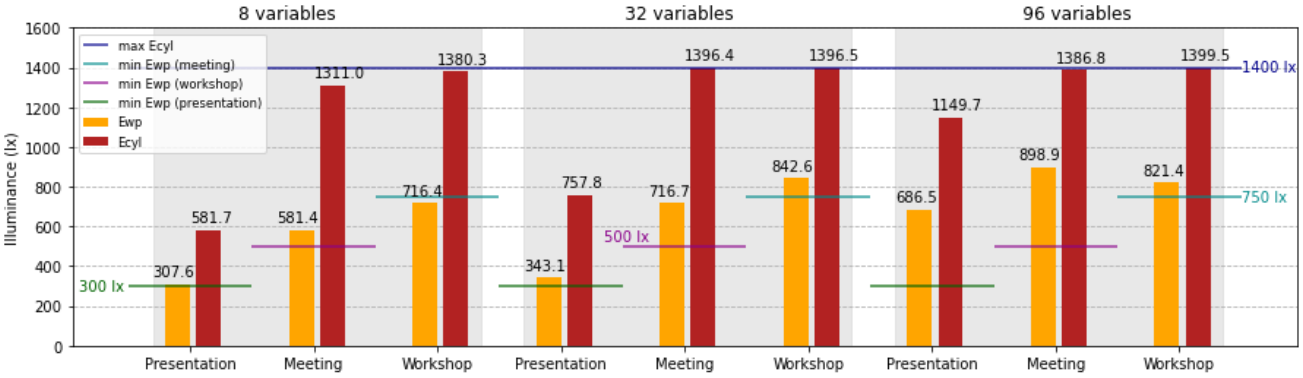

Figure 4.10: Performance comparison between the simplest blinds' operation (8 optimization variables), the one with blinds' movements in sets of three (32 optimization variables) and the totally independent operation of the blinds (96 optimization variables) for the three activity modes.

Table 4.3: Relative errors between the results of the three blinds' operations for the three activity modes, having the 8-variable optimization as a reference.

	Presentation		Meeting		Workshop	
	E_{wp}	E_{cyl}	E_{wp}	E_{cyl}	E_{wp}	E_{cyl}
8 variables	-	-	-	-	-	-
32 variables	0.115	0.303	0.233	0.065	0.176	0.012
96 variables	1.232	0.976	0.546	0.058	0.147	0.014

4.4. Validation of the control strategy & evaluation of E_{cyl}

4.4.1. Clear sky conditions

As the simultaneous operation of the blinds in each facade was proven flexible enough for adequate regulation of daylight entry, the 8-variable optimization was employed for the validation process. Firstly, the results of the test period with constant sunny conditions, high GHI and low solar altitude (18.03.2022 between 10.00-16.00) are presented. The detailed results of the following graphs can be found in Tables A.25, A.26, A.27, A.28 of the Appendix.

Figure 4.11 demonstrates the blinds' states decided by the control strategies, for each time step of the event's duration. It is evident that the shades' movement is mostly smooth for the current control, while it is more erratic in all modes of the optimized control. The abrupt changes, especially of the increments, might cause disturbance or distraction to the occupants during a session. Nevertheless, thanks to the 20% increment step, there are intervals where the shades are lowered or raised to the next increment step, facilitating the provision of visual comfort with small movements and hence without causing much nuisance to the users. The level of smoothness can be quantified as the percentage of blinds' consecutive changes with an increment difference lower than or equal to 20%. The higher the percentage, the smoother the blinds' operation. This smoothness metric considers only the increment modifications, as those movements are the most distracting. Table 4.4 reports the smoothness percentages of the blinds' movements on each facade for the current and the optimized control.

The overall performance of the control strategies for the three activities, in terms of daylight sufficiency, glare risks and view quality, can be seen in Figure 4.12. As regards the amount of daylight in the indoor space, the existing control system results in higher E_{wp} values most of the time than the other controls, meaning that more light is allowed to pass through the facades. This is desired when a meeting or a workshop takes place, but it is unwanted during a presentation when the occupants' focus should be on the projection screen. On the other hand, the optimized control for the presentation mode most of the time manages to minimize E_{wp} close to the target value of 300 lx, without creating the need for electric lighting. There is only one exception, at 15.15, when E_{wp} drops just slightly below 300 lx. In the case of a meeting and workshop, the maximum limit of E_{cyl} makes the developed control stricter, letting less daylight enter the space than the current control, but usually enough to meet the minimum limits. Only for a few time steps, the minimum thresholds of 500 lx and 750 lx are not exceeded, but this is reasonable as energy minimization was not the priority of the developed control strategy.

The middle graph in Figure 4.12 clearly shows that the high daylight admission of the currently implemented control leads to high glare risks; throughout the whole duration of the session, at least one of the nine tested positions experiences glare. On the contrary, the developed control system successfully prevents glare most of the time for all activity scenarios, except for only a few time steps where E_{cyl} exceeds 1400 lx. For those instances, the algorithm shows some difficulty to converge to a non-glare solution, probably due to incoming direct or diffuse daylight passing through the unshaded western and eastern doors.

As regards the view quality, the bottom graph in Figure 4.12 demonstrates the average percentage of the occupants' view that is not blocked by the blinds, over the test period. The graph proves that the lower amount of admitted daylight in the optimized control does not compromise essentially the occupants' view to the outside, although it is clear that the current control provides higher view quality. Between the three activity modes of the optimized control, no large differences occur. Table 4.5 summarizes the ranges where the view percentages fluctuate for the whole test period for both control strategies. Figure 4.13 presents an example of the view analysis performed in *Grasshopper*. Here it can be seen that the grid next to mostly closed louvers is colored dark pink, implying that the view to the outside is limited. On the contrary, wherever the louvers are more open and in the areas close to the unshaded doors, the grid is colored light green-blue, indicating a higher visual contact with the exterior.

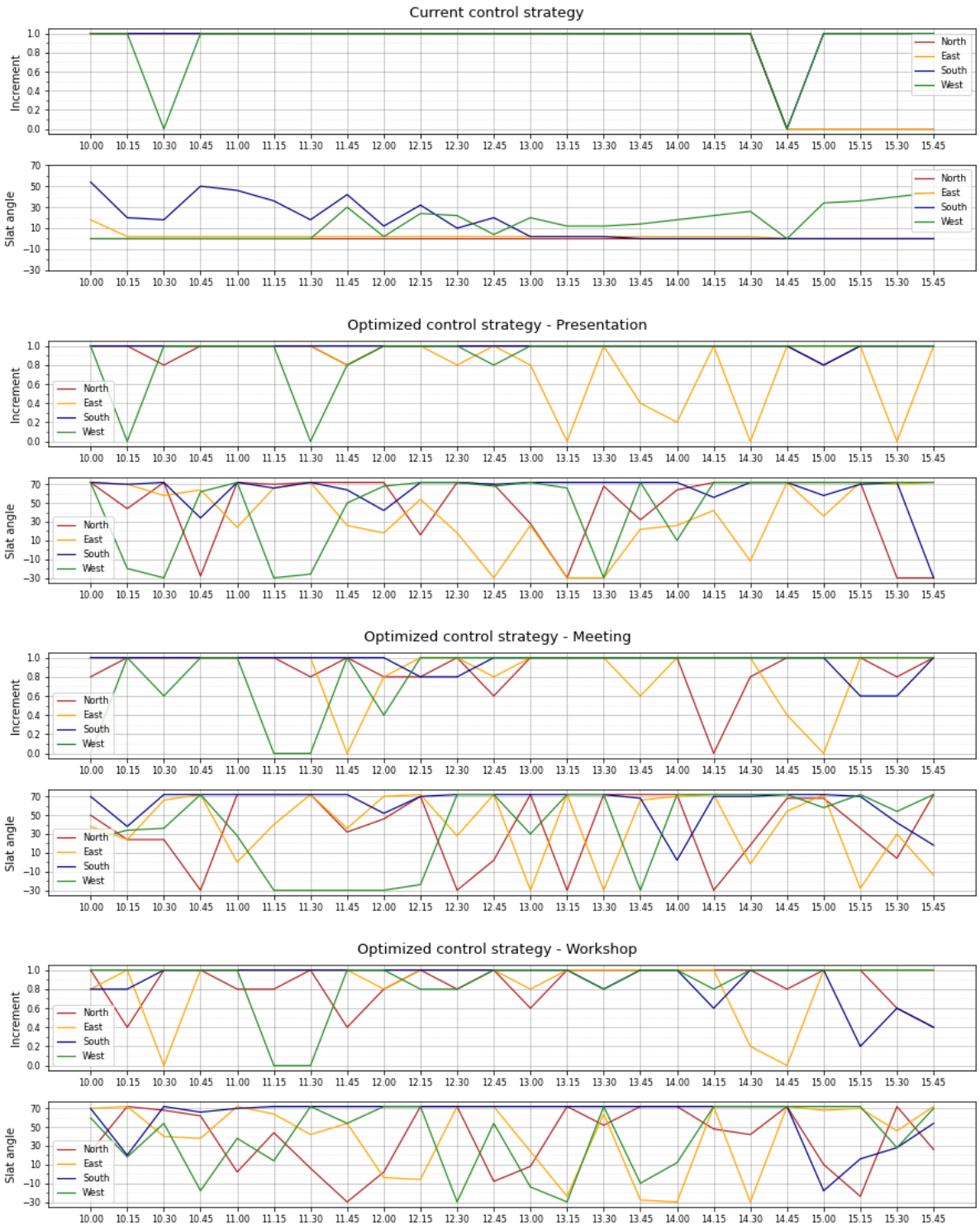

Figure 4.11: Blinds' states decided by the current control and the optimized one for the presentation, meeting and workshop mode over the test period on 18.03.2022.

Table 4.4: Percentages indicating the smoothness of blinds' movements on each facade for the current control and the optimized one for the three activity modes during the test period on 18.03.2022. The higher the percentage, the smoother the blinds' operation.

	Current control	Optimized control Presentation	Optimized control Meeting	Optimized control Workshop
Smoothness - N (%)	96	100	83	70
Smoothness - E (%)	96	65	70	83
Smoothness - S (%)	91	100	91	83
Smoothness - W (%)	83	83	70	91

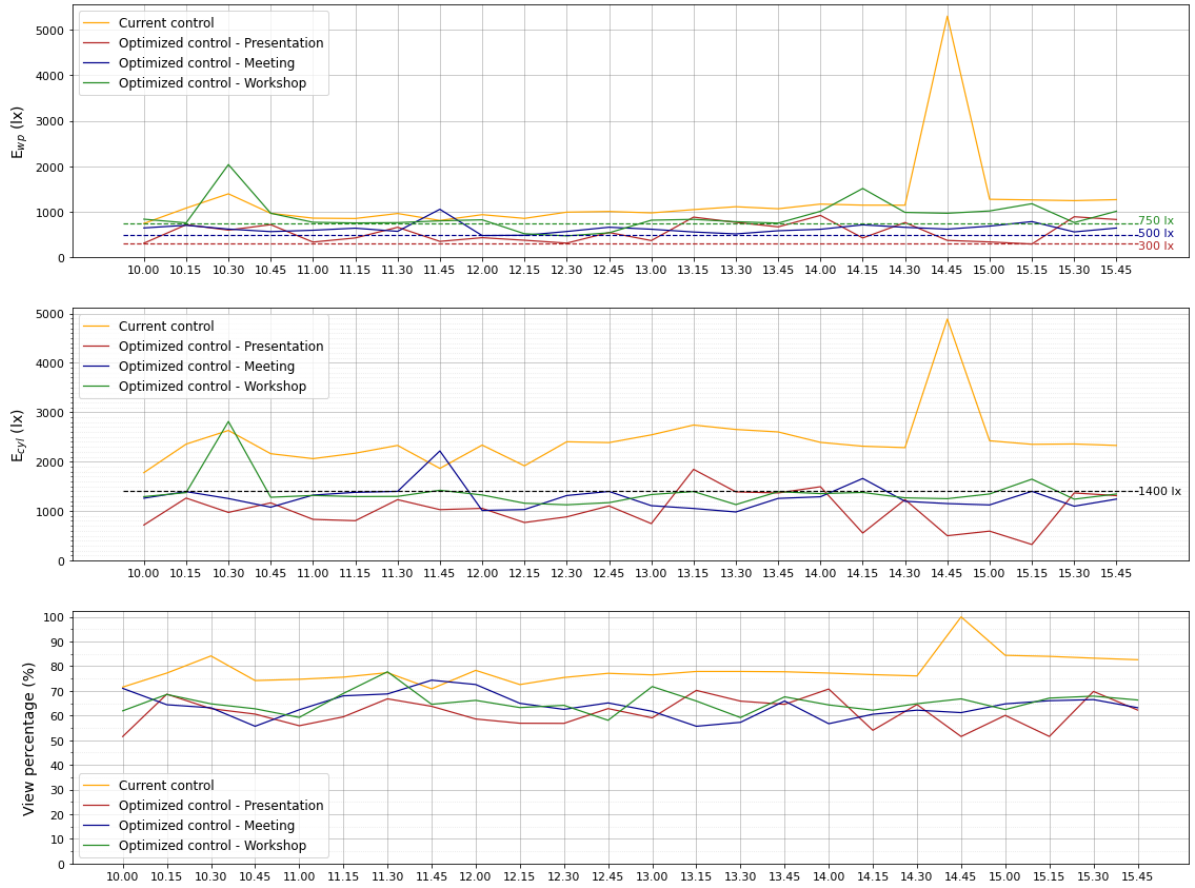

Figure 4.12: Workplane illuminance, cylindrical illuminance and view percentage for all control strategies throughout the test period on 18.03.2022.

Table 4.5: Ranges where the average view percentages for the current and the optimized control fluctuate during the test period on 18.03.2022.

	Current control	Optimized control Presentation	Optimized control Meeting	Optimized control Workshop
Average view percentage (%)	70–100	51–71	55–75	58–78

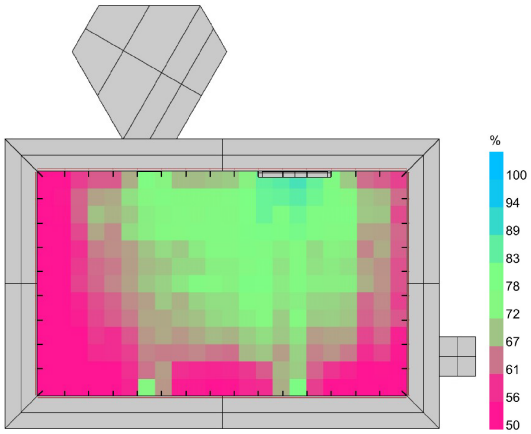

Figure 4.13: View analysis of the optimized control for the meeting mode at 15.45 on 18.03.2022.

Figure 4.14 demonstrates in detail the glare risks distributed over the space during the session on 18.03.2022. Every rectangle represents the floor plan, divided into nine smaller rectangles that outline the nine viewpoints where glare is assessed. Every viewpoint is evaluated based on its maximum DGP value among eight view directions and its E_{cyl} (average of vertical illuminances among the eight directions). As expected, when the blinds are totally raised, the two metrics agree by 100% that there is constantly excessive daylight in the space, causing glare to all positions. This also demonstrates that the selected day is appropriate for a test on glare risk.

With the currently implemented control strategy, only a small improvement of 6.5-9.3% is achieved in glare risks over the test period. Between the two indices, it is noticed that E_{cyl} slightly overestimates the glare positions, noting an 87% correlation with DGP. The reason behind this is that E_{cyl} evaluates glare based only on the amount of light perceived by the occupant's eyes, whereas DGP additionally considers the contrast effect between the background and the glare source's luminance. In other words, in some cases when E_{cyl} identifies glare risks due to high daylight entry, DGP assumes that the daylight amount is appropriate for the users preventing disturbing luminance contrast.

For the vast majority of the time steps, the optimized control strategy guarantees glare protection for all activity modes. In the case of presentation, a 96-98% reduction of glare positions is noticed in comparison to the totally raised blinds, while this percentage is 92-98% for the meeting and workshop modes. Here, contrary to the current control, the DGP-based assessment overestimates glare positions in all activity cases. This can be justified by the higher contrast effects that occur due to the darker indoor conditions and the bright daylight that penetrates unshaded parts of the facades or through the louvers, especially when their slat angle is -30°. Another explanation for the higher glare risks identified by DGP is that, in some time steps, the best solution decided by the optimization algorithm results in an E_{cyl} value very close to the upper threshold of 1400 lx. This means that after rerunning *Honeybee*'s non-deterministic glare analyses for the DGP calculation, results might exceed the threshold of 0.35 indicating glare risks. Generally, the agreement percentage between the two glare indices is satisfactory, equal to 93%, 89% and 87% for the presentation, meeting and workshop respectively. The percentages of glare reduction (in comparison to the blinds-up situation) and the agreement between E_{cyl} - DGP for all cases shown in Figure 4.14, are summarized in Table 4.6.

Overall, in all cases, the blinds' states explain the shading patterns in the space, as glare risks occur close to facades with more open louvers or more raised blinds. Figure 4.15 includes the HDR images resulting from the DGP-based glare assessment in eight view directions of the South-East viewpoint, at 14.00 on 18.03.2022. The blinds' states in the images have resulted from the optimized control strategy, for the meeting mode. At that moment, all facades have totally lowered blinds with closed slats, except for the southern louvers that are placed almost horizontally. Figure 4.15 represents an example of a point's visual conditions, where the small amount of daylight entry decreases E_{cyl}, but creates a contrast effect when daylight passes through the unshaded parts, leading to a higher value of DGP. Based on

E_{cyl}, there is no glare risk at that viewpoint, whereas based on DGP, the viewpoint experiences glare towards the South and the South-West view directions (visible in the fifth and sixth fish-eye images of Figure 4.15). It is noticeable that the illuminance contrast is caused by the daylight coming through the blinds of the southern facade, while the sunlight and daylight coming through the unshaded western and eastern doors respectively illuminate the space rather uniformly, without provoking glare.

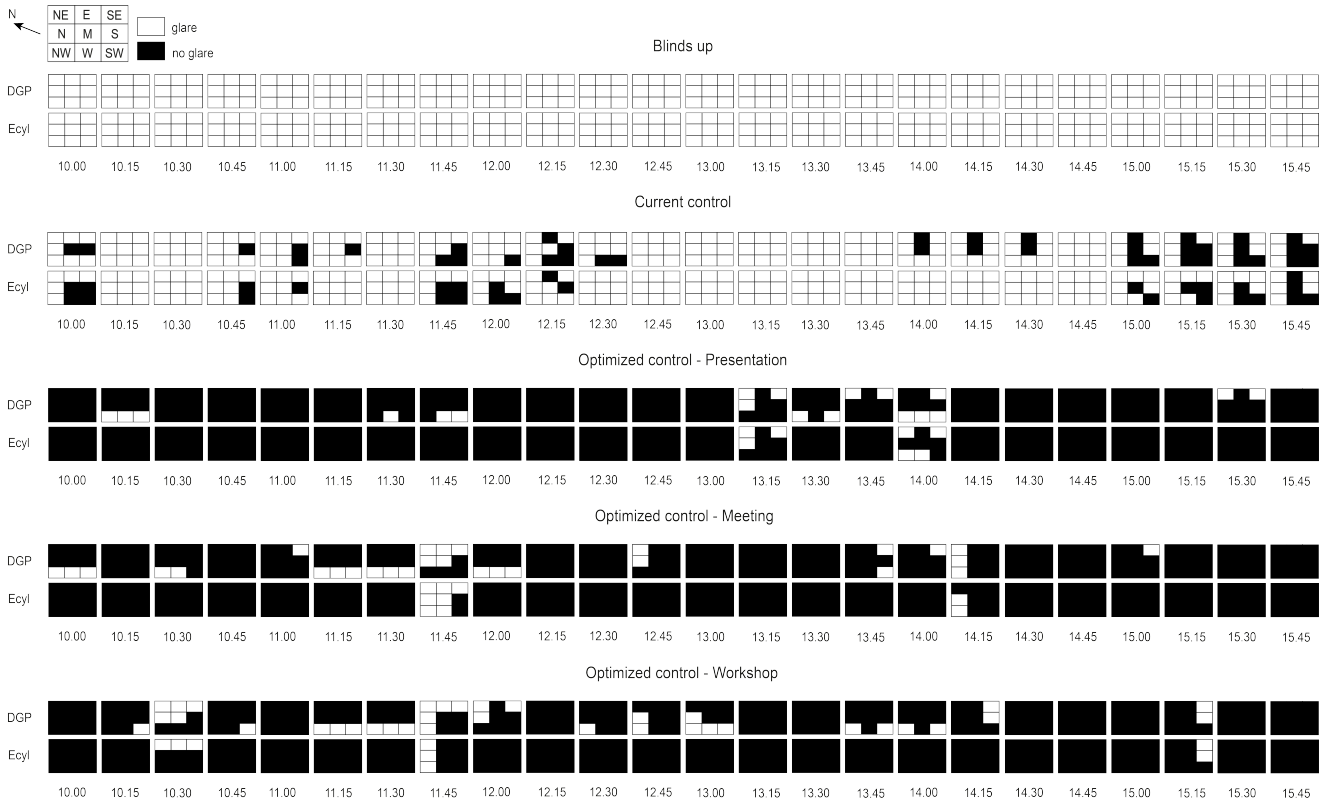

Figure 4.14: Demonstration of glare and no glare positions over the test period on 18.03.2022 for totally raised blinds, the current control and the optimized one for the presentation, meeting and workshop mode.

Table 4.6: Improvement of glare conditions compared to totally raised blinds based on E_{cyl} and DGP, and agreement between the two glare indices for the different blinds' operations during the test period on 18.03.2022.

	Blinds up	Current control	Optimized control Presentation	Optimized control Meeting	Optimized control Workshop
Improvement based on DGP (%)	-	9.3	96	93	92
Improvement based on E_{cyl} (%)	-	6.5	98	98	98
E_{cyl} - DGP agreement (%)	100	87	93	89	87

Figure 4.16a presents the lighting energy demands for each activity scenario under the currently implemented control and the optimized one. It should be clear that the current control's energy demands shown in the chart are calculated assuming that the lighting system works properly, supplementing daylight only in case of illuminance insufficiency and without pointless additional energy consumption. In the bar chart, the energy is presented as mean hourly values (kWh/h), in order to be comparable with the corresponding bar chart of the second test period. The large amounts of incoming daylight allowed by the current system results in almost zero lighting energy needs for all activities. On the other hand, the optimized control leads to higher energy consumption in all cases, with the workshop demanding a more considerable energy amount. This is reasonable, as the strict E_{cyl} threshold of 1400 lx, makes the optimization convergence to high E_{wp} values ($>$ 750 lx) difficult.

The solar heat gains resulting from the four controls are demonstrated in Figure 4.16b. Again, the mean hourly values are shown in the bar chart. It is clear that the admitted solar radiation is higher

in the optimized control than in the existing one, despite the higher daylight entry observed in the latter. The reason behind this is that the current control avoids direct sunlight penetration, while the optimized algorithm usually allows that. In fact, it is noticed that the highest solar heat gains occur when sunlight passes through louvers with negative angles. During meetings and workshops, the incoming solar radiation is higher than during presentations, since for the former the maximization of incoming daylight is targeted, whereas for the latter its minimization is pursued.

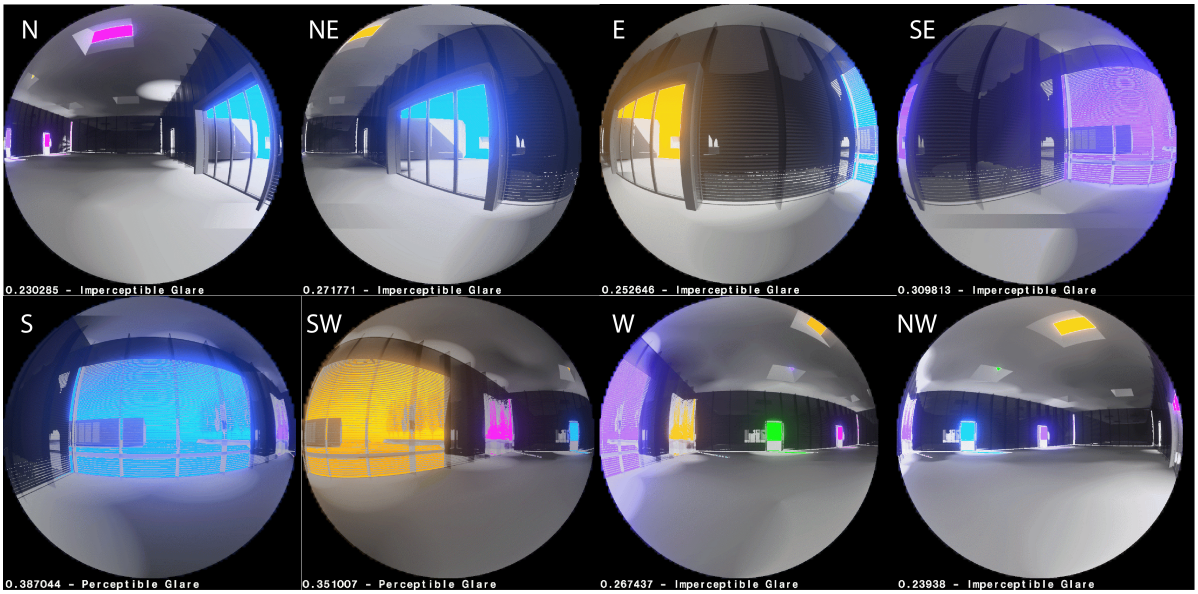

Figure 4.15: HDR images resulting from DGP-based glare assessment for eight view directions of the SE viewpoint at 14.00 on 18.03.2022. The blinds' states have resulted from the optimized control for the meeting mode. The viewpoint experiences glare towards the South and the South-West view directions (visible in the fifth and sixth fish-eye images).

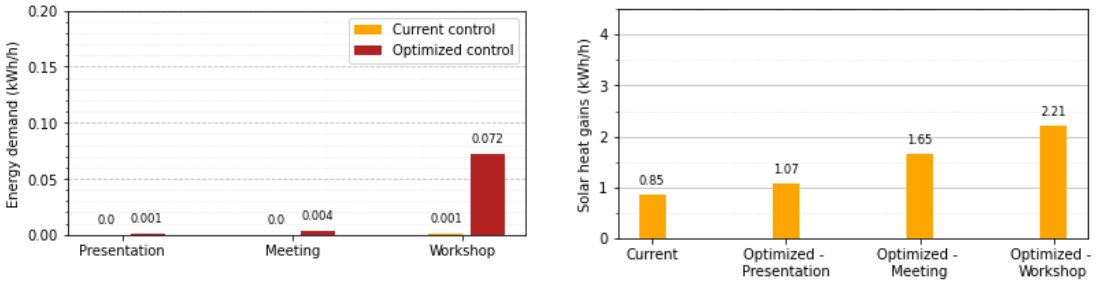

(a) **(b)**

Figure 4.16: (a) Energy demands for electric lighting resulting from the two control systems for the three activity scenarios on 18.03.2022. (b) Solar heat gains for the current control and the optimized one for the three activity modes on 18.03.2022.

4.4.2. Variable weather conditions

After testing the blinds' operation under clear sky conditions, the investigation of the performance of the different control strategies under sunny and cloudy sky variations is also of interest. The chosen test period on 24.10.2022 gives insight into that. The detailed results of the next graphs can be seen in Tables A.29, A.30, A.31, A.32 of the Appendix.

Figure 4.17 shows the blinds' states decided by the existing control and the optimized one for each time step of the event's duration. Here again, the optimized control results in a more abrupt louvers' operation, even though there are subsequent time steps where small movements (20% raising or lowering) correct effectively the visual conditions in the building when the weather conditions change.

On the other hand, the constantly stable blinds of the current control system satisfy its requirement of causing minimum disturbance to the occupants during the session. The level of smoothness of the blinds' operation on each facade for the two control strategies is presented in Table 4.7.

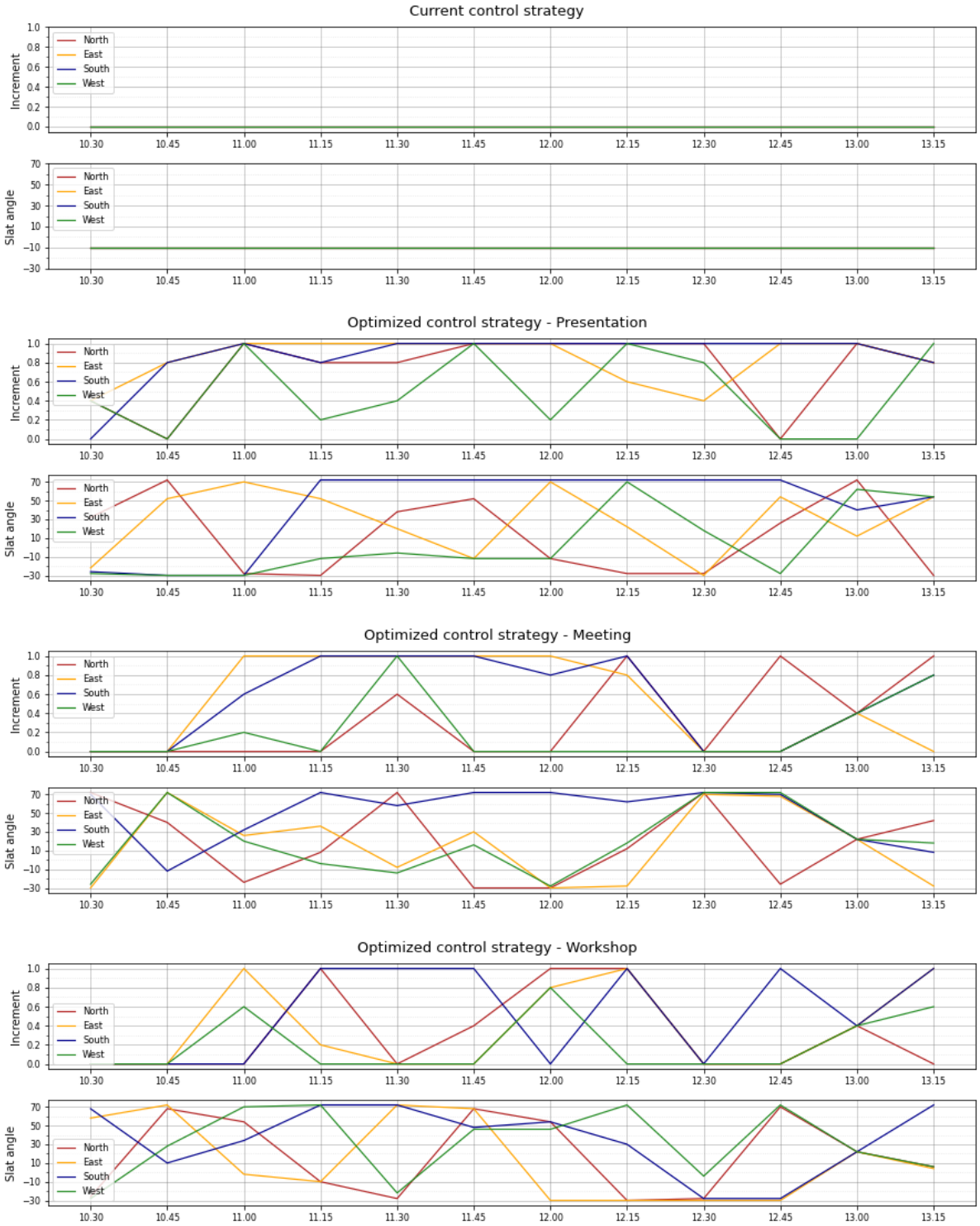

Figure 4.17: Blinds' states decided by the current control and the optimized one for the presentation, meeting and workshop mode over the test period on 24.10.2022.

Figure 4.18 summarizes the overall performance of the control strategies regarding E_{wp}, E_{cyl} and the percentage of the occupants' view to the outside. The continuously raised blinds of the existing

control allow adequate daylight entry into the space most of the time, but such an amount of light is rather disturbing for the presentation mode. The high daylight admission also leads to high glare risks, especially around noon when the direct irradiance is high and therefore direct sunlight enters the space. On the contrary, the optimized algorithm manages to prevent glare for the whole duration of the session, regardless of the activity mode, maintaining sufficient daylight almost continuously. It is worth noticing that, at the beginning of the session, when the global, direct and diffuse irradiance is very low, neither of the two control strategies manages to keep E_{wp} above the minimum thresholds of the meeting and workshop, although they both have totally raised blinds. As for the view quality, the current control constantly provides 100% visual contact with the external environment, while in the optimized algorithm, the average view percentage displays higher fluctuations during the test period. Table 4.8 shows the ranges where the view percentages fluctuate for the two control modes for the whole duration of the session. The higher amount of daylight entry during the meeting and workshop modes slightly increases the view quality in comparison to the presentation mode, although no large differences are observed.

Table 4.7: Percentages indicating the smoothness of blinds' movements on each facade for the current control and the optimized one for the three activity modes during the test period on 24.10.2022. The higher the percentage, the smoother the blinds' operation.

	Current control	Optimized control Presentation	Optimized control Meeting	Optimized control Workshop
Smoothness - N (%)	100	64	36	36
Smoothness - E (%)	100	73	64	45
Smoothness - S (%)	100	91	55	55
Smoothness - W (%)	100	27	64	55

Figure 4.18: Workplane illuminance, cylindrical illuminance and view percentage for all control strategies throughout the test period on 24.10.2022.

Table 4.8: Ranges where the average view percentages for the current and the optimized control fluctuate during the test period on 24.10.2022.

	Current control	Optimized control Presentation	Optimized control Meeting	Optimized control Workshop
Average view percentage (%)	100	63–96	74–100	68–100

A detailed demonstration of glare and non-glare positions distributed over the space during the event on 24.10.2022 is presented in Figure 4.19. Here again, both DGP-based and E_{cyl}-based glare assessments are shown. Due to the low irradiance conditions, the current control does not move the blinds at all during the session. However, the two glare indices agree by 94% that glare risks occur in the building at some time steps, when diffuse irradiance exceeds 120 W/m^2 or direct sunlight enters the space. As noticed in the previous test period, the E_{cyl}-based assessment tends to slightly overestimate the blinds positions.

The optimized control strategy guarantees zero glare risks for the whole duration of the session, regardless of the activity mode. This concerns the E_{cyl}-based glare evaluation, by which the optimization is steered. On the other hand, DGP identifies glare risks when bright daylight enters the dim space and creates luminance contrast. Nevertheless, the correlation between the two indices is still high, reaching 97%, 94% and 92% for the presentation, meeting and workshop modes respectively. The overall improvement of glare risks provided by the optimized control strategy in relation to the current one (totally raised blinds), is around 95-100% for the presentation and 87-100% for the meeting and workshop. The percentages of glare reduction and E_{cyl} - DGP agreement for all cases shown in Figure 4.19 are summarized in Table 4.9.

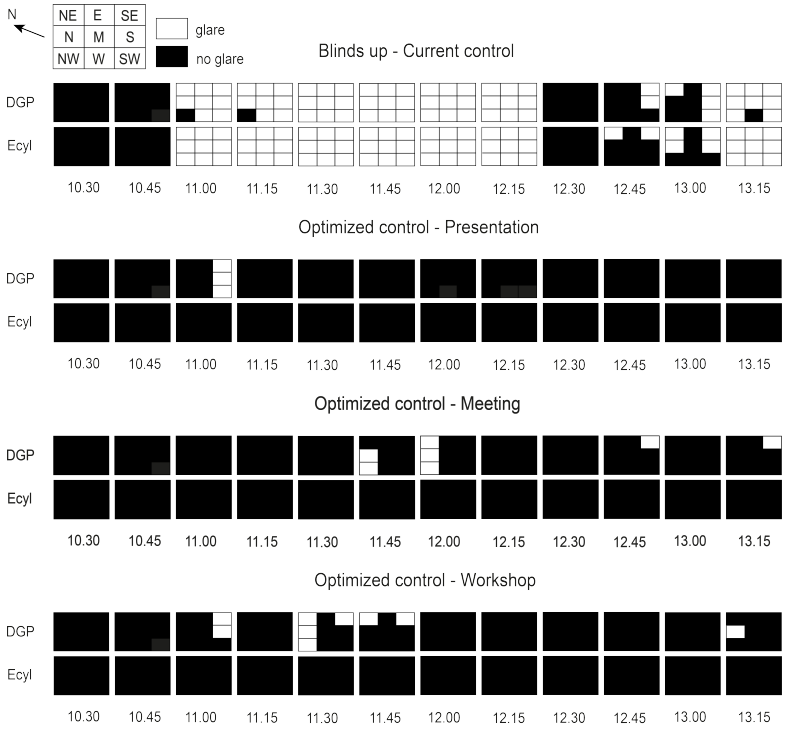

Figure 4.19: Demonstration of glare and no glare positions over the test period on 24.10.2022 for the current control (totally raised blinds) and the optimized control for the presentation, meeting and workshop mode.

In Figure 4.20, the HDR images resulting from the DGP-based glare assessment for the North viewpoint, at 12.00 on 24.10.2022, are presented. The blinds' states in the images have been determined by the optimized control strategy, for the meeting mode. For that time step, the North and West facades have totally raised blinds, while the South facade is shaded by 80% of its height by completely closed louvers and the East blinds are totally down with a -30° slat angle. Although E_{cyl} estimates that there

are zero glare risks, DGP is higher towards the North facade, where large amounts of incoming diffuse daylight create a noticeable contrast effect. As a consequence, the viewpoint experiences perceptible glare towards the North and North-East view directions (visible in the first and second fish-eye images of Figure 4.20).

Table 4.9: Improvement of glare conditions compared to totally raised blinds based on E_{cyl} and DGP, and agreement between the two glare indices for the different blinds' operations during the test period on 24.10.2022.

	Blinds up - Current control	Optimized control Presentation	Optimized control Meeting	Optimized control Workshop
Improvement based on DGP (%)	-	95	89	86
Improvement based on E_{cyl} (%)	-	100	100	100
E_{cyl} - DGP agreement (%)	94	97	94	92

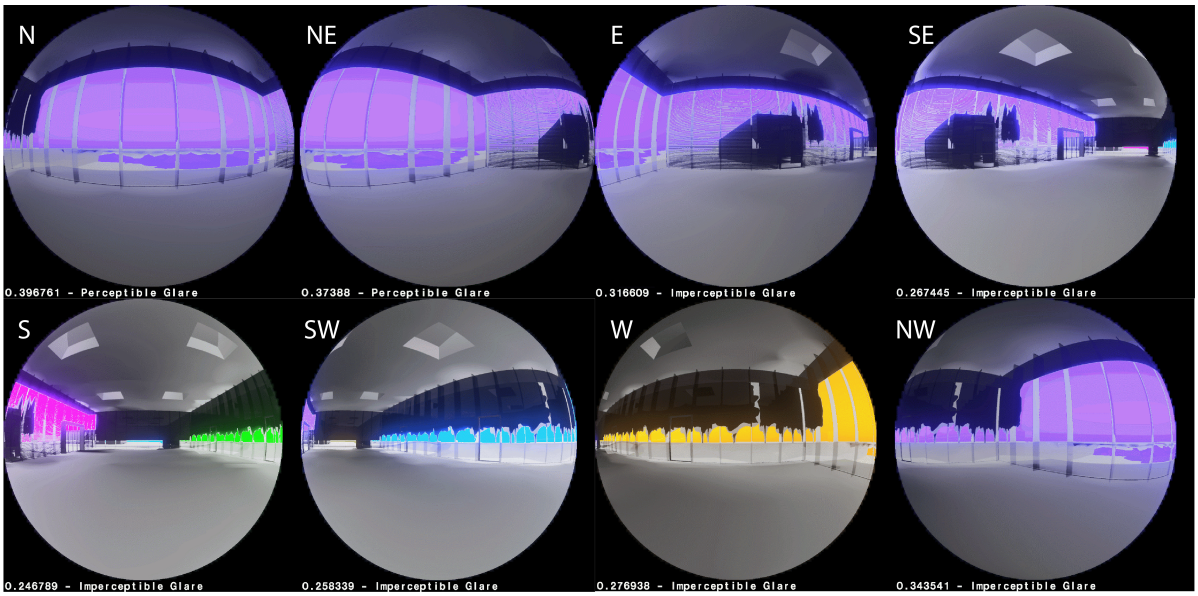

Figure 4.20: HDR images resulting from the DGP-based glare assessment for eight view directions of the N viewpoint at 12.00 on 24.10.2022. The blinds' states have resulted from the optimized control for the meeting mode. The viewpoint experiences glare towards the North and North-East view directions (visible in the first and second fish-eye images).

Figure 4.21a presents the lighting energy demands for each activity scenario under the current control strategy and the optimized one for the whole duration of the event. As regards the existing control, the constantly raised blinds allow large amounts of admitted daylight that result in zero lighting energy needs for the presentation mode. However, the low irradiance levels at some time steps do not suffice to meet the minimum requirements of E_{wp} for the meeting and workshop and hence electric lighting is needed. On the other hand, the aim of the optimized control to minimize glare risks leads to higher energy consumption for the meeting and workshop modes, with the latter demanding a more considerable energy amount, as expected.

Finally, the bar chart in Figure 4.21b demonstrates the solar heat gains resulting from the current and optimized control during the event on 24.10.2022. The incoming solar radiation is slightly higher in the existing control due to the high daylight admission, especially around noon. However, the generally low irradiance values result in low differences between the two controls, especially for the meeting and workshop modes, although the blinds are often lowered in the optimized control. In the presentation case, the admitted solar radiation of the optimized strategy is much lower, as desired, leading to low solar heat gains in the building.

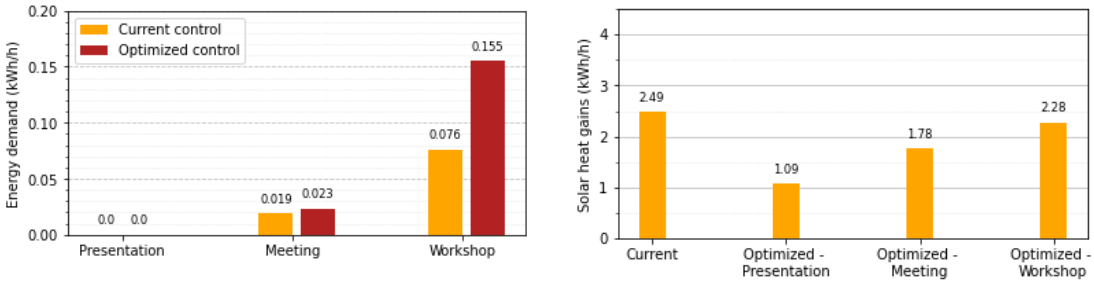

(a) (b)

Figure 4.21: (a) Energy demands for electric lighting resulting from the two control systems for the three activity scenarios on 24.10.2022. (b) Solar heat gains for the current control and the optimized one for the three activity modes on 24.10.2022.

4.4.3. Summary

Comparing the performance of the optimized control algorithm in the two test periods, it is noticed that under low irradiance conditions, which include low glare risks, the algorithm can converge faster/easier to a satisfactory result, especially when there is no direct sunlight. Furthermore, it is evident that variable weather conditions lead to a more erratic operation of the blinds and therefore to larger fluctuations in the provided view quality. In spite of the different blinds' operations between the two analyzed periods, the optimized control results in fairly constant incoming solar radiation in terms of daylight and energy, for all activity types, as the blinds' states are controlled in a way to constantly maintain visual comfort, meeting the requirements for E_{wp} and E_{cyl}. For the same reason, the energy consumption for electric lighting does not differ essentially between the two test periods. The small difference is due to the low solar irradiance during the second, more cloudy, period, which results in less daylight in the indoor space and therefore in a slightly bigger need for electric lighting.

The daylight performance of the developed control algorithm is overall satisfactory, providing visual comfort most of the time for all viewpoints. Figure 4.22 presents the percentage of the time steps of the two test periods where sufficient daylight, zero glare risks and both of them occur for the three activity modes under the two control systems. In terms of daylight adequacy, the current system slightly outperforms the proposed one, but at the cost of glare risks. On the contrary, the optimized algorithm keeps a balance between daylight sufficiency and glare prevention, reducing the time steps with glare risks by an average of 85% in all cases, but increasing the time steps where electric lighting is needed by only 7%, in comparison to the existing control. In total, ideal visual conditions with adequate daylight and zero glare over the space, are achieved at a much higher average percentage of the tested time (80%) than in the current control, with the workshop being the most complex case for the algorithm to converge.

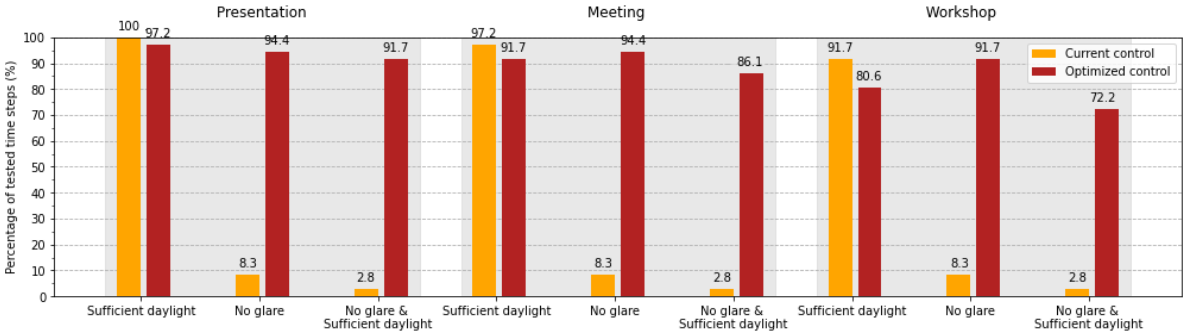

Figure 4.22: Percentage of time steps of the two test periods where sufficient daylight, zero glare risks, and both of them are noted for each of the activity scenarios. Here, the percentages refer to E_{cyl}-based glare assessment.

Regarding the view quality, it is noticed that the current control outperforms the optimized one, as it provides more visual contact with the outdoor environment, by an average of 15% under a clear

sky and 17% when the sky conditions are mostly cloudy. Those percentages are similar but not generalisable, as they depend on the exact weather conditions and the corresponding commands of the control systems. However, they show that the optimized system does not differ extremely from the current situation and provides an overall satisfactory view, although it does not include view-related constraints. As for the solar heat gains of the two control systems during the heating period, no certain conclusions can be drawn, because the differences between them seem small and unstable. However, it is clear that solar heat gains during a session are generally low since both controls prioritize visual comfort.

Finally, the glare assessments by DGP and E_{cyl} were overall similar, reaching a mean agreement percentage of 92.5%. This proves that the *a priori* correlation of the two indices was necessary and was performed thoroughly and correctly, including test periods with various sun conditions.

5

Discussion

5.1. Reflection on results

The developed control strategy for the automatic operation of Venetian blinds was proven generally successful in the complex case of the Co-Creation Center. Despite the difficult assessment of the indoor visual conditions due to the four totally glazed facades, the optimization algorithm managed to prevent glare in the vast majority of the tested time steps, noticeably improving the visual comfort in comparison to the existing control system. Prioritizing glare led to stricter results in terms of daylight quantity in the space and therefore the energy demands for electric lighting were slightly higher than in the current control. The fact that the developed control logic worked effectively in such a complex case as the CCC, suggests that it can be trustfully implemented universally, in similarly complex or common buildings as well, such as office spaces and classrooms.

The time resolution of the validation process was considered high enough, balancing accuracy and total computational time. Besides, a time step of 15 minutes (or less) is usually employed in practice, as within this interval there is no drastic change of external conditions or sun position. Moreover, this frequency of blinds' movements does not cause significant distraction to the occupants. The chosen 20% resolution of blinds' increments was proven beneficial for the provision of visual comfort and the smoothness of blinds' operations. That constitutes an advantage of the proposed control over the existing one, which regulates daylight entry in a less flexible way, as totally raising or lowering the blinds many times during the session would cause high nuisance.

Results indicated that simultaneously operating the blinds of each facade is flexible enough to provide visual comfort in the building, avoiding the high computational effort of a more independent blinds' movement. However, the runtime of 1 hour is still prohibitive for a real-time controller of a shading system that responds instantaneously to sensors' measurements in each time step. Although the scope of the developed control strategy did not explicitly include the short runtime requirement, it should be admitted that its computational cost constitutes a limitation. The long runtime was not related to the algorithm itself, but it was due to *Grasshopper*, which was proved currently unsuitable for point-in-time optimization problems, since the ray-tracing analyses using the *rtrace* command for the point-in-time simulations were noticeably time-consuming. At the same time, although RBFOpt was proved a successful optimization tool for fast convergence, its component in *Grasshopper* (*Opossum*) was rather inconvenient, because it needed manual commencement of the optimization process for each time step. Nevertheless, in real-life control systems, other software with low-level programming languages that accelerate daylight analyses, are generally used.

The outputs of the optimized algorithm were obtained after 20 iterations. This means that the results were not the deterministically optimal ones (global minimum or maximum), but, in most of the cases, they converged and were found to be acceptable. This guarantees that after re-performing the

optimizations, they would generally produce similar results. More iterations might provide a higher probability that the actual best solution is reached, but at the cost of computational time. Of course, reaching the optimal solution does not necessarily imply that the algorithm would converge to a satisfactory result, as this depends on the conditions of the specific time step.

For a few time steps, the control algorithm didn't achieve finding a satisfactory solution. This means that probably more iterations would be needed to facilitate the convergence to a good result, although this is not guaranteed. Results revealed that there wasn't a certain relation between the convergence difficulty and those instances, and thus one cannot easily predict the time step where the algorithm will not converge. This is because the optimization process is not deterministic –if not run for a long time– and there is always a degree of randomness in its iterations. However, the validation process proved that unsuccessful optimizations that resulted in glare or insufficient daylight, occurred with a small average percentage of 16% for the three activity modes. This indicates that the algorithm is reliable with a high possibility to converge to a satisfactory solution.

In terms of glare assessment, E_{cyl} was proven a generally reliable index for the identification of glare risks due to large daylight amounts in the space. However, when the room is mostly dim and solar beams or daylight pass through the louvers, high contrast effects may occur, which are not taken into account by E_{cyl}. Although this constitutes a limitation for the universal use of E_{cyl} as a glare index, its application in complex cases with multiple glare sources (i.e. windows) is encouraged since it can represent well reality most of the time, with low computational effort.

Overall, the results of the present study are considered reliable, as they were obtained using the real sky conditions of the specific location and a high level of detail for the ray-tracing process, thanks to the calibration of the ambient parameters. The accuracy of the results can also be guaranteed by the thorough calibration of the 3D model of the building and its surroundings. Finally, the chosen time periods for the validation of the developed control algorithm, correspond to different scenarios of high global irradiance and weather variations and hence they are considered representative of the daylight performance of the control strategy.

5.2. General comments on control strategies for shading systems

The automatically controlled shading systems implemented in practice aim at the provision of visually comfortable indoor environments to the occupants. The most commonplace way to achieve that is by following rule-based strategies, which are the easiest and most straightforward way to regulate indoor visual conditions. However, smart blinds' operation usually neglects the energy performance of the buildings in terms of heating and cooling, focusing only on daylight.

Over the last decades, research has been implemented on the development of automatic shading controllers that consider both daylight and energy. These control strategies operate the shading system in a way that maintains a visually comfortable environment while minimizing the energy demands for electric lighting, heating and cooling. Nevertheless, multiple studies (Lee, Cho, & Jo, 2021; Le et al., 2022; Yao, 2014) have shown that balancing the daylight and the energy performance of a building, by utilizing one shading system, is a challenging task. In fact, it is proven that it is difficult to improve both visual comfort, thermal comfort and energy consumption simultaneously; the level of improvement in the various performance indicators depends on their order of priority.

The aforementioned conclusions of the literature are supported by the findings of the present study. The investigation of the performance of the optimized control strategy revealed that the solar heat gains do not change essentially when the weather changes and only small amounts of solar gains are admitted. This indicates that the priority of the control to maintain visual comfort when the building is occupied does not allow for large differentiation of the admitted solar radiation depending on the weather conditions. This observation raises concerns about the solar heat gains during the cooling season; as the system operates the blinds always the same way (keeping E_{cyl} and E_{wp} within the desired limits), regardless of the sky conditions, the admitted solar radiation will probably display a constant

trend over the year. Of course, this assumption should be confirmed with extra analyses in the cooling season, as data limitations didn't allow testing summer periods within this study.

The fact that glare-based control systems aim to constantly maintain the same desired visual conditions in the building on a yearly basis, while an energy-based control should adjust its behavior depending on the season, creates an incompatibility between them. This probably explains why the CCC utilizes two modes of shading control, for daylight and thermal performance separately, following a similar approach as Guillemin and Morel (2001). Nevertheless, apart from implementing two control strategies depending on the occupancy periods, a more advanced way to constantly balance daylight entry and heating/cooling demands at the same time is to utilize two shading devices in the same control system. For instance, outdoor Venetian blinds could be operated only for constant solar heat gains regulation, while indoor roller blinds could be applied to provide visual comfort.

6

Conclusion

This Master thesis supported the development of a glare-based control strategy for the automatic operation of Venetian blinds in spaces with multiple daylight sources (i.e. windows). The project was based on the case study of the Co-Creation Center, an event space with four fully glazed facades and variable occupancy patterns depending on the activity (presentation, meeting, workshop). The general aim was to improve the current control in the building, as well as to offer a new control algorithm that can be used universally. The deployed control strategy was steered by a black-box optimization process based on RBFOpt. Within the scope of this research, the performance of cylindrical illuminance (E_{cyl}) as a glare index was additionally assessed.

A parametric model was first created in *Grasshopper* to give the opportunity for adjustments for the investigation of the control's performance in other similar buildings. In order to ensure the reliability of the results of the control algorithm, a number of calibrations had to be initially implemented in the model of the case study. Thus, after setting the *Radiance* parameters and validating the accuracy of the sky model used for the analyses, the geometrical and optical properties of the building and its context were calibrated based on measurements of the building's sensors. Subsequently, the optimized control strategy was devised, aiming at the regulation of daylight admission, maintaining a sufficient amount of daylight in the space for each activity case, while preventing noticeable glare.

The comparison of the overall performance of the optimized and the currently implemented control system yielded results that proved the effectiveness of the developed control. In fact, the latter achieved providing visual comfort (zero glare risks and daylight sufficiency) for the majority of the tested time steps, reaching 92%, 86% and 72% for the presentation, meeting and workshop modes respectively. The priority of the optimized control to prevent glare led to an average increase of 7% in the time steps where electric lighting was needed, in comparison to the current control. In total, results indicated that the optimized algorithm can improve the existing visual conditions in the Co-Creation Center by an average of 80% for all event types. This implies that the effectiveness of the optimized control algorithm can be universal, after performing the necessary calibrations. Nevertheless, the time-consuming visualization tools and ray-tracing process utilized by *Grasshopper* and the inconvenient use of the component *Opossum*, slowed down the optimizations and made their use unsuitable for the real-life implementation of the control strategy. As an optimization tool, RBFOpt worked successfully, providing satisfactory results within a short runtime, and therefore its use is encouraged in complex daylight problems.

As regards the glare assessment, E_{cyl} displayed an overall agreement of 92.5% with DGP, proving that their correlation was done successfully. This indicates that in spaces with multiple windows, and uncertain occupants' view direction, a view-independent index can predict glare risks adequately well, after being carefully correlated with another reliable view-dependent index. However, it was noticed that the disagreement between the two metrics occurred when a high luminance contrast is created by the dim indoor space and the bright incoming daylight. This contrast effect cannot be identified by E_{cyl}, which is based only on the overall vertical illuminance at eye level. Although this constitutes a

limitation for E_{cyl}, its low computational cost and overall good performance support its use for glare evaluations in complex cases, like the Co-Creation Center.

To conclude, this Master thesis managed to offer an overall successful state-of-the-art control strategy for Venetian blinds, based on optimization tools that gain more and more ground in contemporary sustainable architectural designs. The fact that the logic of the control algorithm was effective in such a complex case as the Co-Creation Center, is an optimistic sign for its broad use, in any kind of building geometry and usage. This thesis and other studies have proven the predominance of optimized techniques over rule-based ones improving occupants' visual comfort while keeping energy demands at low levels, and this probably suggests the gradual obsolescence of rule-based methods in the future.

7

Recommendations

This Master thesis highlighted the limitations faced throughout the development of a control strategy for Venetian blinds, based on a model in *Rhino* - *Grasshopper*. To overcome those limitations, lack of time did not allow for further investigation of the tackled topics. Therefore, some recommendations for improvements and further research, as well as for in-practice applications in the future, are pointed out in this chapter.

7.1. Improvements and further research

First and foremost, the calibration process was done manually under multiple weather conditions, by modifying the geometry of the trees, tweaking the optical properties and checking the results step-by-step, in order to achieve small rMBEs. In this way, one can have high control over the process and get a feeling of how the modifications affect the outcome. Therefore, it is generally suggested to perform manual calibrations of a model, at least at the beginning, by using realistic and justifiable values for the input parameters. However, to ensure the validity of the selected optical properties, the manual calibration of the model could generally be supplemented by an algorithm, which can automatically find the optical properties that result in very low rMBEs between the calculations and the measurements. As the influence of the input properties on the results is investigated during the manual part of the calibration, the optical characteristics can be used as variables with certain thresholds-constraints. Having the rMBEs as objectives, the algorithm would then identify the set of variables that minimize them. The deployment of such an algorithm would ensure the validity or the arbitrariness of the manual modifications and would correct them in case of minor or large mistakes.

The validation of the control strategy was implemented for two representative time periods, trying to test its performance under the difficult scenarios of a sunny sky with low solar altitude, as well as of variable weather conditions. Nevertheless, it would be valuable to assess its effectiveness for events' periods spread throughout the year, with various GHI values and solar altitudes (e.g. summer during sunset). In this manner, one can get a more general idea of its behavior under a wide variety of weather conditions. Moreover, testing the algorithm during summer can give insight into its energy performance in the cooling season and thus more robust conclusions can be drawn about the independence of glare-based control systems from weather conditions and their combination with energy-based controls, discussed in chapter 5.2.

This study devised a control strategy, considering indoor visual comfort when the building is occupied. However, more factors affect the occupants' comfort, such as the blinds' movements and view quality. Hence, although the results were overall satisfactory regarding the smoothness of the blinds' operation and the view to the outdoors, including smoothness- and view-related constraints in the algorithm would further improve its performance. Moreover, the Venetian blinds' control system could also include a zero-occupancy mode, where the regulation of the energy performance of the building would

be prioritized, minimizing the energy needs for heating and cooling. An even more demanding task would be the deployment of a control algorithm that combines both daylight and energy control simultaneously, utilizing two shading devices (e.g. Venetian blinds and roller blinds). The investigation of the influence of such control on indoor visual conditions and energy demands would be of great interest.

The main problem identified in the performance of the developed control strategy was the high computational cost that makes *Grasshopper* an inefficient software for that scope due to its time-consuming visualization tools and point-in-time simulations. Improving the overall performance of the parametric software by its developers is a necessity, as this would facilitate the development of a control strategy at least in the design stage. Besides, the real-time control strategy is executed by other, more appropriate programs in real-life applications. Currently, aiming to drastically reduce the runtime, choosing another programming language (e.g. Python, Matlab, C++) would help execute faster the optimization iterations, probably performing more iterations within a shorter time period and thus providing more accurate results. Developing a component that could translate the whole *Grasshopper* script into those programming languages, would facilitate the exploitation of *Grasshopper*'s parametric and visualization skills, as well as the fast optimizations of the control strategy performed by another software. Additionally, using the 5-phase method (either in *Grasshopper* or in another software), would save computational effort, as the light transport in the exterior could be calculated only once throughout the optimization iterations for each time step.

Although *Opossum* is a user-friendly optimization tool, its use is limited by the lack of automation. This issue can be solved by updating *Opossum* component and making it able to connect with other *Grasshopper* components. In particular, *Opossum* should have a *Boolean Toggle* as input, which, when set to *True*, would start the optimization. In this way, within the Python script used to define the objective function, one could automate the optimization process as a loop for each time step of the tested period, setting the *Boolean* to *True* at the beginning of the optimization and to *False* after a certain number of iterations. This method would avoid the need for manual commencement of the optimization process for each time step. In case Python (instead of *Grasshopper*) is employed to speed up the calculations, it is possible to perform RBFOpt using a certain suite of commands (Nannicini, 2021).

7.2. Recommendations for applications in practice

The computational time demanded by the optimization process is prohibitive for its real-time implementation in a real-life control system. Nevertheless, the "optimal" louvers' increments and slat angles decided by the optimization algorithm, can be used for the population of a database, depending on the time step of the year and GHI. Each time step corresponds to a specific day of the year and a certain solar altitude, which, coupled with GHI, are enough to estimate DNI and DHI. In this manner, the shading control implicitly considers both direct and diffuse daylight. The optimization can be performed for every hour of the year and for various GHI values, resulting in the respective blinds' states of all facades. An algorithm can then use the data and, by applying an interpolation method, can determine the blinds' states for time steps and GHI values that are not included in the database.

Based on this algorithm, the control system can be trained via a machine learning approach (reinforcement learning) based on rewards and punishments learned through trials and errors, seeking the maximum reward. More specifically, the trained algorithm will "read" the current time step of the year, as well as the current GHI, and it will decide the blinds' positions. If its decision is close to the training algorithm's imported dataset or interpolation results, the system will be rewarded. The training process is time-consuming and in order to obtain a well-trained control algorithm, the latter should confront a large variety of weather conditions. However, when the system produces correct results and the rewards are maximized, the *training phase* ends and then, the control system starts its normal function (*operational phase*), responding instantly to the new conditions of each time step. A detailed example of such systems was presented by Motamed et al. (2020), although this research focused on a rule-based control strategy that was trained with a supervised learning approach.

With the aforementioned approach, the database doesn't have to include the blinds' positions for a dense time discretization of the year (time step smaller than 1 hour) and for an exhaustive list of GHI values, and thus the needed disk storage is limited. Furthermore, with this technique, the results are independent of a certain meteorological year's GHI, being more flexible towards weather variations. Of course, to ensure a more well-responding blinds' operation by the controller, it is suggested that its training should be repeated in regular maintenance periods. A limitation of the above-described method is its dependence on the digital model of the building that should represent as accurately as possible the real environment. In case of important changes in the model's scene, the correlation between simulation and reality would be compromised.

After applying the developed control algorithm in practice in the CCC, it would be valuable to validate its effectiveness through questionnaires during presentations, meetings and workshops. In this way, it can be seen how the daylight entry is regulated by the shading control in the occupants' interest and comfort, as well as if the natural and electric lighting are well integrated. Besides, occupants' response to a smart control system is the best way to judge its value. If the results are positive, then the logic of the control strategy can be generally applied. Based on the questionnaires, a better assessment of E_{cyl} as a glare index can be done, as this research would prove if E_{cyl} can correspond well to real-life visual conditions perceived by the human eye.

Even though the created *Grasshopper* script is currently inefficient for a control strategy, it can be used to import a *Rhino* model of a building similar to the CCC, and adjust the input parameters to perform the calibration process. For instance, in order to reduce the rMBE between the measurement and calculation for a certain time step, the simulated trees' geometry may need corrections based on that moment's solar altitude. In this example, the ability to visualize the sun position provided by *Rhino-Grasshopper* allows for a better understanding of the scene and sky model, facilitating the manual calibration process. Furthermore, the visualization of results gives a better insight into the visual conditions in the space (e.g. shadows from lowered blinds when direct solar beams pass through them, specific direction where glare occurs for each viewpoint, etc.). Finally, the parametric script in *Grasshopper* can also be used for further design parametric/optimization problems. Such examples would be the implementation of a sensitivity analysis about the effect that the lamellas' geometrical design has on direct solar beams' entry, or a parametric analysis regarding geometrical characteristics of a building (e.g. optimal depth of overhang, optimal height of facade, etc.).

References

Brembilla, E. (2021). *Solar radiation analysis for the Converge project*. Tech. rep.

— (2022a). *Analysis on glare discomfort in the CCC*. Tech. rep.

— (2022b). *Analysis on the electric lighting control in the CCC*. Tech. rep.

Brembilla, E., C. J. Hopfe, and J. Mardaljevic (May 2018). "Influence of input reflectance values on climate-based daylight metrics using sensitivity analysis". In: *Journal of Building Performance Simulation* 11.3, pp. 333–349.

Brembilla, E. et al. (2017). "Inter-model Comparison of Five Climate-Based Daylight Modelling Techniques: Redirecting Glazing/Shading Systems". In: *Building Simulation Conference 2017*.

Brembilla, E. et al. (Nov. 2019). "Evaluation of climate-based daylighting techniques for complex fenestration and shading systems". In: *Energy and Buildings* 203.

Bueno, B. et al. (May 2015). "Fener: A Radiance-based modelling approach to assess the thermal and daylighting performance of complex fenestration systems in office spaces". In: *Energy and Buildings* 94, pp. 10–20.

Carlucci, S. et al. (Aug. 2015). "A review of indices for assessing visual comfort with a view to their use in optimization processes to support building integrated design". In: *Renewable and Sustainable Energy Reviews* 47, pp. 1016–1033.

Chan, Y. C. and A. Tzempelikos (2013). "Efficient venetian blind control strategies considering daylight utilization and glare protection". In: *Solar Energy* 98.PC, pp. 241–254.

Čongradac, V. et al. (Sept. 2012). "Algorithm for blinds control based on the optimization of blind tilt angle using a genetic algorithm and fuzzy logic". In: *Solar Energy* 86.9, pp. 2762–2770.

Duff, J. T. (2012). "Code for Lighting: the Impact on Design and Commissioning". In: *SDAR* Journal of Sustainable Design & Applied Research* 1.2.

Eltaweel, A. and Y. Su (Mar. 2017). "Controlling venetian blinds based on parametric design; via implementing Grasshopper's plugins: A case study of an office building in Cairo". In: *Energy and Buildings* 139, pp. 31–43.

Forrester, A., A. Sobester, and A. Keane (July 2008). *Engineering Design via Surrogate Modelling: A Practical Guide*. Chichester, UK: Wiley, J.

Giovannini, L. et al. (Dec. 2020). "GLANCE (GLare ANnual Classes Evaluation): An approach for a simplified spatial glare evaluation". In: *Building and Environment* 186.

Guillemin, A. and N. Morel (2001). "An innovative lighting controller integrated in a self-adaptive building control system". In: *Energy and Buildings*.

Gunay, H. B. et al. (Jan. 2014). "On adaptive occupant-learning window blind and lighting controls". In: *Building Research and Information* 42.6, pp. 739–756.

Gunay, H. B. et al. (Feb. 2017). "Development and implementation of an adaptive lighting and blinds control algorithm". In: *Building and Environment* 113, pp. 185–199.

Hewitt, H., D. J. Bridgers, and R. H. Simons (1965). "Lighting and the Environment: Some Studies in Appraisal and Design". In: *Transactions of the Illuminating Engineering Society*.

Hirning, M. B., G. L. Isoardi, and I. Cowling (Feb. 2014). "Discomfort glare in open plan green buildings". In: *Energy and Buildings* 70, pp. 427–440.

Jakubiec, J A. and C. F. Reinhart (2012a). *Overview and Introduction to DAYSIM and Current Research Developments*. Tech. rep. Massachusetts Institute of Technology.

Jakubiec, J. A. (2022). "Data-Driven Selection of Typical Opaque Material Reflectances for Lighting Simulation". In: *LEUKOS - Journal of Illuminating Engineering Society of North America*.

Jakubiec, J. A. and C. F. Reinhart (2012b). "The 'adaptive zone'-A concept for assessing discomfort glare throughout daylit spaces". In: *Lighting Research and Technology* 44.2, pp. 149–170.

Jones, D. R. (2001). "Direct Global Optimization Algorithm". In: *Encyclopedia of Optimization*. Ed. by C. A. Floudas and P. M. Pardalos. Boston, MA: Springer US, pp. 431–440.

Kharvari, F. (Sept. 2020). “An empirical validation of daylighting tools: Assessing radiance parameters and simulation settings in Ladybug and Honeybee against field measurements”. In: *Solar Energy* 207, pp. 1021–1036.

Konstantoglou, M. and A. Tsangrassoulis (July 2016). “Dynamic operation of daylighting and shading systems: A literature review”. In: *Renewable and Sustainable Energy Reviews* 60, pp. 268–283.

Konstantzos, I. and A. Tzempelikos (2014). “Daylight Glare Probability Measurements And Correlation With Indoor Illuminances In A Full-Scale Office With Dynamic Shading Controls”. In: *3rd International High Performance Buildings Conference*.

Konstantzos, I., A. Tzempelikos, and Y. C. Chan (May 2015). “Experimental and simulation analysis of daylight glare probability inoffices with dynamic window shades”. In: *Building and Environment* 87, pp. 244–254.

Le, D. M. et al. (Sept. 2022). “Multi-criteria decision making for adaptive façade optimal design in varied climates: Energy, daylight, occupants’ comfort, and outdoor view analysis”. In: *Building and Environment* 223.

Lee, D., Y. H. Cho, and J. H. Jo (Mar. 2021). “Assessment of control strategy of adaptive façades for heating, cooling, lighting energy conservation and glare prevention”. In: *Energy and Buildings* 235.

Mahdavi, A. (Mar. 2008). “Predictive simulation-based lighting and shading systems control in buildings”. In: *Building Simulation* 1.1, pp. 25–35.

Mardaljevic, J et al. (2012). “Daylighting Metrics: Is there a relation between Useful Daylight Illuminance and Daylight Glare Probability?” In: *First Building Simulation and Optimization Conference*.

Mardaljevic, J. (2000). “Daylight Simulation: Validation, Sky Models and Daylight Coefficients”. PhD thesis. Loughborough University, UK.

— (2006). “Examples of Climate-Based Daylight Modelling”. In: *CIBSE National Conference 2006: Engineering the Future*.

Mardaljevic, John (1995). “Validation of a lighting simulation program under real sky conditions”. In: *Lighting Research and Technology*.

McNeil, A. et al. (Dec. 2013). “A validation of a ray-tracing tool used to generate bi-directional scattering distribution functions for complex fenestration systems”. In: *Solar Energy* 98.PC, pp. 404–414.

Mecanoo (n.d.). *Co-Creation Centre and Nonohouse*. URL: `https://www.mecanoo.nl/Projects/project/261/Co-Creation-Centre-and-Nonohouse`.

Motamed, A. et al. (Mar. 2020). “Self-commissioning glare-based control system for integrated venetian blind and electric lighting”. In: *Building and Environment* 171.

Nabil, A. and J. Mardaljevic (July 2006). “Useful daylight illuminances: A replacement for daylight factors”. In: *Energy and Buildings* 38.7, pp. 905–913.

Naderi, E. et al. (Feb. 2020). “Multi-objective simulation-based optimization of controlled blind specifications to reduce energy consumption, and thermal and visual discomfort: Case studies in Iran”. In: *Building and Environment* 169.

Nagy, Zoltán et al. (May 2015). “Occupant centered lighting control for comfort and energy efficient building operation”. In: *Energy and Buildings* 94, pp. 100–108.

Nannicini, G. (Feb. 2021). *RBFOpt user manual*. Tech. rep. NY: IBM T.J. Watson.

Nassar, A. et al. (2003). “Cylindrical illuminance and its importance in integrating daylight with artificial light”. In: *Lighting Research and Technology* 35.3, pp. 217–222.

NEN-EN 17037 (2018). “Natural lighting of buildings – Assessment of daylight in buildings”. *CEN (European Committee for Standardization)*.

Nielsen, M. V., S. Svendsen, and L. B. Jensen (May 2011). “Quantifying the potential of automated dynamic solar shading in office buildings through integrated simulations of energy and daylight”. In: *Solar Energy* 85.5, pp. 757–768.

Osterhaus, W. K.E. (Aug. 2005). “Discomfort glare assessment and prevention for daylight applications in office environments”. In: *Solar Energy*. Vol. 79. 2, pp. 140–158.

Reindl, D. T., W. A. Beckman, and J. A. Duffie (1990). *DIFFUSE FRACTION CORRELATIONS*. Tech. rep. Solar Energy Laboratory, University of Wisconsin-Madison, p. 7.

Saint-Gobain (2019). *Calumen III 1.8*. Tech. rep.

Skartveit, A. and J. A. Olseth (1987). “A MODEL FOR THE DIFFUSE FRACTION OF HOURLY GLOBAL RADIATION”. In: *Solar Energy* 38.4, pp. 271–274.

Subramaniam, S. (Oct. 2017). *Daylighting Simulations with Radiance using Matrix-based Methods*. Tech. rep. Berkeley Lab.

Suk, J. and M. Schiler (2013). "Investigation of Evalglare software, daylight glare probability and high dynamic range imaging for daylight glare analysis". In: *Lighting Research and Technology* 45.4, pp. 450–463.

Talbi, E. G. (2009). *Metaheuristics: from design to implementation*. Wiley, J., p. 593.

Torres, S. and V. R.M. Lo Verso (Nov. 2015). "Comparative analysis of simplified daylight glare methods and proposal of a new method based on the cylindrical illuminance". In: *Energy Procedia*. Vol. 78. Elsevier Ltd, pp. 699–704.

Van den Engel, P. et al. (2022). "CONVERGE: Low energy with active passiveness in a transparent highly occupied building". In: *REHVA 14th HVAC World Congress*. Vol. 111.

Velux (Apr. 2022). *Optimaal wooncomfort met de nieuwe standaard glaseigenschappen van VELUX dakramen*. Tech. rep.

Vos, J. J. (1984). "Disability Glare: a State of the Art Report". In: *Commission Int. de l' Eclairage*, pp. 39–53.

Wagdy, A. and F. Fathy (July 2015). "A parametric approach for achieving optimum daylighting performance through solar screens in desert climates". In: *Journal of Building Engineering* 3, pp. 155–170.

Wang, Y., Y. Weibin, and Q. Wang (Nov. 2022). "Multi-objective parametric optimization of the composite external shading for the classroom based on lighting, energy consumption, and visual comfort". In: *Energy and Buildings* 275.

Wassink, J. (Apr. 2018). *The Green Village plans self-sufficient glass hall*. URL: `https://www.delta.tudelft.nl/article/green-village-plans-self-sufficient-glass-hall#`.

Wienold, J. (July 2009). "DYNAMIC DAYLIGHT GLARE EVALUATION". In: *Eleventh International IBPSA Conference*.

Wienold, J. and J. Christoffersen (July 2006). "Evaluation methods and development of a new glare prediction model for daylight environments with the use of CCD cameras". In: *Energy and Buildings* 38.7, pp. 743–757.

Wienold, J. et al. (Nov. 2019). "Cross-validation and robustness of daylight glare metrics". In: *Lighting Research and Technology* 51.7, pp. 983–1013.

Wortmann, T. (2017). "Model-based Optimization for Architectural Design: Optimizing Daylight and Glare in Grasshopper". In: *Technology Architecture and Design* 1.2, pp. 176–185.

Wortmann, T. et al. (May 2017). "Are Genetic Algorithms Really the Best Choice in Building Energy Optimization?" In.

Si-X (2021). *Co-Creation Centre op The Green Village Delft*. URL: `https://si-x.nl/project/co-creation-centre-op-the-greenvillage-delft/`.

Xiong, J. and A. Tzempelikos (Sept. 2016). "Model-based shading and lighting controls considering visual comfort and energy use". In: *Solar Energy* 134, pp. 416–428.

Xiong, J. et al. (June 2019). "A personalized daylighting control approach to dynamically optimize visual satisfaction and lighting energy use". In: *Energy and Buildings* 193, pp. 111–126.

Yao, J. (Jan. 2014). "An investigation into the impact of movable solar shades on energy, indoor thermal and visual comfort improvements". In: *Building and Environment* 71, pp. 24–32.

Zhang, S. and D. Birru (Mar. 2012). "An open-loop venetian blind control to avoid direct sunlight and enhance daylight utilization". In: *Solar Energy* 86.3, pp. 860–866.

A

Appendix

A.1. In-situ Measurements

Table A.1 lists the measured luminance (L) and illuminance (E) of various opaque surfaces in the CCC and its context. Based on these values, their reflectance (ρ) is computed using equation 3.1. The average value is imported into the model.

Table A.1: Field measurements and reflectance calculations for opaque surfaces.

	L (cd/m^2)	E (lx)	ρ (%)
Floor	6.63	860	2.4
	13.9	1247	3.5
	9.89	1049	3.0
	11.34	1096	3.3
Frames	4.68	533	2.8
	4.88	583	2.6
	6.56	694	3.0
Venetian blinds	30.35	2720	3.5
	60.66	4750	4.0
	69	5290	4.1
Sill	370	4200	27.7
	380	4350	27.4
	1090	6140	55.8
Climate tower	3.75	1095	1.1
	3.61	1111	1.0
	4.18	1125	1.2
Pavement	616	8310	23.3
	530	7780	21.4
	510	8250	19.4
Dark-colored walls of surrounding buildings	83.6	6550	4.0
	91.3	7260	4.0
	90.4	7340	3.9
Light-colored walls of surrounding buildings	171	6590	8.2
	173	7910	6.9
	195	7530	8.1

Table A.2 lists the iterative measurements of the vertical indoor and outdoor illuminance ($E_{v,in}$, $E_{v,out}$) of the window panes and the doors of the CCC. These values are used for the calculation of

the transmittance (τ) of the glazings using equation 3.2. Again, the average value is imported into the model.

Table A.2: Field measurements and transmittance calculations for facades' windows and doors.

	$E_{v,in}$ (lx)	$E_{v,out}$ (lx)	τ (%)
Facades' windows	2360	3630	65.0
	2405	3920	61.4
	2250	3860	58.3
	3160	5100	62.0
Facades' doors	5130	6600	77.7
	4320	5350	80.7

A.2. Model Calibration Details

A.2.1. Calibration of ambient parameters

Tables A.3 and A.4 present the iterations done for the step-by-step calibration of the ambient parameters for blinds up and down. The tables detail the calculated values of $E_{middle,wp}$ for different sets of rendering parameters, by gradually increasing the resolution of the ray-tracing process.

Table A.3: Calibration of ambient parameters for blinds up.

Blinds up							
Iteration	-ab	-aa	-ar	-ad	-as	$E_{middle,wp}$	Error
1	1	0.4	8	32	16	317.13	
2	1	0.4	8	64	32	170.2	-0.463
3	1	0.4	8	128	64	232.81	0.368
4	1	0.4	8	256	128	276.37	0.187
5	1	0.4	8	512	256	284.76	0.030
6	1	0.4	8	1024	512	227.02	-0.203
7	1	0.4	8	2048	1024	284.07	0.251
8	1	0.4	8	**4096**	**2048**	268.77	-0.054
9	1	0.4	8	8192	4096	278.89	0.038
1	1	0.4	8	4096	2048	292.67	
2	1	0.4	16	4096	2048	265.15	-0.094
3	1	0.4	32	4096	2048	304.71	0.149
4	1	0.4	**64**	4096	2048	281.36	-0.077
5	1	0.4	128	4096	2048	273.46	-0.028
6	1	0.4	256	4096	2048	289.12	0.057
1	1	0.4	64	4096	2048	281.41	
2	1	**0.2**	64	4096	2048	283.64	0.008
3	1	0.1	64	4096	2048	278.02	-0.020
4	1	0.05	64	4096	2048	285.76	0.028
1	1	0.2	64	4096	2048	285.37	
2	2	0.2	64	4096	2048	287.63	0.008
3	3	0.2	64	4096	2048	285.55	-0.007
4	4	0.2	64	4096	2048	281.22	-0.015
5	**5**	0.2	64	4096	2048	283.84	0.009
6	6	0.2	64	4096	2048	287.62	0.013
7	7	0.2	64	4096	2048	291.34	0.013
8	8	0.2	64	4096	2048	282.59	-0.030

The lowest values that clearly lead to an error of less than 10% are chosen as final parameters (bold

values). Exceptionally, in order to be on the safe side, -ab = 5 is chosen even though lower values result in low errors.

Table A.4: Calibration of ambient parameters for blinds down with horizontal slats.

Blinds down - Horizontal slats							
Iteration	-ab	-aa	-ar	-ad	-as	$E_{middle,wp}$	Error
1	1	0.4	8	32	16	17.94	
2	1	0.4	8	64	32	126.71	6.063
3	1	0.4	8	128	64	101.56	-0.198
4	1	0.4	8	256	128	213.26	1.100
5	1	0.4	8	512	256	143.91	-0.325
6	1	0.4	8	1024	512	220.67	0.533
7	1	0.4	8	2048	1024	206.99	-0.062
8	1	0.4	8	**4096**	**2048**	190.53	-0.080
9	1	0.4	8	8192	4096	182.7	-0.041
1	1	0.4	8	4096	2048	204.43	
2	1	0.4	16	4096	2048	196.49	-0.039
3	1	0.4	32	4096	2048	191.92	-0.023
4	1	0.4	**64**	4096	2048	198.24	0.033
5	1	0.4	128	4096	2048	186.09	-0.061
6	1	0.4	256	4096	2048	207.62	0.116
1	1	0.4	64	4096	2048	199.48	
2	1	**0.2**	64	4096	2048	187.46	-0.060
3	1	0.1	64	4096	2048	203.4	0.085
4	1	0.05	64	4096	2048	175.47	-0.137
1	1	0.2	64	4096	2048	194.35	
2	2	0.2	64	4096	2048	187.8	-0.034
3	3	0.2	64	4096	2048	196.75	0.048
4	4	0.2	64	4096	2048	198.99	0.011
5	**5**	0.2	64	4096	2048	193.33	-0.028
6	6	0.2	64	4096	2048	186.82	-0.034
7	7	0.2	64	4096	2048	174.37	-0.067
8	8	0.2	64	4096	2048	191.04	0.096

A.2.2. Calibration of optical properties

Tables A.5, A.6 and A.7 broadly describe the logic followed for the calibration of the optical properties of the ground, the canal and the trees for all test days. On the other hand, the calibration process for the CCC's materials is demonstrated in Tables A.8, A.9, A.10, A.11 and A.12. To discover the sets of properties that produce the desired results for the two calibrations, many trials were done, composing an exhaustive procedure. For reasons of simplicity, the most determinant iterations are presented in the tables. The rMBEs steer the whole process for each case and based on them, the optical properties for the next step of the calibration are decided. The aim is to minimize the rMBEs as much as possible, allowing a maximum value of 20% for the first calibration and 30% for the second one. The decision-making process is written in the last row of the tables. The columns "Calculation 0" of the tables refer to the initially imported optical properties.

Calibration of context materials' properties

This calibration was performed for three days: an overcast day (24.12.2022), a sunny with high solar altitude (09.07.2022) and a sunny day with low solar altitude (02.10.2022). The latter was chosen as the starting point of the process, as it would determine the geometry of the trees. However, it should be clear that the calibration was not a linear process and at some point, it was done for the three days in parallel, considering how a modification in the optical properties would affect the results of all days simultaneously.

Table A.5: Calibration of ground, canal and trees properties for a sunny day with low solar altitude.

	Sunny day with low solar altitude (09.07.2022) – E_v (lx)														
	Measurements			Calculation 0 ρ_{gr}=0.2 ρ_{can}=0.5 τ_{tr}=0.1			Calculation 1 (extra trees) ρ_{gr}=0.2 ρ_{can}=0.3 τ_{tr}=0.1			Calculation 2 (extra trees) ρ_{gr}=0.3 ρ_{can}=0.2 τ_{tr}=0.1			Calculation 3 (extra trees) ρ_{gr}=0.25 ρ_{can}=0.3 τ_{tr}=0.1		
Hour	West	South	East	West	South	East	West	South	East	West	South	East	West	South	East
0.00	0	0	35.8	0	0	0	0	0	0	0	0	0	0	0	0
1.00	0	5.83	39.2	0	0	0	0	0	0	0	0	0	0	0	0
2.00	0	8.33	25	0	0	0	0	0	0	0	0	0	0	0	0
3.00	0	0	34.2	0	0	0	0	0	0	0	0	0	0	0	0
4.00	0	0	35	0	0	0	0	0	0	0	0	0	0	0	0
5.00	0	2.5	59.2	0	0	0	0	0	0	0	0	0	0	0	0
6.00	5	47.5	113	0	0	0	0	0	0	0	0	0	0	0	0
7.00	914	2730	3610	0	0	0	0	0	0	0	0	0	0	0	0
8.00	2630	7900	9510	2632	20337	22456	2293	6415	7786	2349	6659	8176	2452	17476	20833
9.00	1850	16100	14700	4878	32680	26169	4334	13909	12203	4466	14515	12809	4534	27631	24801
10.00	6320	39800	20900	7569	49660	28870	6464	45100	22408	6448	45934	24307	6728	48457	25907
11.00	9080	35800	16500	9772	48041	22095	8408	44306	13915	8271	45169	17149	8582	46661	17458
12.00	27600	55000	15400	16903	55097	19090	15436	50938	11421	15469	51927	14896	15755	52903	14630
13.00	34800	72200	18700	48288	92365	18202	47258	87369	13598	47569	89385	18239	47750	89495	17189
14.00	7450	51000	16200	10327	63971	12184	9922	59282	10110	9950	60599	11966	9893	60811	10970
15.00	6980	19400	10300	9243	19492	9379	8790	16364	8437	8787	16667	9213	8890	17200	8840
16.00	4580	4760	5280	2756	3938	3850	2503	3326	3555	2513	3535	3794	2565	3666	3689
17.00	1270	2090	2730	1387	1978	1973	1267	1673	1821	1265	1775	1949	1293	1847	1893
18.00	90.8	205	302	556	826	811	526	592	708	531	623	736	536	685	706
19.00	0	0	27.5	0	0	0	0	0	0	0	0	0	0	0	0
20.00	0	0	44.2	0	0	0	0	0	0	0	0	0	0	0	0
21.00	0	0	15	0	0	0	0	0	0	0	0	0	0	0	0
22.00	0	0	42.5	0	0	0	0	0	0	0	0	0	0	0	0
23.00	0	0	65.8	0	0	0	0	0	0	0	0	0	0	0	0
rMBE	-	-	-	0.104	0.265	0.227	0.035	0.072	-0.213	0.039	0.097	-0.085	0.052	0.195	0.091
R^2	-	-	-	0.877	0.969	0.833	0.862	0.983	0.949	0.861	0.983	0.963	0.864	0.967	0.848
Comments	-			Aim to reduce the South and East sensors' calculations: add extra trees to the South-West and to the East and reduce ρ_{can}			Aim to increase the East sensor's calculations, but not the West and South ones: increase ρ_{gr} and reduce ρ_{can}			Good results			Final results with changed properties due to the other two days' calibrations		

Table A.6: Calibration of ground, canal and trees properties for an overcast day.

	Overcast day (24.12.2022) – E_v (lx)														
	Measurements			Calculation 0 ρ_{gr}=0.2 ρ_{can}=0.5 τ_{tr}=0.1			Calculation 1 (extra trees) ρ_{gr}=0.3 ρ_{can}=0.2 τ_{tr}=0.7			Calculation 2 (extra trees) ρ_{gr}=0.25 ρ_{can}=0.3 τ_{tr}=0.7			Calculation 3 (extra trees) ρ_{gr}=0.25 ρ_{can}=0.3 τ_{tr}=0.8		
Hour	West	South	East	West	South	East	West	South	East	West	South	East	West	South	East
0.00	14.2	0	75	0	0	0	0	0	0	0	0	0	0	0	0
1.00	3.33	0	88.3	0	0	0	0	0	0	0	0	0	0	0	0
2.00	2.5	1.67	91.7	0	0	0	0	0	0	0	0	0	0	0	0
3.00	5.83	2.5	85	0	0	0	0	0	0	0	0	0	0	0	0
4.00	15.8	0	64.2	0	0	0	0	0	0	0	0	0	0	0	0
5.00	0	0	75.8	0	0	0	0	0	0	0	0	0	0	0	0
6.00	0	0	90	0	0	0	0	0	0	0	0	0	0	0	0
7.00	0	0	94.2	0	0	0	0	0	0	0	0	0	0	0	0
8.00	22.5	59.2	180	0	0	0	0	0	0	0	0	0	0	0	0
9.00	886	1680	1710	0	0	0	0	0	0	0	0	0	0	0	0
10.00	1620	2710	2650	1778	10519	5346	1098	9817	4991	2136	10332	5244	2455	10396	5297
11.00	4570	17800	5360	3032	14629	6007	3535	13667	5740	3656	14217	5926	4192	14343	6005
12.00	7470	20800	6060	5959	21979	6860	5789	20663	6782	6973	21269	6819	7740	21356	6911
13.00	8520	20700	6410	4549	19249	6238	6503	17495	6217	6629	18166	6196	8090	18200	6262
14.00	7820	14900	6210	4092	16040	5419	5928	11348	5383	6034	12019	5324	7763	12762	5399
15.00	5850	6390	4030	2814	11386	4049	4575	6785	3962	4614	7136	3920	6464	8058	3994
16.00	432	488	523	845	1917	1361	1477	1700	1341	1478	1816	1321	2017	1942	1348
17.00	0	0.833	83.3	0	0	0	0	0	0	0	0	0	0	0	0
18.00	0	0	102	0	0	0	0	0	0	0	0	0	0	0	0
19.00	0	2.5	102	0	0	0	0	0	0	0	0	0	0	0	0
20.00	4.17	0	80	0	0	0	0	0	0	0	0	0	0	0	0
21.00	0	0.833	73.3	0	0	0	0	0	0	0	0	0	0	0	0
22.00	4.17	0	95.8	0	0	0	0	0	0	0	0	0	0	0	0
23.00	1.67	0	45.8	0	0	0	0	0	0	0	0	0	0	0	0
rMBE	-	-	-	-0.381	0.119	0.026	-0.223	-0.047	0.001	-0.154	-0.007	0.011	0.040	0.018	0.024
R^2	-	-	-	0.935	0.915	0.915	0.974	0.922	0.925	0.973	0.922	0.916	0.976	0.922	0.916
Comments	-			Aim to increase the West sensor's calculations: increase τ_{tr} and make the modifications that led to good results previously			Aim to increase the West sensor: increase ρ_{can} & decrease ρ_{gr} due to the calibration of the sunny day with high solar altitude			Aim to increase the West sensor: increase τ_{tr}			Final results		

Table A.7: Calibration of ground, canal and trees properties for a sunny day with high solar altitude.

	Sunny day with high solar altitude (09.07.2022) – E_v (lx)											
	Measurements			Calculation 0 ρ_{gr}=0.2 ρ_{can}=0.5 τ_{tr}=0.1			Calculation 1 (extra trees) ρ_{gr}=0.3 ρ_{can}=0.3 τ_{tr}=0.1			Calculation 2 (extra trees) ρ_{gr}=0.25 ρ_{can}=0.3 τ_{tr}=0.1		
Hour	West	South	East	West	South	East	West	South	East	West	South	East
0.00	0	191	16.7	0	0	0	0	0	0	0	0	0
1.00	0	186	24.2	0	0	0	0	0	0	0	0	0
2.00	0	168	16.7	0	0	0	0	0	0	0	0	0
3.00	0	177	25	0	0	0	0	0	0	0	0	0
4.00	9.09	220	77.3	0	0	0	0	0	0	0	0	0
5.00	577	1580	3480	1171	2110	12664	1148	1740	12512	1095	1833	4815
6.00	1900	6180	17500	2619	5740	22043	2553	4692	21498	2421	4933	10476
7.00	3840	15400	31300	4754	14690	38423	4620	12583	37232	4442	13240	34050
8.00	5260	16300	23600	6200	18789	30530	5955	15934	28609	5707	17663	27742
9.00	7600	33400	38400	9294	40147	53651	8742	36613	51513	8308	39296	51599
10.00	8820	40500	38000	12051	46433	43970	10824	43751	42824	10505	45693	42900
11.00	11200	53400	32800	14437	69980	39665	12250	69408	40955	11694	61690	39815
12.00	15500	34700	22700	16399	42243	22434	15002	40464	22652	14730	41307	21931
13.00	34200	44000	20700	34750	58965	16388	32632	58471	18408	32307	53414	16768
14.00	34200	27800	17400	34098	36683	16885	33470	35316	17981	33073	35688	16738
15.00	60800	19300	15800	56750	29821	14721	56579	29079	16101	56254	28924	14636
16.00	59600	11500	13200	55363	15285	12752	55121	14393	13589	54855	14613	12511
17.00	10800	8640	12000	15273	12624	11668	14970	11122	11722	14874	11678	11086
18.00	7190	6720	8660	10691	8639	8581	10389	7392	8395	10262	8002	8039
19.00	10700	4280	5550	6447	5082	5349	6309	4219	5111	6172	4623	4922
20.00	2020	1430	1660	1557	1972	2099	1500	1775	2080	1478	1866	2001
21.00	8.33	233	62.5	0	0	0	0	0	0	0	0	0
22.00	0	154	2.5	0	0	0	0	0	0	0	0	0
23.00	0	152	15	0	0	0	0	0	0	0	0	0
rMBE	-	-	-	0.028	0.253	0.161	-0.008	0.185	0.159	-0.022	0.177	0.056
R^2	-	-	-	0.987	0.989	0.952	0.991	0.981	0.965	0.991	0.990	0.957
Comments	-			Make the modifications that led to good results in the two previous calibrations			Aim to decrease the South & East sensor: decrease ρ_{gr}			Final results		

Calibration of building materials' properties

This calibration is done for two days, under overcast sky (24.12.2022) and under clear sky (02.10.2022). The calibration of the materials' properties inside the CCC is a demanding process, since the illuminance values of nine sensors for two days have to be simultaneously correlated with the corresponding measurements. The overcast day is chosen as a starting point, because the daylight hours are few and thus the simulations demanded a shorter time. In the second row of the tables, only the materials' properties that are eventually changed, are written. It should be noted that the increase in the optical properties in "Calculation 1" of Table A.9 was initially implemented step-by-step, by modifying one material's properties at a time.

Table A.8: Calibration of building materials' properties for an overcast day (Part A).

	Overcast day (24.12.2022) – $E_{ceiling}$ (lx)																	
	Measurements									Calculation 0 $\tau_{windows}$=τ_{fins}=0.60 $\tau_{skylights}$=0.65 ρ_{floor}=$\rho_{ceiling}$=0.03 ρ_{frames}=0.03								
Hour	NE	N	NW	E	M	W	SE	S	SW	NE	N	NW	E	M	W	SE	S	SW
0.00	1	1	1	1	1	1	1	1	1	0	0	0	0	0	0	0	0	0
1.00	1	1	1	1	1	1	1	1	1	0	0	0	0	0	0	0	0	0
2.00	1	1	1	1	1	1	1	1	1	0	0	0	0	0	0	0	0	0
3.00	1	1	1	1	1	1	1	1	1	0	0	0	0	0	0	0	0	0
4.00	1	1	1	1	1	1	1	1	1	0	0	0	0	0	0	0	0	0
5.00	1	1	1	1	1	1	1	1	1	0	0	0	0	0	0	0	0	0
6.00	1	1	1	1	1	1	1	1	1	0	0	0	0	0	0	0	0	0
7.00	1	1	1	1	1	1	1	1	1	0	0	0	0	0	0	0	0	0
8.00	3.25	4.5	3.08	3.17	3.83	3.08	3.17	3.67	2.58	0	0	0	0	0	0	0	0	0
9.00	41.5	60.3	45.7	32	25.8	33.3	50.1	46.3	32.3	0	0	0	0	0	0	0	0	0
10.00	64.2	95.6	74.9	48.4	38	54.6	77.3	69.7	51	45.8	50.6	54.2	43.1	45.3	48.4	60.7	55.6	53.6
11.00	173	255	201	175	188	188	238	242	165	77.9	83.5	84.2	80.3	80.9	78.5	106.9	99.0	88.9
12.00	185	282	233	207	167	210	337	293	196	101.2	103.5	119.3	112.6	109.9	107.0	165.7	146.9	128.5
13.00	187	367	286	153	157	223	269	234	186	85.0	92.2	104.8	80.0	81.3	88.4	124.5	106.0	98.5
14.00	205	341	264	143	159	215	204	192	166	81.6	83.0	97.8	66.5	71.4	80.3	101.1	87.8	87.3
15.00	142	239	199	93.5	102	155	143	143	144	61.8	65.2	75.0	50.0	55.1	63.6	63.1	59.6	62.0
16.00	12.8	21.3	17.4	9.08	8.33	12.7	14.7	13.9	11.5	18.2	18.4	20.8	13.7	14.8	16.8	19.0	16.5	16.8
17.00	1	1	1	1	1	1	1	1	1	0	0	0	0	0	0	0	0	0
18.00	1	1	1	1	1	1	1	1	1	0	0	0	0	0	0	0	0	0
19.00	1	1	1	1	1	1	1	1	1	0	0	0	0	0	0	0	0	0
20.00	1	1	1	1	1	1	1	1	1	0	0	0	0	0	0	0	0	0
21.00	1	1	1	1	1	1	1	1	1	0	0	0	0	0	0	0	0	0
22.00	1	1	1	1	1	1	1	1	1	0	0	0	0	0	0	0	0	0
23.00	1	1	1	1	1	1	1	1	1	0	0	0	0	0	0	0	0	0
rMBE	-	-	-	-	-	-	-	-	-	-0.542	-0.705	-0.585	-0.492	-0.469	-0.565	-0.526	-0.544	-0.448
R^2	-	-	-	-	-	-	-	-	-	0.955	0.933	0.948	0.967	0.930	0.950	0.975	0.967	0.950
Comments	-									Aim to significantly increase all sensors' calculations: gradually increase materials' properties that affect all sensors								

Table A.9: Calibration of building materials' properties for an overcast day (Part B).

	Overcast day (24.12.2022) – $E_{ceiling}$ (lx)																	
	Calculation 1 $\tau_{windows}$=τ_{fins}=0.65 $\tau_{skylights}$=0.80 ρ_{floor}=$\rho_{ceiling}$=0.30 ρ_{frames}=0.08									Calculation 2 $\tau_{windows}$=τ_{fins}=0.68 $\tau_{skylights}$=0.80 ρ_{floor}=$\rho_{ceiling}$=0.40 ρ_{frames}=0.08								
Hour	NE	N	NW	E	M	W	SE	S	SW	NE	N	NW	E	M	W	SE	S	SW
0.00	0	0	0	0	0	0	0	0	0	0	0	0	0	0	0	0	0	0
1.00	0	0	0	0	0	0	0	0	0	0	0	0	0	0	0	0	0	0
2.00	0	0	0	0	0	0	0	0	0	0	0	0	0	0	0	0	0	0
3.00	0	0	0	0	0	0	0	0	0	0	0	0	0	0	0	0	0	0
4.00	0	0	0	0	0	0	0	0	0	0	0	0	0	0	0	0	0	0
5.00	0	0	0	0	0	0	0	0	0	0	0	0	0	0	0	0	0	0
6.00	0	0	0	0	0	0	0	0	0	0	0	0	0	0	0	0	0	0
7.00	0	0	0	0	0	0	0	0	0	0	0	0	0	0	0	0	0	0
8.00	0	0	0	0	0	0	0	0	0	0	0	0	0	0	0	0	0	0
9.00	0	0	0	0	0	0	0	0	0	0	0	0	0	0	0	0	0	0
10.00	78.6	88.1	92.7	75.0	79.4	82.3	99.8	97.9	90.6	127.0	146.2	148.6	118.7	131.3	134.7	164.7	157.6	141.5
11.00	131.5	140.7	141.9	133.9	140.4	133.3	175.8	170.3	149.2	218.1	240.6	224.4	225.3	239.2	222.4	298.3	282.5	240.3
12.00	166.9	170.8	183.4	196.8	189.6	183.3	276.1	250.9	217.7	285.2	295.0	306.8	338.0	335.9	309.1	473.8	430.1	354.6
13.00	143.2	156.1	170.6	134.5	136.4	152.2	199.1	173.8	162.4	233.2	258.6	270.9	225.5	233.1	241.8	345.5	293.6	250.7
14.00	131.9	141.0	162.3	111.1	119.7	132.4	166.0	149.2	144.4	213.1	237.3	262.3	186.3	203.1	228.8	274.5	246.5	232.8
15.00	102.6	112.3	124.7	87.2	96.2	107.2	109.2	102.1	101.5	176.6	190.7	207.8	146.8	168.7	181.4	177.9	170.7	174.4
16.00	30.3	32.9	34.6	25.9	27.0	29.7	32.0	29.9	28.7	50.0	53.2	57.2	41.0	44.9	48.6	51.6	47.4	45.5
17.00	0	0	0	0	0	0	0	0	0	0	0	0	0	0	0	0	0	0
18.00	0	0	0	0	0	0	0	0	0	0	0	0	0	0	0	0	0	0
19.00	0	0	0	0	0	0	0	0	0	0	0	0	0	0	0	0	0	0
20.00	0	0	0	0	0	0	0	0	0	0	0	0	0	0	0	0	0	0
21.00	0	0	0	0	0	0	0	0	0	0	0	0	0	0	0	0	0	0
22.00	0	0	0	0	0	0	0	0	0	0	0	0	0	0	0	0	0	0
23.00	0	0	0	0	0	0	0	0	0	0	0	0	0	0	0	0	0	0
rMBE	-0.237	-0.499	-0.320	-0.131	-0.087	-0.261	-0.217	-0.222	-0.077	0.267	-0.154	0.104	0.458	0.570	0.232	0.322	0.300	0.485
R^2	0.952	0.934	0.952	0.960	0.925	0.946	0.974	0.964	0.945	0.948	0.931	0.949	0.963	0.922	0.947	0.976	0.964	0.948
Comments	Aim to increase most sensors' calculations: increase $\tau_{windows}$=τ_{fins} and ρ_{floor}=$\rho_{ceiling}$									Aim to decrease most sensors' calculations (mostly E, M, SW) – no particular local effects: decrease ρ_{floor}=$\rho_{ceiling}$								

Table A.10: Calibration of building materials' properties for an overcast day (Part C).

	Overcast day (24.12.2022) – $E_{ceiling}$ (lx)																	
	Calculation 3 $\tau_{windows}$=τ_{fins}=0.68 $\tau_{skylights}$=0.80 ρ_{floor}=$\rho_{ceiling}$=0.35 ρ_{frames}=0.08									Calculation 4 $\tau_{windows}$=τ_{fins}=0.68 $\tau_{skylights}$=0.80 ρ_{floor}=$\rho_{ceiling}$=0.30 ρ_{frames}=0.08								
Hour	NE	N	NW	E	M	W	SE	S	SW	NE	N	NW	E	M	W	SE	S	SW
0.00	0	0	0	0	0	0	0	0	0	0	0	0	0	0	0	0	0	0
1.00	0	0	0	0	0	0	0	0	0	0	0	0	0	0	0	0	0	0
2.00	0	0	0	0	0	0	0	0	0	0	0	0	0	0	0	0	0	0
3.00	0	0	0	0	0	0	0	0	0	0	0	0	0	0	0	0	0	0
4.00	0	0	0	0	0	0	0	0	0	0	0	0	0	0	0	0	0	0
5.00	0	0	0	0	0	0	0	0	0	0	0	0	0	0	0	0	0	0
6.00	0	0	0	0	0	0	0	0	0	0	0	0	0	0	0	0	0	0
7.00	0	0	0	0	0	0	0	0	0	0	0	0	0	0	0	0	0	0
8.00	0	0	0	0	0	0	0	0	0	0	0	0	0	0	0	0	0	0
9.00	0	0	0	0	0	0	0	0	0	0	0	0	0	0	0	0	0	0
10.00	102.1	121.4	125.1	96.9	104.3	106.0	140.3	130.1	114.8	84.9	94.5	96.9	82.7	84.5	87.0	110.1	103.8	95.7
11.00	177.3	186.5	189.3	181.1	188.8	180.2	241.8	227.0	194.5	135.4	149.3	148.2	139.1	147.6	141.9	193.8	186.6	163.4
12.00	227.3	237.2	254.9	266.5	266.2	257.9	379.4	339.2	287.3	179.0	189.0	203.3	210.6	200.6	190.7	297.5	268.5	225.1
13.00	199.3	207.9	234.8	181.4	189.0	201.2	288.3	247.2	218.0	153.9	165.0	186.4	149.2	151.2	164.8	221.1	195.8	181.9
14.00	176.0	194.0	212.5	148.8	160.0	175.5	209.2	196.1	191.1	137.3	151.2	168.6	116.9	125.7	139.7	174.6	154.7	153.3
15.00	139.1	150.3	165.7	120.1	135.4	147.9	144.1	139.1	136.7	111.6	121.8	134.5	92.5	102.4	116.3	117.4	111.2	114.5
16.00	40.7	44.3	45.9	34.3	36.2	40.8	42.4	40.0	39.9	33.7	34.8	38.4	27.3	28.1	29.9	34.0	31.1	29.7
17.00	0	0	0	0	0	0	0	0	0	0	0	0	0	0	0	0	0	0
18.00	0	0	0	0	0	0	0	0	0	0	0	0	0	0	0	0	0	0
19.00	0	0	0	0	0	0	0	0	0	0	0	0	0	0	0	0	0	0
20.00	0	0	0	0	0	0	0	0	0	0	0	0	0	0	0	0	0	0
21.00	0	0	0	0	0	0	0	0	0	0	0	0	0	0	0	0	0	0
22.00	0	0	0	0	0	0	0	0	0	0	0	0	0	0	0	0	0	0
23.00	0	0	0	0	0	0	0	0	0	0	0	0	0	0	0	0	0	0
rMBE	0.032	-0.321	-0.083	0.171	0.250	0.000	0.070	0.053	0.220	-0.188	-0.461	-0.271	-0.069	-0.028	-0.216	-0.150	-0.160	-0.006
R^2	0.952	0.930	0.949	0.963	0.921	0.942	0.973	0.965	0.949	0.947	0.930	0.950	0.955	0.925	0.950	0.974	0.967	0.955
Comments	Good results for the overcast day, but not for the sunny day: reduce ρ_{floor}=$\rho_{ceiling}$ due to the calibration of the sunny day									Final results								

Table A.11: Calibration of building materials' properties for a sunny day (Part A).

	Sunny day (02.10.2022) – $E_{ceiling}$ (lx)																	
	Measurements									Calculation 0 $\tau_{windows}$=τ_{fins}=0.60 $\tau_{skylights}$=0.65 ρ_{floor}=$\rho_{ceiling}$=0.03 ρ_{frames}=0.03								
Hour	NE	N	NW	E	M	W	SE	S	SW	NE	N	NW	E	M	W	SE	S	SW
0.00	1	1	1	1	1	1	1	1	1	0	0	0	0	0	0	0	0	0
1.00	1	1	1	1	1	1	1	1	1	0	0	0	0	0	0	0	0	0
2.00	1	1	1	1	1	1	1	1	1	0	0	0	0	0	0	0	0	0
3.00	1	1	1	1	1	1	1	1	1	0	0	0	0	0	0	0	0	0
4.00	1	1	1	1	1	1	1	1	1	0	0	0	0	0	0	0	0	0
5.00	1	1	1	1	1	1	1	1	1	0	0	0	0	0	0	0	0	0
6.00	3.25	5.08	3.33	2.33	2.58	2.67	4.08	3.42	2.75	0	0	0	0	0	0	0	0	0
7.00	71.8	122	73.6	58.9	57.7	57.3	95	82.4	57.2	0	0	0	0	0	0	0	0	0
8.00	186	313	199	152	151	158	236	211	149	7.6	7.7	8.5	8.2	6.9	7.1	10.7	8.3	7.9
9.00	328	500	329	278	238	260	450	411	286	15.4	14.9	15.6	16.4	13.0	13.7	23.8	18.4	17.8
10.00	457	703	467	460	403	472	1034	1015	687	22.2	21.3	25.0	25.2	19.7	22.2	38.4	31.3	31.4
11.00	445	724	551	423	372	447	1202	983	566	24.4	23.8	30.1	23.2	21.4	26.2	42.5	34.2	35.3
12.00	437	809	841	430	426	687	1549	1417	790	25.1	26.7	38.5	22.9	22.8	32.7	46.0	37.1	41.7
13.00	314	570	510	273	274	394	1017	693	370	22.6	26.1	23.8	20.0	22.7	19.3	33.4	29.6	20.9
14.00	438	734	442	312	294	317	1025	561	317	18.0	17.7	18.5	15.3	15.5	20.4	41.3	25.4	17.7
15.00	286	482	266	181	162	174	283	241	138	14.7	14.7	16.9	9.5	9.5	12.7	15.9	12.6	14.3
16.00	147	255	138	86.2	86.3	91.3	120	105	68.3	6.2	6.0	7.1	4.0	3.7	4.9	6.5	4.9	5.5
17.00	74.2	119	62.4	45.6	43.1	42.3	58.3	50	30.1	3.1	3.0	3.6	2.0	1.9	2.5	3.3	2.5	2.8
18.00	8.58	13.5	7.08	5.58	5.08	4.58	6.92	5.75	3.58	0.9	0.8	1.0	0.5	0.5	0.6	0.8	0.6	0.6
19.00	1	1	1	1	1	1	1	1	1	0	0	0	0	0	0	0	0	0
20.00	1.08	1.42	1	1.08	1.42	1.08	1	1.08	1	0	0	0	0	0	0	0	0	0
21.00	1.42	2.92	1.25	1.67	2.83	1.67	1.17	1.58	1.33	0	0	0	0	0	0	0	0	0
22.00	1	1	1	1	1	1	1	1	1	0	0	0	0	0	0	0	0	0
23.00	1	1	1	1	1	1	1	1	1	0	0	0	0	0	0	0	0	0
rMBE	-	-	-	-	-	-	-	-	-	-0.950	-0.970	-0.952	-0.946	-0.946	-0.948	-0.963	-0.965	-0.944
R^2	-	-	-	-	-	-	-	-	-	0.954	0.943	0.980	0.978	0.952	0.973	0.965	0.940	0.968
Comments	-									Aim to significantly increase all sensors' calculations: made the modifications that led to good results previously								

Table A.12: Calibration of building materials' properties for a sunny day (Part B).

	Sunny day (02.10.2022) – $E_{ceiling}$ (lx)																	
	Calculation 1 $\tau_{windows}$=τ_{fins}=0.68 $\tau_{skylights}$=0.80 ρ_{floor}=$\rho_{ceiling}$=0.35 ρ_{frames}=0.08									Calculation 2 $\tau_{windows}$=τ_{fins}=0.68 $\tau_{skylights}$=0.80 ρ_{floor}=$\rho_{ceiling}$=0.30 ρ_{frames}=0.08								
Hour	NE	N	NW	E	M	W	SE	S	SW	NE	N	NW	E	M	W	SE	S	SW
0.00	0	0	0	0	0	0	0	0	0	0	0	0	0	0	0	0	0	0
1.00	0	0	0	0	0	0	0	0	0	0	0	0	0	0	0	0	0	0
2.00	0	0	0	0	0	0	0	0	0	0	0	0	0	0	0	0	0	0
3.00	0	0	0	0	0	0	0	0	0	0	0	0	0	0	0	0	0	0
4.00	0	0	0	0	0	0	0	0	0	0	0	0	0	0	0	0	0	0
5.00	0	0	0	0	0	0	0	0	0	0	0	0	0	0	0	0	0	0
6.00	0	0	0	0	0	0	0	0	0	0	0	0	0	0	0	0	0	0
7.00	0	0	0	0	0	0	0	0	0	0	0	0	0	0	0	0	0	0
8.00	227.8	285.5	271.0	305.4	319.7	278.0	372.5	346.1	292.3	185.0	221.0	212.7	237.3	240.6	213.5	286.9	258.9	216.9
9.00	425.2	431.3	365.2	530.8	509.1	428.8	725.1	699.7	582.3	338.2	352.3	287.4	412.6	387.1	331.6	556.6	527.1	452.9
10.00	487.9	469.4	498.4	647.4	593.2	555.9	1161.9	1163.0	928.4	397.9	373.9	392.9	530.0	465.6	434.6	916.8	884.3	734.6
11.00	491.6	494.2	575.2	562.3	542.6	557.2	1177.9	1110.9	904.2	388.5	395.0	456.7	457.8	422.1	448.4	935.4	853.4	710.4
12.00	474.9	526.1	662.3	541.3	537.1	639.8	1273.3	1131.7	970.6	399.4	429.9	564.3	435.9	426.5	535.2	990.9	900.0	774.7
13.00	368.1	415.3	408.5	357.0	394.8	389.0	525.8	501.6	391.2	299.4	322.6	351.7	288.6	328.1	337.1	436.0	415.2	351.9
14.00	371.6	461.0	511.1	349.7	501.1	805.5	897.0	592.6	419.5	293.5	352.9	411.0	273.8	378.8	622.7	719.2	472.8	345.6
15.00	317.6	328.0	370.5	227.2	249.6	289.5	336.0	308.0	310.4	254.2	261.0	294.1	189.5	199.0	228.8	283.5	240.5	251.3
16.00	135.4	135.2	146.2	91.2	91.6	103.8	121.9	100.7	100.4	105.3	108.5	124.8	77.1	75.4	84.1	110.2	90.3	93.1
17.00	69.4	68.9	71.9	48.2	46.7	53.4	67.3	56.3	57.0	52.6	53.2	59.1	30.2	31.8	40.8	47.4	36.8	38.6
18.00	23.6	25.0	24.5	17.0	19.0	19.1	20.7	18.7	17.0	19.1	20.1	20.5	13.9	14.7	14.6	16.4	14.9	14.0
19.00	0	0	0	0	0	0	0	0	0	0	0	0	0	0	0	0	0	0
20.00	0	0	0	0	0	0	0	0	0	0	0	0	0	0	0	0	0	0
21.00	0	0	0	0	0	0	0	0	0	0	0	0	0	0	0	0	0	0
22.00	0	0	0	0	0	0	0	0	0	0	0	0	0	0	0	0	0	0
23.00	0	0	0	0	0	0	0	0	0	0	0	0	0	0	0	0	0	0
rMBE	0.058	-0.321	0.001	0.352	0.505	0.321	-0.058	0.041	0.431	-0.148	-0.461	-0.186	0.084	0.175	0.055	-0.253	-0.189	0.146
R^2	0.972	0.974	0.945	0.957	0.952	0.832	0.917	0.929	0.957	0.970	0.972	0.961	0.962	0.960	0.859	0.922	0.942	0.965
Comments	Aim to decrease E, M, W, SW sensors – no local effects, except for the N sensor: reduce ρ_{floor}=$\rho_{ceiling}$									Final results								

A.3. Initial Optimizations of the Control Strategy

A.3.1. Multi-objective optimizations

A MOO problem was first run for the three activity modes for 02.10.2022 at 10.00 under sunny conditions. This problem used E_{wp} and E_{cyl} as objectives. The results obtained after 10 iterations are listed in Tables A.13, A.14, A.15. The results that belong to the same rank are equally good, with the zero rank being the best. The values are listed from worst to best rank, from highest to lowest daylight entry in each rank. It is noticed that higher values of E_{wp} yield higher E_{cyl} values.

Table A.13: MOO results for the presentation mode after 10 iterations.

Presentation		
Rank	Objective 1: E_{wp} (lx)	Objective 2: E_{cyl} (lx)
0	840.0	1373.5
0	831.9	1372.7
0	827.6	1372.4
0	797.6	1362.4
0	666.9	1321.8
0	630.6	1152.2
0	626.6	1049.6
0	542.8	1022.3
0	488.2	818.9
0	299.3	588.0

Table A.14: MOO results for the meeting mode after 10 iterations.

Meeting		
Rank	Objective 1: E_{wp} (lx)	Objective 2: E_{cyl} (lx)
1	830.1	1374.9
1	604.9	1190.8
1	566.1	1010.9
0	840.2	1367.7
0	738.4	1347.7
0	701.3	1231.2
0	605.5	1167.6
0	580.4	946.5
0	392.0	802.6
0	390.5	615.9

Table A.15: MOO results for the workshop mode after 10 iterations.

Workshop		
Rank	Objective 1: E_{wp} (lx)	Objective 2: E_{cyl} (lx)
2	633.6	1297.8
1	685.8	1232.2
1	611.9	1141.4
0	848.4	1377.0
0	829.6	1375.4
0	791.2	1340.1
0	726.5	1082.2
0	574.1	943.4
0	417.1	753.8
0	322.9	575.4

A.3.2. Single-objective optimizations

In Tables A.16, A.17, A.18 the results of the optimizations performed for the three scenarios on 02.10.2022 at 10.00 under clear sky conditions are detailed. Those optimizations were executed with the simplest case of 8 variables. The results indicate the convergence of the developed control algorithm after 20 iterations. It should be noted that the iterations are listed from worst to best solution, although during the optimization process, their sequence was random.

In Tables A.19, A.20, A.21 the results of the optimizations for the same instant, using 32 variables, are presented. This case refers to the blinds' operation in sets of three. For those optimizations, 150 iterations are needed to obtain satisfactory results. For reasons of simplicity, only the first and last 10 iterations are shown in the tables.

Finally, in Tables A.22, A.23, A.24 the optimization results for the same instant, using 96 variables, are demonstrated. This case refers to the totally independent blinds' operation. For those optimizations, 250 iterations are needed to obtain satisfactory results. Again, for reasons of simplicity, only the first and last 10 iterations are shown in the tables.

Table A.16: SOO results for the presentation mode after 20 iterations, with the simplest blinds' operation.

Presentation (8 variables)			
Iteration	Value of Objective Function	E_{wp} (lx)	E_{cyl} (lx)
1	498886.5	2411.0	4988.9
2	476896.1	1971.9	4769.0
3	453369.1	1908.4	4533.7
4	424100.3	1935.3	4241.0
5	422788.4	1730.4	4227.9
6	405737.0	1772.1	4057.4
7	399145.3	1517.7	3991.5
8	333963.9	1567.3	3339.6
9	333198.9	1399.6	3332.0
10	247722.9	1090.2	2477.2
11	243544.8	1123.1	2435.4
12	196385.9	857.7	1963.9
13	183058.7	922.4	1830.6
14	140534.8	749.1	1405.3
15	5861.1	285.3	586.1
16	5399.1	286.2	539.9
17	876.4	432.0	876.5
18	774.4	321.6	774.4
19	726.1	368.9	726.1
20	581.7	307.6	581.7

Table A.17: SOO results for the meeting mode after 20 iterations, with the simplest blinds' operation.

Meeting (8 variables)			
Iteration	Value of Objective Function	E_{wp} (lx)	E_{cyl} (lx)
1	480853.8	2500.3	4808.5
2	455527.4	2243.6	4555.3
3	348746.9	2153.3	3487.5
4	346535.5	2121.2	3465.4
5	345253.8	1942.3	3452.5
6	337993.1	1947.6	3379.9
7	326958.4	1731.5	3269.6
8	260708.9	1260.4	2607.1
9	231140.8	1219.7	2311.4
10	178007.6	614.6	1780.1
11	177722.7	871.3	1777.2
12	174230.4	643.1	1742.3
13	-720.0	234.3	720.0
14	-897.4	380.8	897.4
15	-1108.5	472.9	1108.5
16	-1150.8	490.6	1150.8
17	-11913.5	524.0	1191.3
18	-11927.2	556.6	1192.7
19	-12294.1	564.1	1229.4
20	-13109.5	581.4	1311.0

Table A.18: SOO results for the workshop mode after 20 iterations, with the simplest blinds' operation.

Workshop (8 variables)			
Iteration	Value of Objective Function	E_{wp} (lx)	E_{cyl} (lx)
1	496485.4	2383.6	4964.9
2	493476.2	2278.6	4934.8
3	450712.6	2180.7	4507.1
4	398558.4	1715.1	3985.6
5	391089.5	1673.7	3910.9
6	345519.1	1702.4	3455.2
7	336405.4	1597.5	3364.1
8	311723.6	1698.0	3117.2
9	309483.2	1562.6	3094.8
10	266202.8	1082.7	2662.0
11	215991.2	981.1	2159.9
12	215299.7	1161.1	2153.0
13	154346.1	675.6	1543.5
14	-892.5	428.4	892.5
15	-895.1	426.6	895.1
16	-908.4	452.2	908.4
17	-918.6	431.3	918.6
18	-921.3	425.3	921.3
19	-1191.2	512.5	1191.2
20	-1380.3	716.4	1380.3

Table A.19: SOO results for the presentation mode after 150 iterations, with blinds' operation in sets of three.

Presentation (32 variables)			
Iteration	Value of Objective Function	E_{wp} (lx)	E_{cyl} (lx)
1	486040.7	1874.3	4860.4
2	482829.7	1812.7	4828.3
3	476631.8	1796.5	4766.3
4	472656.5	1764.3	4726.6
5	468524.1	1739.2	4685.2
6	464902.7	1721.1	4649.0
7	463935.9	1731.4	4639.4
8	453932.6	1667.6	4539.3
9	428311.9	1534.7	4283.1
10	403583.0	1448.6	4035.8
...	...	...	...
141	911.2	884.4	911.2
142	896.7	624.8	896.7
143	877.5	529.6	877.5
144	867.5	443.8	867.5
145	848.0	406.1	848.0
146	839.9	411.8	839.9
147	808.6	396.1	808.6
148	798.3	327.3	798.3
149	782.3	338.1	782.3
150	757.8	343.1	757.8

Table A.20: SOO results for the meeting mode after 150 iterations, with blinds' operation in sets of three.

Meeting (32 variables)			
Iteration	Value of Objective Function	E_{wp} (lx)	E_{cyl} (lx)
1	484156.0	1889.9	4841.6
2	483256.0	1887.9	4832.6
3	482813.6	1938.5	4828.1
4	476235.2	1909.5	4762.4
5	475233.6	1818.0	4752.3
6	469113.1	1790.8	4691.1
7	457154.8	1639.0	4571.5
8	443479.9	1574.4	4434.8
9	433328.2	1497.3	4333.3
10	427225.7	1445.7	4272.3
...	...	...	...
141	-12614.9	571.6	1261.5
142	-12774.9	662.3	1277.5
143	-12859.0	628.9	1285.9
144	-12873.5	601.0	1287.4
145	-12883.1	617.8	1288.3
146	-13028.4	605.2	1302.8
147	-13323.7	650.2	1332.4
148	-13593.0	679.7	1359.3
149	-13875.4	728.7	1387.5
150	-13963.8	716.7	1396.4

Table A.21: SOO results for the workshop mode after 150 iterations, with blinds' operation in sets of three.

Workshop (32 variables)			
Iteration	Value of Objective Function	E_{wp} (lx)	E_{cyl} (lx)
1	484981.2	2206.1	4849.8
2	479920.7	2092.0	4799.2
3	479402.8	1849.2	4794.0
4	474427.2	1866.3	4744.3
5	472333.1	1720.6	4723.3
6	463386.2	1586.3	4633.9
7	462817.5	1436.3	4628.2
8	455271.3	1402.5	4552.7
9	448760.4	1361.1	4487.6
10	447973.9	1307.6	4479.7
...	...	...	...
141	140846.8	987.7	1408.5
142	140317.9	980.6	1403.2
143	-12587.2	751.0	1258.7
144	-12898.1	775.8	1289.8
145	-13436.3	824.6	1343.6
146	-13448.3	843.2	1344.8
147	-13452.8	831.2	1345.3
148	-13692.9	821.4	1369.3
149	-13889.7	834.0	1389.0
150	-13965.1	842.6	1396.5

Table A.22: SOO results for the presentation mode after 250 iterations, with totally independent blinds' operation.

Presentation (96 variables)			
Iteration	Value of Objective Function	E_{wp} (lx)	E_{cyl} (lx)
1	447912.3	1833.0	4479.1
2	436839.8	1637.8	4368.4
3	436217.7	1589.4	4362.2
4	431732.5	1470.1	4317.3
5	428134.7	1396.0	4281.3
6	421339.6	1393.2	4213.4
7	418650.6	1321.1	4186.5
8	415634.3	1350.4	4156.3
9	413404.0	1368.9	4134.0
10	412106.3	1257.1	4121.1
...	...	...	...
241	1228.0	1149.5	1228.0
242	1226.7	745.8	1226.7
243	1222.2	759.4	1222.2
244	1218.7	730.8	1218.7
245	1215.3	724.5	1215.3
246	1197.2	758.0	1197.2
247	1197.0	766.3	1197.0
248	1196.1	704.6	1196.1
249	1150.0	711.4	1150.0
250	1149.7	686.5	1149.7

Table A.23: SOO results for the meeting mode after 250 iterations, with totally independent blinds' operation.

Meeting (96 variables)			
Iteration	Value of Objective Function	E_{wp} (lx)	E_{cyl} (lx)
1	458016.0	1252.5	4580.2
2	449477.6	1251.0	4494.8
3	447853.5	1141.7	4478.5
4	447433.9	1157.0	4474.3
5	441728.4	1103.8	4417.3
6	430638.0	1171.4	4306.4
7	424800.8	1261.0	4248.0
8	416998.1	1247.1	4170.0
9	404892.2	1303.3	4048.9
10	398231.3	1344.3	3982.3
...	...	...	...
241	-13306.7	703.4	1330.7
242	-13398.4	954.5	1339.8
243	-13465.9	875.0	1346.6
244	-13491.5	648.5	1349.2
245	-13513.0	618.9	1351.3
246	-13540.5	657.6	1354.0
247	-13712.7	790.2	1371.3
248	-13738.7	831.8	1373.9
249	-13794.4	798.6	1379.4
250	-13868.5	898.9	1386.8

Table A.24: SOO results for the workshop mode after 250 iterations, with totally independent blinds' operation.

Workshop (96 variables)			
Iteration	Value of Objective Function	E_{wp} (lx)	E_{cyl} (lx)
1	461140.7	1985.8	4611.4
2	442642.5	1761.8	4426.4
3	442368.7	1682.6	4423.7
4	436867.9	1704.1	4368.7
5	419174.6	1572.8	4191.7
6	417464.4	1556.4	4174.6
7	413903.6	1375.0	4139.0
8	409077.1	1382.3	4090.8
9	403763.3	1336.1	4037.6
10	400442.7	1717.7	4004.4
...	...	...	...
241	-13149.0	804.3	1314.9
242	-13158.1	758.9	1315.8
243	-13173.4	763.5	1317.3
244	-13174.3	787.5	1317.4
245	-13214.8	803.2	1321.5
246	-13345.6	848.3	1334.6
247	-14691.3	821.7	1469.1
248	-13831.2	816.3	1383.1
249	-13896.4	849.8	1389.6
250	-13995.3	821.4	1399.5

A.4. Detailed Results of the Control Strategies

A.4.1. Clear sky conditions

Tables A.25, A.26, A.27, A.28 detail the blinds' states decided by the current and the optimized control for each time step of the test period on 18.03.2022, as well as the respective results in terms of visual comfort, view quality, lighting energy demand and solar heat gains.

A.4.2. Variable weather conditions

Tables A.29, A.30, A.31, A.32 detail the blinds' states decided by the controls for each time step of the test period on 24.10.2022, as well as the respective results in terms of visual comfort, view quality, lighting energy demand and solar heat gains.

Table A.25: Detailed results of the current control for the test period on 18.03.2022.

Current control strategy																			
Hour	Increments				Slat angles (°)				average E_{wp} (lx)	max E_{cyl} (lx)	max DGP	View percentage (%)	Light dimming levels			Energy demand (kWh)			Solar heat gains (kWh)
	N	E	S	W	N	E	S	W					Presentation	Meeting	Workshop	Presentation	Meeting	Workshop	
10.00	1	1	1	1	0	18	54	0	743.2	1776.6	0.611	71.5	0	0	0.01	0	0	0.005	0.094
10.15	1	1	1	1	0	2	20	0	1081.4	2354.8	0.779	77.2	0	0	0	0	0	0	0.202
10.30	1	1	1	0	0	2	18	0	1395.0	2631.3	0.873	84.2	0	0	0	0	0	0	0.456
10.45	1	1	1	1	0	2	50	0	966.8	2160.6	0.650	74.2	0	0	0	0	0	0	0.266
11.00	1	1	1	1	0	2	46	0	860.1	2060.0	0.389	74.7	0	0	0	0	0	0	0.038
11.15	1	1	1	1	0	2	36	0	852.7	2170.6	0.391	75.6	0	0	0	0	0	0	0.179
11.30	1	1	1	1	0	2	18	0	962.5	2328.5	0.452	77.4	0	0	0	0	0	0	0.168
11.45	1	1	1	1	0	2	42	30	809.0	1862.4	0.386	70.8	0	0	0	0	0	0	0.038
12.00	1	1	1	1	0	2	12	2	936.9	2335.0	0.457	78.3	0	0	0	0	0	0	0.038
12.15	1	1	1	1	0	2	32	24	854.7	1915.0	0.389	72.6	0	0	0	0	0	0	0.038
12.30	1	1	1	1	0	2	10	22	992.2	2402.1	0.465	75.4	0	0	0	0	0	0	0.038
12.45	1	1	1	1	0	2	20	4	1007.4	2385.3	0.428	77.1	0	0	0	0	0	0	0.038
13.00	1	1	1	1	0	2	2	20	975.9	2541.8	0.477	76.5	0	0	0	0	0	0	0.038
13.15	1	1	1	1	0	2	2	12	1048.0	2741.2	0.468	77.9	0	0	0	0	0	0	0.038
13.30	1	1	1	1	0	2	2	12	1111.1	2651.0	0.472	77.9	0	0	0	0	0	0	0.155
13.45	1	1	1	1	0	2	0	14	1067.0	2601.3	0.476	77.8	0	0	0	0	0	0	0.080
14.00	1	1	1	1	0	2	0	18	1169.1	2389.7	0.423	77.2	0	0	0	0	0	0	0.109
14.15	1	1	1	1	0	2	0	22	1146.1	2311.9	0.421	76.6	0	0	0	0	0	0	0.117
14.30	1	1	1	1	0	2	0	26	1144.6	2283.4	0.420	76.1	0	0	0	0	0	0	0.134
14.45	0	0	0	0	0	0	0	0	5297.2	4885.3	0.644	100.0	0	0	0	0	0	0	2.672
15.00	0	0	1	1	0	0	0	34	1274.3	2422.3	0.420	84.4	0	0	0	0	0	0	0.038
15.15	0	0	1	1	0	0	0	36	1260.4	2350.6	0.419	84.0	0	0	0	0	0	0	0.038
15.30	0	0	1	1	0	0	0	40	1244.7	2357.4	0.420	83.3	0	0	0	0	0	0	0.038
15.45	0	0	1	1	0	0	0	44	1266.8	2327.8	0.424	82.6	0	0	0	0	0	0	0.038

Table A.26: Detailed results of the optimized control for the presentation mode for the test period on 18.03.2022.

Optimized control strategy - Presentation															
Hour	Increments				Slat angles (°)				average E_{wp} (lx)	max E_{cyl} (lx)	max DGP	View percentage (%)	Light dimming levels	Energy demand (kWh)	Solar heat gains (kWh)
	N	E	S	W	N	E	S	W							
10.00	1	1	1	1	72	72	72	72	310	717	0.346	51.5	0	0	0.041
10.15	1	1	1	0.0	44	70	70	-20	715	1262	0.787	68.7	0	0	0.236
10.30	0.8	1	1	1	72	58	72	-30	598	972	0.348	62.8	0	0	0.038
10.45	1	1	1	1	-28	64	34	62	717	1165	0.347	60.6	0	0	0.038
11.00	1	1	1	1	72	24	72	72	335	831	0.329	55.9	0	0	0.038
11.15	1	1	1	1	70	66	66	-30	425	804	0.318	59.5	0	0	0.151
11.30	1	1	1	0	72	72	72	-26	660	1230	0.405	66.8	0	0	0.191
11.45	0.8	0.8	1	0.8	72	26	64	50	350	1028	0.359	63.8	0	0	0.038
12.00	1	1	1	1	72	18	42	68	431	1054	0.336	58.6	0	0	0.119
12.15	1	1	1	1	16	54	72	72	375	767	0.334	56.9	0	0	0.082
12.30	1	0.8	1	1	72	18	72	72	312	882	0.335	56.8	0	0	0.038
12.45	1	1	1	0.8	70	-30	70	68	545	1103	0.337	62.8	0	0	1.142
13.00	1	0.8	1	1	28	26	72	72	368	745	0.306	59.1	0	0	0.065
13.15	1	0	1	1	-30	-30	72	66	883	1844	0.397	70.2	0	0	0.221
13.30	1	1	1	1	68	-30	72	-30	768	1388	0.36	65.8	0	0	2.320
13.45	1	0.4	1	1	32	22	72	72	669	1366	0.386	64.5	0	0	0.128
14.00	1	0.2	1	1	64	26	72	10	921	1492	0.379	70.8	0	0	0.368
14.15	1	1	1	1	72	42	56	72	425	554	0.299	54.0	0	0	0.015
14.30	1	0	1	1	72	-12	72	72	764	1231	0.349	64.5	0	0	0.384
14.45	1	1	1	1	72	72	72	72	371	500	0.293	51.5	0	0	0.146
15.00	0.8	1	0.8	1	72	36	58	72	338	593	0.302	60.1	0	0	0.038
15.15	1	1	1	1	72	72	70	72	292	322	0.31	51.5	0.01	0.005	0.065
15.30	1	0	1	1	-30	70	72	72	891	1366	0.371	69.8	0	0	0.327
15.45	1	1	1	1	-30	72	-30	72	830	1312	0.345	62.2	0	0	0.197

Table A.27: Detailed results of the optimized control for the meeting mode for the test period on 18.03.2022.

Optimized control strategy - Meeting															
Hour	Increments				Slat angles (°)				average E_{wp} (lx)	max E_{cyl} (lx)	max DGP	View percentage (%)	Light dimming levels	Energy demand (kWh)	Solar heat gains (kWh)
	N	E	S	W	N	E	S	W							
10.00	0.8	1	1	0	50	38	70	24	645.4	1260.0	0.768	71.0	0	0	0.274
10.15	1	1	1	1	24	24	38	34	703.5	1393.0	0.349	64.4	0	0	0.085
10.30	1	1	1	0.6	24	66	72	36	619.8	1253.0	0.357	63.2	0	0	0.251
10.45	1	1	1	1	-30	72	72	72	564.9	1077.6	0.345	55.7	0	0	0.222
11.00	1	1	1	1	72	0	72	28	594.4	1322.5	0.383	62.3	0	0	0.038
11.15	1	1	1	0	72	40	72	-30	639.9	1378.5	0.408	68.0	0	0	0.522
11.30	0.8	1	1	0	72	72	72	-30	570.5	1397.9	0.412	68.8	0	0	0.573
11.45	1	0	1	1	32	36	72	-30	1054.8	2216.5	0.488	74.3	0	0	0.367
12.00	0.8	0.8	1	0.4	46	70	52	-30	478.2	1011.3	0.421	72.6	0.03	0.016	1.808
12.15	0.8	1	0.8	1	70	72	70	-24	484.6	1029.8	0.338	65.0	0.02	0.011	0.615
12.30	1	1	0.8	1	-30	28	72	72	567.5	1313.7	0.341	62.5	0	0	0.712
12.45	0.2	0.8	1	1	2	72	72	50	660.7	1396.5	0.442	65.1	0	0	0.192
13.00	1	1	1	1	72	-30	72	30	616.9	1108.2	0.335	61.7	0	0	0.101
13.15	1	1	1	1	-30	72	72	72	556.2	1051.9	0.333	55.7	0	0	0.082
13.30	1	1	1	1	72	-30	72	72	514.2	980.8	0.323	57.3	0	0	0.088
13.45	1	0.6	1	1	72	66	68	-30	583.4	1255.4	0.363	65.9	0	0	2.006
14.00	1	1	1	1	72	70	2	72	615.8	1288.5	0.387	56.7	0	0	0.040
14.15	0	1	1	1	-30	72	70	72	713.2	1659.0	0.407	60.5	0	0	0.145
14.30	0.8	1	1	1	18	-2	70	72	659.0	1196.7	0.341	62.2	0	0	0.124
14.45	1	0.4	1	1	68	54	72	72	619.0	1150.4	0.346	61.2	0	0	0.157
15.00	1	0	1	1	68	72	72	58	684.7	1123.8	0.357	64.7	0	0	0.211
15.15	1	1	0.6	1	36	-28	70	72	784.6	1398.8	0.340	66.0	0	0	0.646
15.30	0.8	1	0.6	1	4	30	42	54	558.1	1097.4	0.331	66.5	0	0	0.527
15.45	1	1	1	1	72	-14	18	72	642.9	1241.4	0.328	63.2	0	0	0.109

Table A.28: Detailed results of the optimized control for the workshop mode for the test period on 18.03.2022.

Optimized control strategy - Workshop															
Hour	Increments				Slat angles (°)				average E_{wp} (lx)	max E_{cyl} (lx)	max DGP	View percentage (%)	Light dimming levels	Energy demand (kWh)	Solar heat gains (kWh)
	N	E	S	W	N	E	S	W							
10.00	1.0	0.8	0.8	1.0	24	70	70	60	837.7	1291.6	0.345	61.9	0	0	0.368
10.15	0.4	1.0	0.8	1.0	72	72	20	18	756.7	1372.7	0.468	68.6	0	0	0.420
10.30	1.0	0.0	1.0	1.0	68	40	72	54	2037.1	2813.1	0.581	64.7	0	0	0.545
10.45	1.0	1.0	1.0	1.0	62	38	66	-18	967.6	1278.4	0.716	62.7	0	0	0.154
11.00	0.8	1.0	1.0	1.0	2	72	70	38	769.6	1315.5	0.349	59.2	0	0	0.038
11.15	0.8	1.0	1.0	0.0	44	64	72	14	755.0	1292.4	0.407	69.0	0	0	0.566
11.30	1.0	1.0	1.0	0.0	6	42	72	72	761.8	1296.2	0.426	77.8	0	0	0.682
11.45	0.4	1.0	1.0	1.0	-30	54	72	54	801.4	1420.1	0.377	64.6	0	0	0.163
12.00	0.8	0.8	1.0	1.0	2	-4	72	72	824.0	1325.0	0.381	66.2	0	0	0.199
12.15	1.0	1.0	1.0	0.8	72	-6	72	72	517.8	1157.8	0.346	63.2	0.26	0.137	0.981
12.30	0.8	1.0	1.0	0.8	72	72	72	-30	470.8	1126.3	0.370	64.1	0.32	0.169	1.045
12.45	1.0	1.0	1.0	1.0	-8	72	72	54	537.9	1169.7	0.394	58.1	0.24	0.127	0.066
13.00	0.6	0.8	1.0	1.0	8	24	72	-14	815.0	1333.5	0.397	71.8	0	0	0.962
13.15	1.0	1.0	1.0	1.0	72	-24	72	-30	833.4	1394.3	0.350	65.9	0	0	1.811
13.30	1.0	1.0	0.8	0.8	52	64	72	72	782.1	1130.2	0.334	59.2	0	0	1.303
13.45	1.0	1.0	1.0	1.0	72	-28	72	-10	751.5	1392.2	0.383	67.6	0	0	0.445
14.00	1.0	1.0	1.0	1.0	72	-30	72	12	1011.0	1352.8	0.376	64.3	0	0	0.335
14.15	1.0	1.0	0.6	0.8	48	72	72	72	1512.8	1376.0	0.384	62.2	0	0	0.923
14.30	1.0	0.2	1.0	1.0	42	-30	72	72	986.6	1266.3	0.344	64.8	0	0	0.189
14.45	0.8	0.0	1.0	1.0	72	72	72	72	967.7	1249.7	0.348	66.8	0	0	0.243
15.00	1.0	1.0	1.0	1.0	10	68	-18	72	1018.5	1345.6	0.348	62.4	0	0	0.124
15.15	1.0	1.0	0.2	1.0	-24	70	16	72	1177.3	1645.0	0.365	67.1	0	0	0.511
15.30	0.6	1.0	0.6	1.0	72	46	28	28	763.4	1239.6	0.340	67.9	0	0	0.712
15.45	0.4	1.0	0.4	1.0	26	72	54	70	1012.8	1344.9	0.348	66.3	0	0	0.478

Table A.29: Detailed results of the current control for the test period on 24.10.2022.

Current control strategy																			
Hour	Increments				Slat angles (°)				average E_{wp} (lx)	max E_{cyl} (lx)	max DGP	View percentage (%)	Light dimming levels			Energy demand (kWh)			Solar heat gains (kWh)
	N	E	S	W	N	E	S	W					Presentation	Meeting	Workshop	Presentation	Meeting	Workshop	
10.30	0	0	0	0	-10	-10	-10	-10	406.4	616.1	0.220	100.0	0	0.11	0.39	0	0.058	0.206	0.219
10.45	0	0	0	0	-10	-10	-10	-10	717.8	1083.4	0.295	100.0	0	0	0.04	0	0	0.021	0.384
11.00	0	0	0	0	-10	-10	-10	-10	2402.0	4320.9	0.970	100.0	0	0	0	0	0	0	0.596
11.15	0	0	0	0	-10	-10	-10	-10	2758.6	4812.6	1.000	100.0	0	0	0	0	0	0	0.739
11.30	0	0	0	0	-10	-10	-10	-10	3790.5	7300.3	1.000	100.0	0	0	0	0	0	0	1.010
11.45	0	0	0	0	-10	-10	-10	-10	3101.5	5981.9	1.000	100.0	0	0	0	0	0	0	0.884
12.00	0	0	0	0	-10	-10	-10	-10	6035.1	12661.4	1.000	100.0	0	0	0	0	0	0	0.939
12.15	0	0	0	0	-10	-10	-10	-10	3391.4	6316.5	1.000	100.0	0	0	0	0	0	0	0.753
12.30	0	0	0	0	-10	-10	-10	-10	1040.6	1366.5	0.338	100.0	0	0	0	0	0	0	0.556
12.45	0	0	0	0	-10	-10	-10	-10	1139.1	1599.4	0.389	100.0	0	0	0	0	0	0	0.474
13.00	0	0	0	0	-10	-10	-10	-10	1334.3	1949.6	0.509	100.0	0	0	0	0	0	0	0.546
13.15	0	0	0	0	-10	-10	-10	-10	2175.2	3966.5	0.851	100.0	0	0	0	0	0	0	0.598

Table A.30: Detailed results of the optimized control for the presentation mode for the test period on 24.10.2022.

Optimized control strategy - Presentation															
Hour	Increments				Slat angles (°)				average E_{wp} (lx)	max E_{cyl} (lx)	max DGP	View percentage (%)	Light dimming levels	Energy demand (kWh)	Solar heat gains (kWh)
	N	E	S	W	N	E	S	W							
10.30	0.4	0.4	0	0.4	32	-22	-26	-28	336.9	487.1	0.215	95.5	0	0	0.204
10.45	0	0.8	0.8	0	72	52	-30	-30	413.9	544.2	0.244	86.9	0	0	0.276
11.00	1	1	1	1	-28	70	-30	-30	501.6	958.7	0.827	68.9	0	0	0.259
11.15	0.8	1	0.8	0.2	-30	52	72	-12	426.7	792.2	0.317	75.1	0	0	0.469
11.30	0.8	1	1	0.4	38	20	72	-6	335.5	618.3	0.325	71.4	0	0	0.489
11.45	1	1	1	1	52	-12	72	-12	555.9	1065.2	0.331	69.5	0	0	0.121
12.00	1	1	1	0.2	-12	70	72	-12	409.4	176.8	0.344	71.3	0	0	0.207
12.15	1	0.6	1	1	-28	22	72	70	466.7	283.1	0.323	63.8	0	0	0.247
12.30	1	0.4	1	0.8	-28	-30	72	18	507.8	233.7	0.293	75.0	0	0	0.285
12.45	0	1	1	0	26	54	72	-28	395.2	85.4	0.288	76.7	0	0	0.279
13.00	1	1	1	0	72	12	40	62	322.1	444.8	0.248	73.7	0	0	0.187
13.15	0.8	0.8	0.8	1	-30	54	54	54	371.3	675.0	0.289	65.1	0	0	0.245

Table A.31: Detailed results of the optimized control for the meeting mode for the test period on 24.10.2022.

Optimized control strategy - Meeting															
Hour	Increments				Slat angles (°)				average E_{wp} (lx)	max E_{cyl} (lx)	max DGP	View percentage (%)	Light dimming levels	Energy demand (kWh)	Solar heat gains (kWh)
	N	E	S	W	N	E	S	W							
10.30	0	0	0	0	72	-30	70	-26	388.8	567.7	0.221	100.0	0.13	0.069	0.219
10.45	0	0	0	0	40	72	-12	72	691.6	1023.9	0.276	100.0	0	0	0.384
11.00	0	1	0.6	0.2	-24	26	32	20	810.5	1166.8	0.309	84.5	0	0	0.471
11.15	0	1	1	0	8	36	72	-4	526.3	1076.8	0.346	78.6	0	0	0.423
11.30	0.6	1	1	1	72	-8	58	-14	617.2	1282.2	0.322	74.7	0	0	0.205
11.45	0	1	1	0	-30	30	72	16	591.7	1196.0	0.359	79.6	0	0	0.540
12.00	0	1	0.8	0	-30	-30	72	-28	853.6	1138.4	0.397	85.9	0	0	0.654
12.15	1	0.8	1	0	12	-28	62	18	702.8	1273.4	0.319	81.3	0	0	0.420
12.30	0	0	0	0	72	70	72	72	949.1	1340.0	0.326	100.0	0	0	0.556
12.45	1	0	0	0	-26	68	70	72	929.5	1376.5	0.359	95.0	0	0	0.511
13.00	0.4	0.4	0.4	0.4	22	22	22	22	841.1	1285.1	0.330	89.6	0	0	0.602
13.15	1	0	0.8	0.8	42	-28	8	18	663.3	1397.8	0.355	78.0	0	0	0.368

Table A.32: Detailed results of the optimized control for the workshop mode for the test period on 24.10.2022.

Optimized control strategy - Workshop															
Hour	Increments				Slat angles (°)				average E_{wp} (lx)	max E_{cyl} (lx)	max DGP	View percentage (%)	Light dimming levels	Energy demand (kWh)	Solar heat gains (kWh)
	N	E	S	W	N	E	S	W							
10.30	0.0	0.0	0.0	0.0	-26	58	68	-28	395.4	577.4	0.222	100.0	0.40	0.211	0.219
10.45	0.0	0.0	0.0	0.0	68	72	10	28	673.0	969.0	0.274	100.0	0.09	0.048	0.384
11.00	0.0	1.0	0.0	0.6	54	-2	34	70	921.0	1297.5	0.563	87.2	0.00	0	0.545
11.15	1.0	0.2	1.0	0.0	-10	-10	72	72	774.1	763.9	0.349	84.9	0	0	0.534
11.30	0.0	0.0	1.0	0.0	-28	72	72	-22	989.9	1313.2	0.396	89.5	0	0	0.881
11.45	0.4	0.0	1.0	0.0	68	68	48	46	874.6	1148.0	0.383	88.6	0	0	0.759
12.00	1.0	0.8	0.8	0.8	54	-30	54	46	566.6	1163.5	0.245	68.5	0.21	0.111	0.963
12.15	1.0	1.0	1.0	0.0	-30	-30	30	72	932.8	1359.1	0.337	81.0	0	0	0.517
12.30	0.0	0.0	0.0	0.0	-28	-30	-28	-4	949.6	1333.8	0.326	100.0	0	0	0.556
12.45	0.0	0.0	1.0	0.0	70	-30	-28	72	936.9	1373.9	0.340	95.0	0	0	0.511
13.00	0.4	0.4	0.4	0.4	22	22	22	22	842.8	1280.8	0.327	89.6	0	0	0.602
13.15	0.0	1.0	1.0	0.6	6	4	72	6	596.5	1365.3	0.358	78.2	0.18	0.095	0.355